RADC-TR-88-298
Final Technical Report
February 1989

AD A207-451

DEVELOPMENT OF THEORETICAL AND NUMERICAL TECHNIQUES FOR ACHIEVING STABILITY IN GYROTRON TRAVELING-WAVE AMPLIFIERS

University of Utah

Jeff E. Arrington

DTIC
ELECTE
MAY 0 8 1989
S
Cb H
D

ROME AIR DEVELOPMENT CENTER
Air Force Systems Command
Griffiss Air Force Base, NY 13441-5700

This report has been reviewed by the RADC Public Affairs Division (PA) and is releasable to the National Technical Information Service (NTIS). At NTIS it will be releasable to the general public, including foreign nations.

RADC-TR-88-298 has been reviewed and is approved for publication.

APPROVED: *Edward Daniszewski*

EDWARD DANISZEWSKI
Project Engineer

APPROVED:

FRED J. DEMMA
Acting Director of Surveillance

FOR THE COMMANDER: *John A. Ritz*

JOHN A. RITZ
Directorate of Plans & Programs

REPORT DOCUMENTATION PAGE

Form Approved
OMB No. 0704-0188

1a. REPORT SECURITY CLASSIFICATION UNCLASSIFIED		1b. RESTRICTIVE MARKINGS N/A			
2a. SECURITY CLASSIFICATION AUTHORITY N/A		3. DISTRIBUTION / AVAILABILITY OF REPORT Approved for public release; distribution unlimited.			
2b. DECLASSIFICATION / DOWNGRADING SCHEDULE N/A					
4. PERFORMING ORGANIZATION REPORT NUMBER(S) UTEC MD-88-072		5. MONITORING ORGANIZATION REPORT NUMBER(S) RADC-TR-88-298			
6a. NAME OF PERFORMING ORGANIZATION University of Utah	6b. OFFICE SYMBOL (If applicable)	7a. NAME OF MONITORING ORGANIZATION Rome Air Development Center (OCTP)			
6c. ADDRESS (City, State, and ZIP Code) Department of Electrical Engineering Microwave Device & Physical Electronics Lab Salt Lake City UT 84112		7b. ADDRESS (City, State, and ZIP Code) Griffiss AFB NY 13441-5700			
8a. NAME OF FUNDING / SPONSORING ORGANIZATION AFOSR	8b. OFFICE SYMBOL (If applicable) NE	9. PROCUREMENT INSTRUMENT IDENTIFICATION NUMBER F30602-84-C-0153			
8c. ADDRESS (City, State, and ZIP Code) Bolling AFB Wash DC 20332		10. SOURCE OF FUNDING NUMBERS			

10. SOURCE OF FUNDING NUMBERS			
PROGRAM ELEMENT NO.	PROJECT NO.	TASK NO	WORK UNIT ACCESSION NO.
61102F	2305	J9	17

11. TITLE (Include Security Classification)
DEVELOPMENT OF THEORETICAL AND NUMERICAL TECHNIQUES FOR ACHIEVING STABILITY IN GYROTRON TRAVELING-WAVE AMPLIFIERS

12. PERSONAL AUTHOR(S)
Jeff E. Arrington

13a. TYPE OF REPORT Final	13b. TIME COVERED FROM Sep 85 TO Jun 88	14. DATE OF REPORT (Year, Month, Day) February 1989	15. PAGE COUNT 242

16. SUPPLEMENTARY NOTATION
Research accomplished in conjunction with Air Force Thermionics Engineering Research (AFTER) Program. AFTER-32 (See reverse)

17. COSATI CODES			18. SUBJECT TERMS (Continue on reverse if necessary and identify by block number)
FIELD	GROUP	SUB-GROUP	Gyrotron
09	01		Numerical Analysis
			Reverse Injection

19. ABSTRACT (Continue on reverse if necessary and identify by block number)
The gyrotron traveling-wave amplifier is investigated with the purpose of developing the necessary analytical and numerical tools to allow analysis of proposed device based solutions to problems that currently limit the usefulness of the device. These solutions involve a fuller development of a scheme to increase the oscillation start current by use of spatially located, frequency selective loss mechanisms. The second problem considered is the narrow bandwidth of the cyclotron resonance maser interaction. A reverse injection scheme is discussed. It is found that the available analytical techniques are severely limited in their ability to analyze and simulate the proposed solutions, therefore indicating the development of the new tools discussed in this report.

20. DISTRIBUTION / AVAILABILITY OF ABSTRACT ☑ UNCLASSIFIED/UNLIMITED ☐ SAME AS RPT. ☐ DTIC USERS	21. ABSTRACT SECURITY CLASSIFICATION UNCLASSIFIED	
22a. NAME OF RESPONSIBLE INDIVIDUAL Edward Daniszewski	22b. TELEPHONE (Include Area Code) (315) 330-4381	22c. OFFICE SYMBOL RADC (OCTP)

DD Form 1473, JUN 86   Previous editions are obsolete.

Block 16 (Continued)

Jeff E. Arrington was an AFTER student from Hughes Aircraft Company, Electron Dynamics Division. This report was submitted in partial fulfillment of the requirements for the degree of Doctor of Philosophy.

ABSTRACT

The gyrotron traveling-wave amplifier (GTWA) is investigated with
the purpose of developing the necessary analytical and numerical tools
to allow analysis of proposed device-based solutions to problems that
currently limit the usefulness of the device. These solutions involve a
fuller development of a scheme to increase the oscillation start current
by use of spatially located, frequency selective loss mechanisms. The
second problem considered is the narrow bandwidth of the cyclotron
resonance maser interaction. A reverse-injection scheme is discussed.
It is found that the available analytic techniques are severely limited
in their ability to analyze and simulate the proposed solutions, there-
fore indicating the need for the development of new tools.

A self-consistent large signal nonlinear theory of the GTWA for
TE_{mn} modes, operating at arbitrary cyclotron harmonics in a circular
waveguide, is derived as a combination of a transmission line formula-
tion for the RF electromagnetic fields and a single particle trajectory
formulation for the electron beam. The general form for a coupling term
is presented, and the specific form for a circular waveguide is
derived. The theory is capable of analyzing the effects of the device-
based solutions.

The analytic theory is implemented into a computer simulation
code, producing a $9N + 2$ order set of equations. The accuracy of the
code has been rigorously tested and verified with respect to internal
calculations and to published data. Excellent agreement between the
code described herein and previous work by Chu[18,19] and Fliflet[24] has

been established in several different ways. Numerical analysis of the conservation of energy has verified the coupling term to produce results with a normalized error in total power rarely exceeding 0.85 percent. The extensive verification testing has shown that the theory correctly addresses conventional GTWA devices, while also making provision for analysis of nonconventional designs not described by previous theories, but indicated by current experimental work[9] and operational problems.

The code has been used to study the effects of detuning of both RF and dc frequencies. It is found that the optimal magnetic field detuning, for the tested design, occurs at approximately 96 percent of the synchronous value, while RF detuning produces the greatest efficiency for tuning approximately 6 percent above the synchronous value. The zero guiding center drift assumption is examined and found to not always be valid. Specifically, it is found that a normalized drift of 8 percent (corresponding to a 6 percent decrease in linear coupling strength) occurs for a TE_{03} mode operating at the 3rd cyclotron harmonic.

ACKNOWLEDGMENTS

TABLE OF CONTENTS

LIST OF FIGURES AND TABLES

LIST OF SYMBOLS

$\vec{a}$	RF force term vector
B_o	dc magnetic field
B_{or}	Radial component of B_o
B_{oz}	Longitudinal component of B_o
c	Speed of light
C_{mn}	Normalization constant for basis vectors
ds	Cross-section area (r dr dθ)
$|e|$	Unsigned charge of electron
%E	Percent normalized total power error
E_{bf}	Beam→field coupling coefficient
$\vec{e}_n$	Normalized electric basis vector
E_p	Component of RF electric field parallel to wall
$\vec{E}_{tn}$	Transverse electric field for n^{th} mode
E_z	Longitudinal electric field
$f(\vec{r},\vec{p},t)$	Phase space distribution function (subscript 0/1 implies dc/RF perturbed)
$F_n(z)$	Longitudinal profile function
$\vec{F}_o$	dc force term vector
G	Power gain in dB
$\vec{h}_n$	Normalized magnetic basis vector
H_p	Component of RF magnetic field parallel to wall
H_{sm}	Beam/field coupling strength coefficient
$\vec{H}_{tn}$	Transverse magnetic field for n^{th} mode
H_z	Longitudinal magnetic field
I_k	Current coefficient for k^{th} mode

I_o	Electron beam current
I_{st}	Oscillation start current
j	Square root of (-1)
J_m	Bessel function of the first kind
$\vec{J}_t$	Transverse vector current density
k	Free space propagation constant
keV	Kilo electron-volts
k_{mn}, k_{tn}	Transverse propagation constant
k_z	Longitudinal propagation constant
$\hat{\ell}$	Unit vector tangent to cross-section area
L_{sat}	Interaction length required to reach n_{sat}
(KE)	Kinetic energy of particle
M	Number of azimuthal variations per two pi
m_o	Rest mass of electron
$\hat{n}$	Unit normal vector
N	Number of macroparticles
N_{min}	Minimum number of macroparticles
P_{in}, P_{out}	RF power in, out
P_t	Transverse momentum
$P_T\vert_z$	Total power (beam and RF) at z
$\hat{r}$, $\hat{\theta}$, $\hat{z}$	Unit vectors in cylindrical coordinates
Q_{sm}	Minimum current term
$\vec{r}$	Three-dimensional position vector
R	$k_{mn} * r$
r_L	Larmour radius of electron

R_L	$k_{mn} * r_L$
r_o	Radius to dc guiding center
R_o	$k_{mn} * r_o$
$\vec{r}_t$	Transverse position vector
$r_w(z)$	z dependent waveguide radius
R_w	$k_{mn} * r_w(z)$
s	Cyclotron harmonic number
$S(z)$	z dependent cross section
t_o	Time particles entered RF region
$TE(z)$	Total energy of a particle at z
T_{nn}, T_{kn}	Tapered wall induced current coupling coefficients
T_{nn}^*, T_{nk}^*	Tapered wall induced voltage coupling coefficients
$\vec{v}$	Total velocity of particle
V	Beam voltage
V_k	Voltage coefficient for k^{th} mode
v_{ph}	Phase velocity
v_t, (v_{t0})	Transverse velocity (initial value)
v_z, (v_{z0})	Longitudinal velocity (initial value)
x'_{mn}	n^{th} solution to $J'_m(x) = 0$ (without prime is solution to $J_m(x) = 0$)
(X_o, Y_o)	Rectangular coordinates of guiding center
Y_{nk}	Nonideal wall induced voltage coupling coefficient
z	Longitudinal position
z_{f1}	Apparent position of RF field injection
Z_{co}	Longitudinal position for classical cutoff radius
Z_n	Wave impedance of nth mode

Z_{nk}	Nonideal wall induced current coupling coefficient
Z_w	Wall impedance

α	$\Omega\tau + \Phi$
α_o	Ratio of initial transverse to longitudinal velocities
β_{ph}	v_p/c
β_t (β_{to})	v_t/c (v_{to}/c)
β_z	v_z/c
γ	Hot gamma value
γ_o	Initial gamma value
Γ	Composite phase variable
δ	Skin depth
δ_{mn}	Dirac delta function
$\vec{\nabla}$	Vector "Del" operator
Δ	Delta (change in)
ϵ	Permittivity of waveguide medium
ϵ_c	Normalized current/coupling term
η_{el}, η	Electronic efficiency
η_{sat}	Saturation efficiency
θ	Azimuthal angle of electron
θ_o	Azimuthal angle to dc guiding center
θ_T	Wall taper angle
λ	Free space RF wavelength
λ_{cyc}	Cyclotron wavelength
μ	Permeability of waveguide medium

ν	Beam density parameter
ρ	Volume current density
σ	Wall conductivity
τ	RF wave period in time or elapsed time of interaction
ϕ	RF perturbation to dc momentum phase
ψ	Solution to 2-D scalar wave equation
ω	RF field radian frequency
ω_{co}	Waveguide cutoff frequency
Ω	Relativistic cyclotron frequency
Ω_o	Nonrelativistic cyclotron frequency

$\overset{\Delta}{=}$	"Is defined as"
$Z*$	Complex conjugate of Z
$\text{Re}\{\ \}$	Real part of complex number
$\text{Im}\{\ \}$	Imaginary part of complex number
$L_{\pm}$	Scalar differential operator
$\langle \gamma \rangle$	Averaged gamma for ensemble

Note: All barred quantities, e.g., $\bar{\omega}$, are normalized to be dimension-less

- xvi -

I. INTRODUCTION AND EXPLANATION OF RESEARCH WORK

1.1 Introduction

This work is an investigation into techniques for improving the operation of the gyrotron traveling-wave amplifier (GTWA). The GTWA was conceived as a device capable of generating large amounts of radio-frequency (RF) power over a relatively broad bandwidth in the millimeter wavelength regime. This work will propose solutions to several of the identified problems that currently prevent the GTWA from achieving the anticipated results. The device has produced neither the bandwidth nor the power levels, and this research described in this report has been an attempt to address these two shortcomings.

These problems are examined and theoretical solutions are proposed for each of the problems, which are closely related. In view of the limited output of the GTWA, a new large signal theory has been developed and applied to the gyrotron interaction under conditions that model those present in the GTWA. The resulting computer code, AMINUS, has been tested extensively against published data, from experimental results, and results of other well-known researchers and institutions. Preliminary results generated by AMINUS are helpful in illustrating the saturation mechanism of the GTWA and in further validating the usefulness of this research effort.

The development of an explicit form allowing the expression of the coupling of the electron beam to the RF field has been central to this work. This term, which may be expressed equally well in either the cylindrical or the rectangular coordinate system, provides a method for

explicitly considering the impact of the electron beam on the RF field mode injected into the device. Excellent results have been achieved using the derived form of this coupling term as derived within this report.

By suitable selection of analytical approaches, the proposed solutions may be investigated numerically under a broad range of operating conditions. The method chosen for the analysis of the RF fields during the interaction allows the researcher to exert control over the electrical characteristics of the interaction cavity without being forced to approximate the impact of nonstandard waveguide configurations. The ability to examine the operation of the GTWA under such tightly controlled conditions has not previously existed to the knowledge of the author.

1.2 Problems Addressed Within This Report

The two most significant limiting factors in the operation of GTWA devices have been the occurrence of unwanted oscillations at beam currents that seriously limit the efficiency of the device, and the extremely narrow bandwidth of the gyrotron interaction. These problems have been recognized for some time,[45,46,48] but have not been addressed due, at least in part, to limitations in the available analytic approaches. In this section, the problems are discussed in some depth. The form of the proposed physical solutions discussed in Section 1.3 will lead directly to the model chosen for the RF electromagnetic fields.

The problem of unwanted oscillation is a serious limitation to the GTWA device because the onset of oscillation has been shown to be a function of the beam current level. The efficiency of a GTWA device scales as the cube root of the beam current.[17] Thus, the need for high beam current is clear, and the severity of the limitation to low currents is also clear. The oscillation problem is discussed in Section 5.2, with an emphasis on the proposed solution to the problem. Here the problem itself will be discussed in further detail.

The previous analysis of the current at which the oscillations start, I_{st}, was carried out via the use of a dimensionless form of the dispersion relation, which was simplified by dropping a term which is normally insignificant at device operating conditions.[48,17,24] The analysis of these oscillations has been carried out for three cases in the article by Lau, et al.:[48]

1. A cold electron beam with a lossless waveguide.

2. A warm beam with a lossless waveguide.

3. A cold beam with a lossy waveguide.

In each of these three cases, an approximated dispersion relation was derived. Wachtel[79] also performed an analysis of these oscillation tendencies, but from a different and less directly related perspective. These dispersion relations are found in Appendix F. The first case is the only case considered in detail by Lau et al.

The difficulty in using the dispersion relation approach lies in the assumed uniformity of the waveguide in the interaction region. The electrical properties of the waveguide are not easily adjustable for simulation with the given analytical tool. Further, the dispersion

relation approach, which is an application of kinetic theory, describes only linear behavior.

The predictions made by Lau are significant because they place a cap on the current in the electron beam for which the GTWA will operate under the convective instability. The results do show that I_{st} increases when the magnetic field is tuned to a frequency below that required for synchronism, which, as shown in Fig. 5.6 of Section 5.5, corresponds also to the magnetic tuning for which the greatest saturated efficiency is achieved in simulation runs.

Also, according to Lau, the frequency at which the oscillations set in falls below the conventional waveguide cutoff frequency by a small margin. This frequency value (normalized to cutoff) corresponds to a relatively high efficiency interaction, as shown in Fig. 5.7 of Section 5.5. This implies that significant interaction of the RF field and the electron beam is taking place at a frequency below cutoff. This is a serious problem for researchers due to the computational difficulty in dealing with below-cutoff RF propagation. It is well known[37] that the normal mode method of electromagnetic field representation fails in cases where the analysis must include the classical cutoff point due to normalization conventions.

Thus, the consideration of unwanted oscillation in GTWA devices leads directly to two problems. The first is the lack of an analytic theory for the consideration of lossy waveguide walls in which the loss is not uniformly applied over the entire waveguide wall. The second problem is the occurrence of the oscillation below the waveguide cutoff frequency.

The problem of the narrow bandwidth of the GTWA has also been considered previously,[4,7] and an experimental device was built at the Naval Research Laboratory.[6] This limitation is not an operational problem, but is an application limiting problem. The specific need in this case was for a simulation tool to allow detailed numerical studies of the interaction in cavities altered in various ways for the purpose of increasing the bandwidth. In order for a simulation code to be designed and implemented, a large signal theory capable of dealing with the interaction in the cavity was also required.

Thus, from the consideraion of the bandwidth problem, the two specific needs which were identified were the need for a large signal theory and its implementation into a useful simulation tool. These needs are in addition to, but compatible with, the needs identified in the consideration of the oscillation problem.

The identification of the third problem considered in this report arose directly from the proposed solutions to the previous problems. The consideration of this problem will point out shortcomings of previous theoretical analyses and limitations of previous simulation programs. Since understanding this problem is dependent on understanding the proposed solutions, the discussion of the problem will be included in Section 1.3 where the solutions are discussed.

The problems identified for investigation and included in this report are:

1. Unwanted oscillations.

2. Narrow bandwidth.

3. Limitations of the previously available theoretical and numerical tools.

Research objectives related to each of these three problems are proposed in the following section.

1.3 Identification of Objectives

This section presents a discussion of the proposed solutions to the problems identified in the preceding section. The identification of the solution to the device operating limitations will lead directly to the theoretical and numerical research objectives which are identified and discussed in the following section. For the mentioned problems in Section 1.2, there are four identifiable objectives, including:

1. Proposal of feasible device oriented solutions to the limitations discussed previously.

2. Construction of an analytical theory to describe the proposed solutions.

3. Construction of a computer simulation code base on No. 2.

4. Verification of the simulation code for cases studied previously.

Each of these objectives is discussed in some depth here and form the basis for one full section each in this report.

The first category of the objective consists of device oriented solutions to the present problems with GTWA devices, as discussed in Section 1.2. The effect of the solution for the oscillation problem as measured by the gain and efficiency characteristics of the GTWA should be as small as possible. The negative effect of the solution can be

minimized by two means. First, the oscillation should be damped out by some means before a large amount of the RF power is carried in the unwanted oscillation mode. This will decrease the impact on efficiency and gain by ensuring that the majority of the power given up by the beam is coupled into an RF mode which will grow and optimize the gyrotron interaction. Second, the solution should affect a very narrow frequency band, so that RF power carried in nonoscillating modes will be relatively unaffected. This calls for frequency selective loss, with a narrow loss profile as a function of frequency. It is theoretically possible to design a cavity[4] filled with a high loss dielectric with a sufficiently high Q factor that the loss profile can be forced to be infinitesimally narrow.[70] Practically, the presence of the lossy material in the cavity will mean that the cutoff frequency is not as well defined as is the case for an empty perfect waveguide. Thus, the concept of an infinitesimally narrow loss profile, centered at the unwanted oscillation frequency, is physically impossible, but the cavity would still provide a very narrow loss profile. This cavity could be coupled to the interaction waveguide in the region where the oscillation mode is beginning to have a linear gain, or in the case of a nonreflective mode of oscillation, the cavity could be continuously coupled to the interaction waveguide. The cavity could be analyzed so as to include the effects of the coupling slots in the resonant frequency calculations.[70] A second method that is feasible is the use of a lossy coating on the inner surface of the waveguide. A single layer coating can be made to have a fairly narrow loss distribution as a function of frequency.[52] The third method for oscillation control would be to simply build the

entire waveguide out of a dielectric material, such as carbon. This method has been implemented and experimental results have been published.[7] This solution is the simplest to implement, but the crudest in its effect on the operation of the device. Lau[8] published figures showing the impact of the ratio of the skin depth to the waveguide wall radius. These curves are shown in Fig. 1.1. Figure 1.2 is a plot of the skin depth versus the bandwidth of the amplification mechanism. This figure clearly demonstrates the importance of a narrow bandwidth loss mechanism, which is not the case for a cavity made of machined graphite.

Further research on the influence of the normalized skin depth on the frequency selectiveness of absorption is contained in Reference 39. The cases considered there do not relate as directly to the work at hand, but they do address the concept of magnetic materials as a waveguide coating. In any case, all published research indicates that a single thin layer of coating is preferable over a thick coating or a waveguide constructed entirely of nonconductive material.

Thus, three methods have been proposed for realizing a solution to the oscillation problem. The principle behind selecting the best of the solutions is absorption of all RF power <u>at the frequency of the unwanted oscillation</u>. The best solution seems to be the coupled cavity due to the ease in construction of a filled cavity with a very specific resonant frequency. Unfortunately, it also appears that the most desirable solution would be the most expensive to implement.

The proposed solution to the bandwidth problem was first suggested by Lau.[47] The scheme would call for a reverse injection configuration,
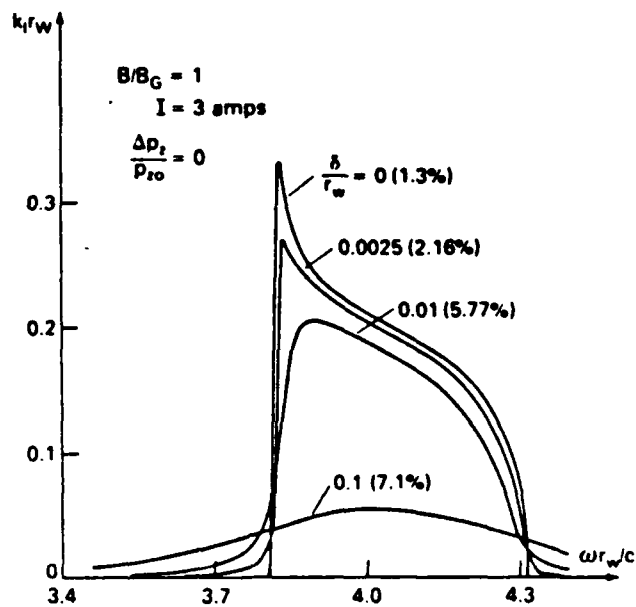
Fig. 1.1. Normalized amplification rate $k_1 r_w$ versus normalized frequency $\omega r_w/c$ at various values of wall resistivity (δ/r_w). All other parameters are fixed as indicated. The numbers shown in the parenthesis in the figure denote the bandwidths. k_1 is defined by $k_z = k_R + jk_1$. (After Reference 38, Fig. 1.)
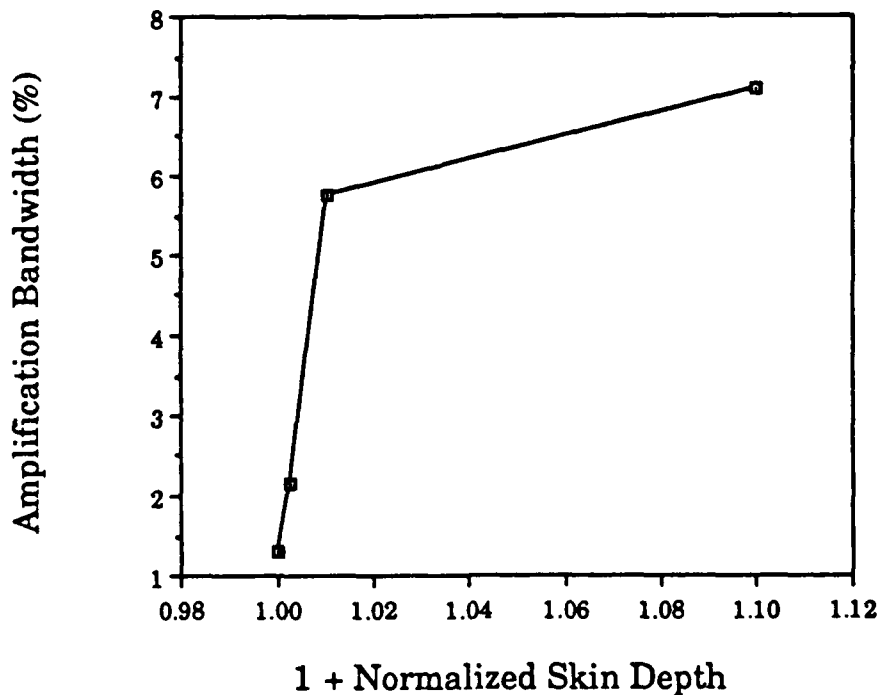
Fig. 1.2. Bandwidth of loss/amplification versus normalized skin depth, taken from Fig. 1.1.

as discussed in Section 5.2. A device based on this principle has been built[6] based on the limited analysis of Lau[*7] and Chu.[21] The problem in the design of a wideband device has been related to the injection of the RF signal. Chu has proposed a side-wall injection scheme[21] in which the input signal would be injected into a rather complicated dual waveguide system. This arrangement is shown in Fig. 1.3.
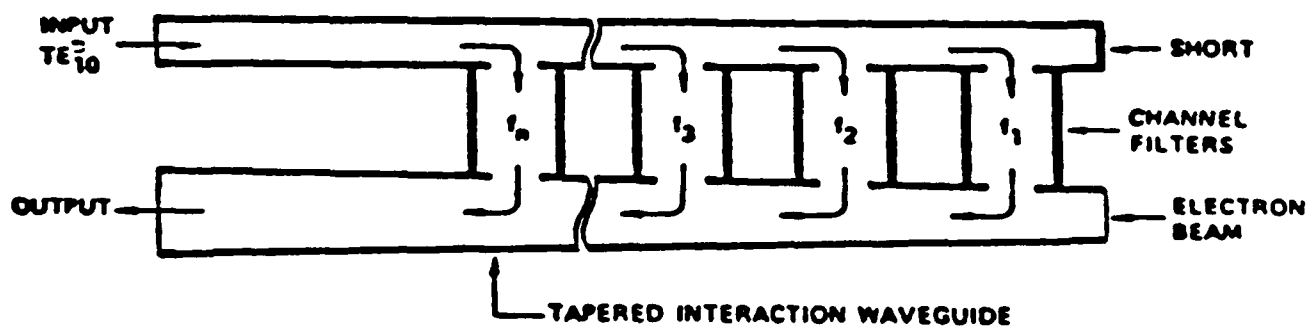
Fig. 1.3. Concept proposed by Chu, et al., for a wideband GTWA device. Each of the channel filters would be designed to provide a specific pass band. Alternate schemes for the design and construction of the filter elements were also proposed. (After Reference 21, Fig. 5.)

This arrangement was not selected due to the complicated construction required and to the likelihood of the generation of spurious competitive modes. Furthermore, it seems less likely for a constant amplification to be attained over the range of frequencies described as f_1 to f_n in the figure for this configuration than for the simpler structure proposed by Lau. The anticipated qualitative gain and bandwidth characteristics are discussed at length in Section 5. The basis of the scheme is similar to the scheme proposed by Lau, and is based on the fact that propagating RF fields reflect when they encounter a region in which they can not propagate. Lau's scheme is known as a reverse injection GTWA, and is pictured in Fig. 1.4.

The problem then is not the basic analysis, nor in the lack of potential solutions to the physical problem, but the lack of in-depth analysis that can be accomplished by the presently available analytic theories and simulation codes. Presently, it is known that a large part of the interaction between the RF field and the electron beam occurs in the region $z_{f1} < z < z_{co}$. It has not been possible previously to model this interaction, rather the simulation has begun at the classical cutoff point and proceeded through saturation. Given the amount of interaction occurring in the unsimulated area, the shortcoming of this method is apparent. There are other limitations to previous analytic methods, which will be discussed in Section 1.4.

The second category of the objective is the construction of a large signal analytic theory capable of accurately describing the interaction mechanics when the proposed solutions are included in the device. Specifically, the derived theory should be self-consistent to
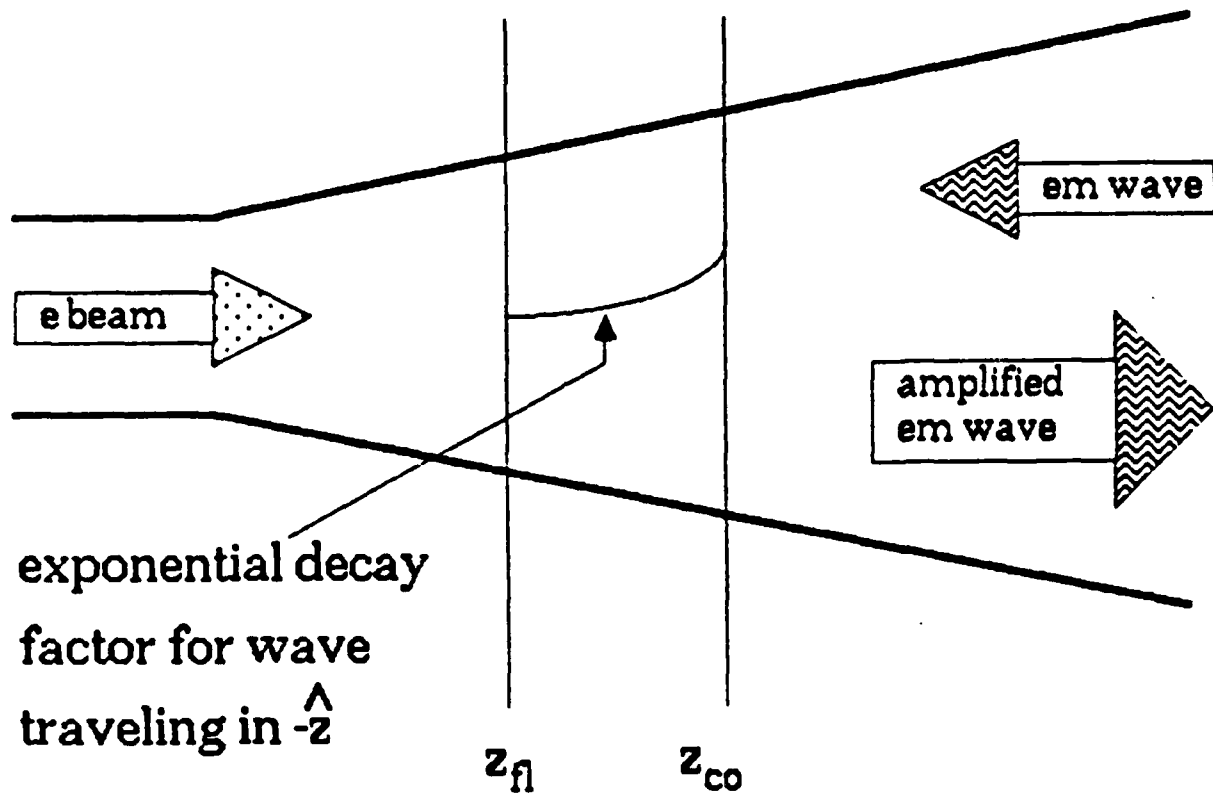
Fig. 1.4. Schematic diagram of the reverse injection GTWA. The transverse plane at z_{co} is the cutoff plane for perfect reflection. The wave will penetrate into the region $z_{fl} < z < z_{co}$, so that a wave launched at z_{fl} will have the same apparent starting point as the reflected wave.

allow calculation in the large current regime where the presence of the beam significantly alters the RF mode from its no current or low current form. The theory should be capable of dealing with frequency selective loss mechanisms in a straightforward manner. The theory should be capable of describing the influence of a tapered magnetic field and/or a tapered radius interaction region. The theory should also describe the motion of the guiding centers, if it is determined that such motion is significant to the interaction physics. The theory should also be able to describe the gyrotron interaction at an arbitrary nonfundamental cyclotron harmonic for any chosen RF mode. It is recognized that several studies have concluded that TM modes do not have the needed characteristics to allow efficient operation of a TM mode based gyro-amplifer,[27][22] thus, it is reasonable to specify that a TE theory be derived.

The third category of objectives identified and dealt with in this report is the implementation of the self-consistent large signal analytic theory into a computer code to allow simulation of GTWA devices for a large range of parameter values for a large numer of parameters. This category would require the transformation of the analytic equations to a form suitable for programming in FORTRAN. The computer code should be sufficiently general so that the researcher has control over any input parameter that would be dealt with in the design of a practical GTWA interaction region, and capable of expressing any change in the electrical characteristic as required by the proposed solutions dis-cussed in previous paragraphs. Recognizing that various approximations are available for special functions and in the derived analytic theory,

the code should be able to compare the time-optimized results with the results found without the benefit of any approximations.

The fourth and final category of the objective for this research effort involves the exercise of the computer simulation code. The first stage of usage should be the verification of accuracy of the code, internally and against other published results where available. The code should demonstrate good agreement with other accepted theoretical approaches for the cases in which the other theories may be applied. The code should then be applied to generate new results and understandings.

These four categories of results: proposed solutions, analytic theory, simulation code, and simulation results are described in Sections II, III, IV, and V, respectively. The process for reaching the objectives, and some of the decisions made in the process are described in the next section.

1.4 Process of Reaching Objectives

This section describes the processes involved in reaching the objectives discussed in Section 1.2. The specific device oriented solutions proposed in Section 1.2 are discussed further in Section 5.7. The purpose of this section will be the discussion of the development of the analytic and numerical tools required to analyze and simulate the device oriented solutions. There are four distinct processes involved:

1. Derivation of a large signal theory with, at least, the capabilities discussed in the previous section.

2. The numerical implementation of the theory derived in part (1).

3. The verification of the results of the numerical implementation.

4. The generation of early results with the derived tools.

An additional focus of this section will be the identification of various options available to the researcher for processes (1), (2), and (3). The basis for the selections made will be discussed from the perspective of the problems being considered in this report.

A self-consistent large signal theory for the GTWA must consist of at least three individual pieces, and may consist of four or more pieces. These pieces describe the RF electromagnetic field, the electron beam, and the influence of the beam on the RF fields. The influence of the RF fields on the electron beam must also be included, but that is usually accomplished with no additional labor. The possible additional piece or pieces may include the equations required to consider guiding center motion and variations in the dc magnetic field or dual RF field input sources. The guiding center motion equations have been derived for this work, in addition to the basic pieces mentioned above. Each of these three portions of a large signal theory will be described, and a discussion of the concept of "self-consistent" theories will be included in the paragraph describing the influence of the beam on the RF fields.

In the derivation of the large signal theory for the GTWA, it was deemed important to achieve the greatest possible degree of consistency between the portions of the theory describing the RF fields and the

electron beam. Practically, this implies that the method chosen to represent the RF fields in the field portion of the theory should also be used to represent the fields in the electron trajectory equations which describe mechanical motion of the electrons within the electron beam. In this particular report, the choice of the field representation scheme was dictated by the problems under consideration, which in turn dictated the form of the trajectory equations as well. It may be recalled from Section 1.3 that the required aspects of the field theory are self-consistency and the ability to simulate the influence of: frequency-selective loss mechanisms, tapered magnetic fields, tapered interaction regions, nonfundamental cyclotron harmonics, and arbitrary TE electromagnetic RF modes. Some of these requirements also will influence the selection of a particle theory as well.

In published works dealing with the analytic description of the RF fields in GTWA devices, there are two principle methods of analysis pursued by researchers. The first of these two methods is known as kinetic theory, and is based on the solution of a linearized form of the Vlasov equation, which is a collision-free form of the Boltzmann equation, which may be written as[5,42]

$$\frac{\partial f_1}{\partial t} + \vec{v} \cdot \vec{\nabla}_r f_1 + q(\vec{E}_o + \vec{v} \times \vec{B}_o) \cdot \vec{\nabla}_p f_1 = -q(\vec{E}_1 + \vec{v} \times \vec{B}_1) \cdot \vec{\nabla}_p f_o \quad (1.1)$$

where f_1 is the RF perturbed electron distribution function, $\vec{\nabla}_p$ is the Del operator for momentum space, $\vec{\nabla}_r$ is the Del operator for configuration space, and field quantities subscripted 0/1 are dc/RF components. The study of the Boltzmann equation provides the basis for a large part

of the field of plasma physics, and thus the kinetic theory is the method of choice for plasma physicists. Kinetic theory, being based on a linearized form of the equation describing the interaction mechanics, produces linear results, which implies that the fundamentally nonlinear process of saturation can not be studied by kinetic theory analysis. The end product in a kinetic theory analysis is a dispersion relation of the general form

$$D(\omega, k) = 0 \tag{1.2}$$

and the analysis is performed by locating the various plasma instabilities with their associated complex values of ω and/or k.[54] The dispersion relation used most often for this type of analysis is[19]

$$\left(\frac{\omega^2}{c^2} - k_z^2 - \frac{x_{mn}^2}{r_w^2} \right) = - \frac{4\nu}{\gamma_o r_w^2 K_{mn}}$$

$$\left[\frac{\left(\omega^2 - k_z^2 c^2 \right) \beta_{to}^2 H_{sm} \left(R_o, R_L \right)}{\left(\omega - k_z v_{zo} - s\Omega_c \right)^2} - \frac{\left(\omega - k_z v_{zo} \right) Q_{sm} \left(R_o, R_L \right)}{\left(\omega - k_z v_{zo} - s\Omega_c \right)} \right]$$

$$\tag{1.3}$$

where ν is a normalized current parameter, K_{mn} is a normalization constant, Ω_c is a relativistically corrected cyclotron frequency, k_z is the longitudinal propagation constant, x_{mn} is the nth zero of $J_m(x) = 0$ for TM modes or $J_m'(x) = 0$ for TE modes. Quantities subscripted 0 refer to initial values, and the functions H_{sm} and Q_{sm} are given as

$$H_{sm} = \left[J_{s-m}\left(R_o\right)\right]^2 \left[J_s'\left(R_L\right)\right]^2 \tag{1.4}$$

$$Q_{sm} = 2H_{sm}\left(R_o, R_L\right) + R_L\left[J_{s-m}^2\left(R_o\right)J_s'\left(R_L\right)J_s''\left(R_L\right)\right.$$

$$\left. + \frac{1}{2} J_{s-m-1}^2\left(R_o\right)J_s'\left(R_L\right)J_{s-1}'\left(R_L\right) - \frac{1}{2} J_{s-m+1}^2\left(R_o\right)J_s'\left(R_L\right)J_{s+1}'\left(R_L\right)\right] \tag{1.5}$$

where $R_o = k_{mn} r_o$, and $R_L = k_{mn} r_L$. Equation 1.3 may be simplified and written in dimensionless form as[4][8]

$$\left(\bar{\omega}^2 - \bar{k}^2 - 1\right)\left(\bar{\omega} - \bar{k}\beta_z - b\right)^2 = -\epsilon_c \tag{1.6}$$

where the normalized quantities, signified by a bar, are defined as

$$\bar{\omega} \triangleq \frac{\omega}{\omega_{co}}$$

$$\bar{k} \triangleq \frac{k_z}{k_{mn}}$$

$$\beta_z \triangleq \frac{v_{zo}}{c}$$

$$\beta_{to} \triangleq \frac{v_{to}}{c}$$

$$b \triangleq \frac{s\Omega_c}{\omega_c}$$

$$\epsilon_c \triangleq \frac{4\nu c^2 \beta_{to}^2 H_{sm}}{\gamma_o r_w^2 k_{mn}^2 \omega_{co}^2}$$

- 18 -

where ω_{co} is the waveguide cutoff frequency. This method of study suffers from limitations required in order to find analytic solutions. It is customary to find assumptions dealing with uniformity in waveguide wall radius and wall electrical characteristics, either explicitly stated or implicitly allowed in kinetic theory analyses. Kinetic theory analysis does offer several significant advantages, although they do not address the problems under consideration in this report.

The second method of field analysis is in the form of a wave equation for a longitudinal profile function, usually defined as $F(z)$. The basic equation for this type of analysis is[37]

$$\left(\nabla^2 - \mu\varepsilon \frac{\partial^2}{\partial t^2}\right)\vec{E}(\vec{r}, t) = \mu \frac{\partial}{\partial t} \vec{J}(\vec{r}, t) + \vec{\nabla} \frac{\rho}{\varepsilon} \qquad (1.7)$$

where ρ is the volume space-charge density. In this approach, the electric field is modeled as a product of a transverse vector function and a scalar function of z, which describes the longitudinal variation of the field magnitude. The left-hand side of Eq. 1.7 may be expanded into three terms, two of which describe tapered wall effects. It is customary, however, for these terms to be dropped (see, for example, References 16 and 48), the Fourier transform theorem is applied, and other approximations are made, so that the final form is[27,28,64]

$$\left(\frac{d^2}{dz^2} + k_z^2\right) F_n(z) = j\omega\mu_o \int_s \vec{J}_t(\vec{r}, \omega) \cdot \vec{e}_{tn}^*(\vec{r}, \omega) \, ds \qquad (1.8)$$

where $\vec{J}_t(\vec{r}, \omega)$ is the fundamental Fourier component of the ac current density. This method of analysis is capable of dealing with taper, but

not with nonideal waveguide walls. The result of the analysis is a second order differential equation for F(z). Another strength of this method is that it is usually employed in a self-consistent manner.

The two customary methods then are kinetic theory and a wave equation approach that leads to a second order differential equation. Neither method satisfies all of the objectives mentioned above.

The method of analysis chosen for this report is known as transmission line field analysis. Transmission line field analysis has not been applied to GTWA devices previously, and so provides a new method for analysis of gyro devices providing decided advantages for the researcher considering interaction regions with the type of special features proposed in Section 1.3. The starting point for this method of analysis is the two curl equations of Maxwell:

$$\vec{\nabla} \times \vec{E} = -j\omega\mu\vec{H} \tag{1.9}$$

$$\vec{\nabla} \times \vec{H} = j\omega\epsilon\vec{E} + \vec{J} \tag{1.10}$$

These equations are separated into longitudinal and transverse parts, and the field components are written in terms of two normalized basis sets, as shown in Eqs. 1.11 and 1.12:

$$\vec{E}_t = \sum_k V_k(z, t)\, \vec{e}_k(\vec{r}, t) \tag{1.11}$$

$$\vec{H}_t = \sum_k I_k(z, t)\, \vec{h}_k(\vec{r}, t) \tag{1.12}$$

After considerable manipulation (described in Section II), the result is in the form

$$\frac{dV}{dz} = \text{ideal waveguide term} + \text{tapered waveguide term}$$
$$+ \text{nonideal waveguide term} \qquad (1.13)$$

$$\frac{dI}{dz} = \text{ideal waveguide term} + \text{tapered waveguide term}$$
$$+ \text{nonideal wall waveguide term}$$
$$+ \text{beam} \rightarrow \text{field coupling term} \qquad (1.14)$$

where the terms labeled in Eqs. 1.13 and 1.14 are described in detail in Section 2.5, and the quantitative equivalents to Eqs. 1.13 and 1.14 are Eqs. 2.103 and 2.104.

A comparison of the various analytic approaches and the benefits of each from the perspective of the specific problems at hand is in order. The kinetic theory approach has a number of advantages over the other two approaches. Bandwidth, velocity spread, and space charge may be considered directly. The basic interaction physics are most available in the kinetic theory. The kinetic theory can not, however, adequately treat the case of a tapered, nonideal wall. For ideal waveguides (i.e., wall radius constant and no loss in the walls), Eqs. 1.13 and 1.14 may be combined into the same form of solution that results from the wave equation method of analysis described above, thus pointing out that the transmission line formulation for the fields contains all the information that may be found in the conventional application of the wave equation method. The transmission line formulation yields two

first order differential equations, which, practically speaking, are simpler to solve numerically than a single second order equation. The transmission line formulation, unlike either of the two other methods, yields specific terms that represent the impact on the RF electromagnetic fields due to tapered waveguide walls and/or electrically nonideal walls.

A final and very significant advantage of the transmission line formulation for the RF fields may be found by examining the coupling terms offered by each method of analysis. The right-hand side of Eqs. 1.6 and 1.8, and the fourth right-hand side term of Eq. 1.14 are coupling terms. They represent the impact of the electron beam on the RF fields. The coupling term in Eq. 1.6 is based on the concept of "smeared" charge, a concept which is discussed further in Section 2.6. As such, it is felt by this researcher that the terms do not represent the degree of accuracy that the forms given by Eqs. 1.8 and 1.14 do. The wave equation and transmission line methods of analysis are very closely related, since the wave equation is formed by substituting Eq. 1.10 into Eq. 1.9, and so it is not surprising that a common coupling term is shared by the two methods.

Summarizing on the selection of a method for representation and analysis of the RF electromagnetic fields, it has been found that no analytic method previously applied to GTWA devices could adequately deal with all the objectives discussed in Section 1.3. Therefore, the transmission line formulation has been adopted. The points at which the chosen formulation is superior to the alternative methods of analysis are: capacity to represent tapered interaction regions, capacity to

represent electrically nonideal waveguide walls, and a straightforward beam-field coupling term. The derivation of the transmission line formulation for the RF electromagnetic fields is found in Section II.

The second major component of the large signal theory is the method chosen to represent the electron trajectories as the beam propagates under the influence of both a dc magnetic field and an injected RF electromagnetic field. As was mentioned above, it was deemed essential that the field theory and the particle theory be as compatible as possible. Given the choice of the transmission line formulation for the RF fields, it follows that the method used to represent the RF fields in the particle theory must also be in the form of normalized basis functions with expansion coefficients that represent the longitudinal profile of the RF fields. The starting point for the particle theory is the Lorentz force equation:[24]

$$\frac{d\vec{p}}{dt} + \frac{|e|}{\gamma m_o} \vec{p} \times \vec{B}_o = -|e| \left[\vec{E} + \frac{\vec{p}}{\gamma m_o} \times \vec{B} \right] \tag{1.15}$$

The beam is modeled as in Fig. 3.2. The position of the ith electron at time t is written as

$$x_i = X_{o_i} + r_{L_i} \cos \left(\Omega_i \tau_i + \phi_i \right) \tag{1.16}$$

$$y_i = Y_{o_i} + r_{L_i} \sin \left(\Omega_i \tau_i + \phi_i \right) \tag{1.17}$$

where

$$\Omega = \frac{e}{m} \frac{B_{oz}}{\gamma_o} \qquad (1.18)$$

and Φ represents the perturbation to the dc orbit caused by the presence of the RF electromagnetic field. The chosen method of proceeding from this starting point produces a system of equations in which the dc and RF contributions to the electron trajectories are clearly defined, as are the contributions from a tapered magnetic field. This separation of terms is helpful in verifying the accuracy of the various segments of the numerical implementation of the analytic theory, as discussed in Section 4.7. The guiding center formulation is formed by considering the time derivative of Eqs. 1.16 and 1.17. The resulting equations from the particle theory and guiding center motion analysis are Eqs. 3.76, 3.77, 3.78, 3.87, 3.88, and 3.97. The fields used in Eq. 1.15 are the fields described by Eqs. 1.13 and 1.14, so that the changes in the RF fields are allowed to produce changes in the forces the fields exert on the moving electrons. The derivation of the electron trajectory formulation is found in Section III.

The large signal theory is then composed of the transmission line formulation for the RF fields and the electron and guiding center trajectory equations described above. The theory is fully self-consistent and nonlinear.

The numerical implementation of the analytic theory involves several steps. The first step is the reduction of the equations into a form specifically tailored to the chosen geometry, which is a generalized circular waveguide. This necessitates the transformation of the trajectory equations so that all the equations are functions of a single

independent variable. The beam-field coupling coefficient must also be written in a geometry specific form. Since all the equations are differential equations, a choice must be made of a numerical algorithm for use in the integration of the system of equations, which, in its final form, is of order $9N + 2$. The selection process is described in Section 4.5, and the algorithm finally selected was a custom written form of the Gill implementation of the fourth order Runge-Kutta method for solution of differential equations. The process of numerical implementation of the analytic theory is discussed in detail in Sections 4.2 through 4.6.

The verification of the numerical code was undertaken in a series of planned phases to insure that the basic structure of the code was correct. There are three distinct phases to the verification. The first phase involves testing the code for simplified cases, such as the dc electron trajectory and the no-beam RF propagation testing. The next level of verification involves checks on the internal consistency of the code. For example, the two available methods of calculating the power of the electron beam were tested and found to agree to within 0.01 percent. The final step in the verification process was performed by running the code with input data taken from published journal articles and comparing the results against those in the articles. As expected, there is very close agreement with the published results. Results from a number of authors were used, and the comparisons are found to be excellent. This verified the ability of the theory to describe the basic interaction mechanism of a GTWA. The discussion of the verification of the numerical implementation is found in Section 4.7.

With the accuracy of the code verified, the next process in reaching the objectives outlined in Section 1.3 is the use of the code to generate results, i.e., using the code to numerically simulate the gyrotron interaction in the chosen geometry under various operating conditions. The motion of the guiding center, neglected in some theories and included in others, is discussed.

The capability to calculate the guiding center motion is included in the large signal theory, as discussed above, but is implemented in the numerical code in such a way that the user may fix the guiding centers or allow them to drift by proper choice of input parameters. It was found that the guiding centers do move for certain combinations of mode and cyclotron harmonic number, while they do not for others. Thus, it was concluded that a complete theory must have the capability to allow the motion to occur, while a good numeric implementation will be run-time optimizable for cases in which the motion is zero or inconsequential. The impact of variation of the other input parameters, primarily in the form of RF frequency and magnetic field (cyclotron frequency) detuning on the saturation efficiency and power gain, is discussed and plotted. In determining the saturation efficiency, the nonlinear aspect of the code is exercised, since, as mentioned previously, saturation is a nonlinear phenomenon. The results based on numerical simulation and limitations on the use of the simulation code are presented in Section 5.5.

In summary, the objectives set forth in Section 1.3 have been attained by the steps discussed in Section 1.4. The proposed device-based solutions have been investigated and the needed analytical and

numerical tools have been developed. The needed large-signal nonlinear theory has been derived as a combination of a transmission line formulation for the RF electromagnetic fields and a single-particle electron trajectory formulation. A guiding center analysis has been derived in a fashion consistent with the two central pieces of the theory. Key contributions of the transmission line formulation include a simple, accurate beam-coupling term and separate terms describing the effects of a physically tapered interaction region and electrically nonideal waveguide walls. The analytic analysis has been supplemented by a numerical implementation, resulting in a simulation code capable of modeling the device-based solutions. The code has been tested for accuracy and found to provide excellent accuracy, internally and as compared to previously published results. The code has been used to examine the effects of various types of detuning from synchronous values, and to examine the significance of guiding center drift. These various accomplishments have satisfied the objectives set forth for this research effort. The detailed analysis of the various aspects of the research may be found in Sections II-V.

1.5 Summary of Results

This section presents a summary of the research results as found in the following sections of the report. In Section II, a transmission line formulation for the RF electromagnetic fields is derived. The analysis begins by representing the RF fields as expansions in terms of normalized basis sets and manipulation of Maxwell's curl relations for $\vec{E}$ and $\vec{H}$. The final results of this analysis, in the form of two nonlinear

first order differential equations, are found in Section 2.6, where the terms required to analyze the simultaneous existence of tapered waveguide walls and electrically nonideal (i.e., lossy) walls in the interaction region of the waveguide are derived and explained. The general form for a beam-field coupling term is also derived and presented, along with the method of representing the electron beam by a "ring" of macroparticles.

Section III presents a model for the electron beam, with the various parameters defined and explained. The chosen beam model allows the total RF effect on the trajectory to be represented in terms of a single variable. The trajectories of the particles are then derived, using the RF field forms derived in Section II in the trajectory equations. The analysis is specific to a circular geometry, but could easily be adapted to rectangular geometry. An equation is derived for the rate of change of the total or kinetic energy for each particle, which allows the trajectory calculations to be verified concerning the prediction of efficiency for a given particle.

Section IV describes the process involved in transforming the analytic theory derived in Sections II and III into a simulation program. The process of combining the equations describing the RF electromagnetic field and the electron beam into a single cohesive unit is discussed. The final geometry specific form for the beam-field coupling coefficient is derived for circular geometry. The choice of the integration algorithm is discussed, and a flow chart for the solution process involved in the simulation code is presented. The final topic

in this section deals with the process used to verify the accuracy of the simulation code.

Section V contains a full discussion of the results of this research effort. The device related solutions are discussed in detail, and the analytic tools derived in Section II and III are discussed as related to the device related solutions. The new beam-field coupling term is discussed further as well. Numerical results dealing with the minimum number of macroparticles and the effects of guiding center motion are discussed. The results of several simulation studies are presented. The variation of operation parameters from their synchronous values is studied and presented graphically.

Section VI contains conclusions and recommendations for further work. It is anticipated that a reasonable next step in the development of analytic tools for the analysis of both oscillation problems and narrow bandwidth problems will be in the form of an optimization code, with the present simulation code as the function being optimized. With this arrangement, it is anticipated that the oscillation start current will be increased by proper selection of loss and taper profiles.

1.6 Special Features of This Report

This section notes some of the special features of this report. The first special feature of note is the list of symbols beginning on page x. All symbols used in the report collected there for the reader's convenience.

The appendices are designed to stand alone. Each addresses a specific need for further explanation of some topic found in the text.

Appendix A contains several general vector relationships. These include relationships between components of the rectangular and cylindrical coordinate systems, vector product rules and expansions, and some integral rules for vector quantities.

Appendix B contains the derivation of a method for expressing a two-component dc magnetic field in terms of a taper in the field. This is utilized in Section III in the derivation of the trajectory equations for electron motion in a tapered dc magnetic field.

Appendix C contains a detailed explanation of the use of Graf's addition theorem for Bessel functions, which is often used and seldom explained. The specific relationships between the angles involved in the theorem and those used in the trajectory expressions are shown. The application of Graf's theorem is followed in detail for one case, and results for the various cases used in the report are listed in the Appendix as well.

Appendix D contains a derivation of an expression for the ensemble efficiency. This expression produces an efficiency value based on the hot γ values, thus providing a method of comparison against the differential equation also predicting the value of the energy for each electron.

Appendix E contains the derivation of a key expression for the transverse velocity. In the chosen form for the trajectory equations, all transverse quantities are expressed in terms of a magnitude and phase. The velocity vector components, v_r and v_θ, are written in terms of a transverse velocity, v_t, and a phase angle, α.

Appendix F contains three dispersion relations derived in References 48 and 50. They describe the interaction of RF fields and particles in three different physical configurations, all of which may be represented and simulated by the theory derived within the report.

II. TRANSMISSION LINE FORMULATION FOR THE RF FIELDS

2.1 Introduction

The transmission line type analysis for the electromagnetic fields in a tapered nonideal wall waveguide is derived in this chapter. The analysis that follows is exact; there are no approximations involved in the derivation of the transmission line equations. The fields are expanded in terms of a complete set of normalized basis functions that are built from solutions to the scalar wave equation. The expansion coefficients used with the basis functions are closely related to the longitudinal profile functions derived in other analysis techniques. In the conventional transmission line analysis, these coefficients are given the names "voltage" and "current." Thus, in the terminology of transmission line theory, a voltage and current may be identified for each RF electromagnetic mode. It will be found that the expansion and normalizations used in the analysis are such that the equations may be integrated through the cutoff region of a mode, a process not possible in normal mode theory.

Tapers may be characterized as azimuthally symmetric or nonsymmetric. The equations derived to deal with the effects of tapered walls are in the form of line integrals around the contour enclosing a cross section, and thus can accomodate nonsymmetric wall tapers. The actual integrals are those defined by Solymar, and are unchanged by the presence of two types of nonuniformity in the waveguide.[71] The equations derived to deal with the presence of nonideal walls in the absence of

taper must be modified, and this modification is presented. The modified equations reduce to Reiter's work for a zero taper angle.[63]

In order for a self-consistent theory to be derived, it is necessary that the magnitude of the electromagnetic field components be dependent on the current and charge densities in the waveguide. The beam-coupling term derived in detail in Section 2.6 expresses this field dependence, using the electron beam as the source of the current and charge. Modeling of various beam configurations is possible by proper selection of phase space distribution functions. Space-charge forces are neglected in the present work, as is the case in most major gyrotron analyses.

Section 2.2 describes the geometry of a tapered general cylindrical waveguide. Section 2.3 presents a definition of the normalized basis functions used to expand a general RF electromagnetic field. The transmission line analogy appears when the expansion coefficients for the basis functions are named. The longitudinal components of the fields are determined in terms of the basis functions and expansion coefficients. Section 2.4 expands the expressions for the transverse electric and magnetic fields given in Section 2.3 by the use of Maxwell's curl relations. A general form of the transmission line equations is derived, with terms present that may be used to represent taper, nonideal walls, and the electron beam. The general equations are reduced to address specific cases in Section 2.5. The final case considered yields equations capable of considering waveguides that are nonuniform in cross section and in the material used to construct the waveguide. The beam-field coupling term is analyzed in Section 2.6. A

comparison of the theory chosen for the present work to the more common theory is presented, and it is shown that the numerical implementation of the two theories actually forces them to be more similar than they appear. The concept of "rings" of electrons is discussed briefly.

2.2 Waveguide Geometry

The geometry of a general tapered cylindrical waveguide will be presented in this section. A circular cylindrical coordinate system consisting of unit vectors, $\hat{r}$, $\hat{\theta}$, and $\hat{z}$ will be augmented by special unit vectors arising from the geometry itself. Figure 2.1 illustrates the basic waveguide geometry used throughout this paper.

Note that the tapered waveguide section depicted has a linear taper, which is characterized by a constant value of θ_T over a length, dz, of the waveguide. This is not a necessary requirement; rather, the taper may be of an arbitrary nature, including the case of an azimuthally asymmetric taper profile, a practical example of which would be a rectangular waveguide tapered in a single transverse dimension. The unit vector $\hat{n}$ is defined to be normal to the boundary of $S(z)$. The unit vector $\hat{\ell}$ is defined as tangent to $S(z)$ at the waveguide boundary. The relationship of $\hat{n}$ and $\hat{\ell}$ to the circular cylindrical unit vectors $\hat{r}$ and $\hat{\theta}$ may be seen by considering Fig. 2.1. For all values of θ_T, $\hat{\ell} = \hat{\theta}$, and the $\hat{z}$ vectors are the same as well. For $\theta_T = 0$, $\hat{n} = \hat{r}$, but for any nonzero value of θ_T, a correction factor must be added to terms involving $\hat{n}$. This term will be derived in Section 2.5.
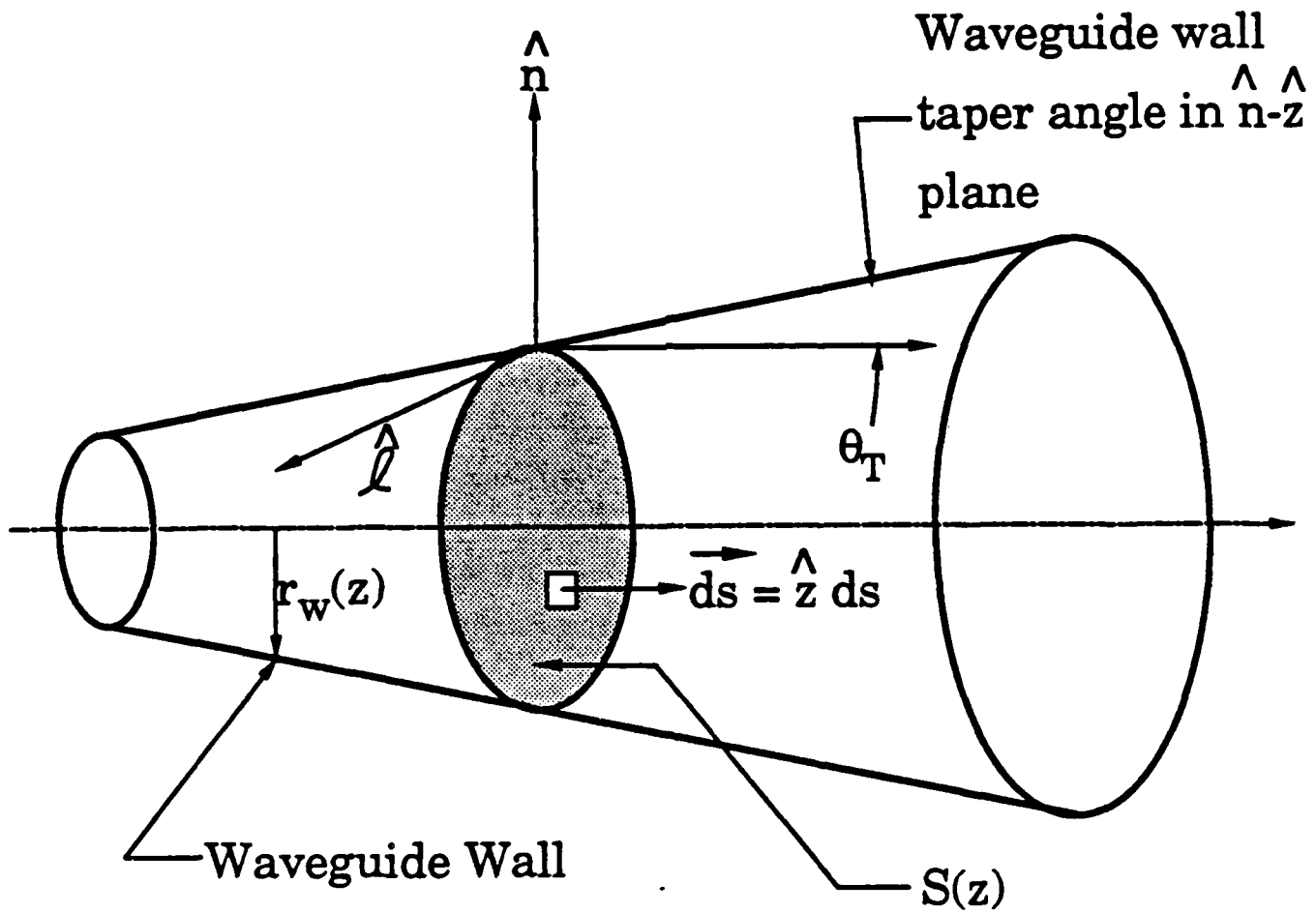
Fig. 2.1. General cylindrical tapered waveguide geometry used in field equation model and derivation. Although drawn as a circular cylindrical waveguide, the formulation is applicable to rectangular waveguides as well. (After Reference 4.)

If a rectangular system were under consideration instead of the circular geometry relationships betwen $\hat{x}$ and $\hat{y}$ in the rectangular system, $\hat{n}$ and $\hat{\ell}$ would be. straightforward. For waveguide faces lying in the $\hat{y}$ - $\hat{z}$ plane, $\hat{n}$ and $\hat{x}$ would share a relationship similar to that between $\hat{r}$ and $\hat{n}$ in the cylindrical system, and $\hat{y}$ and $\hat{\ell}$ would share a relationship similar to that between $\hat{\theta}$ and $\hat{\ell}$ in the cylindrical system. Similar analogies may be drawn for faces lying the in the $\hat{x}$ - $\hat{z}$ plane.

For a reflective mode amplifier, the electron beam would travel in the +z direction. The incident electromagnetic radiation would travel in the -z direction, reflect within the interaction region, and be amplified as it traveled in the +z direction. The field equations to be derived in this section will calculate the change in the electromagnetic field as it travels in the +z direction. This configuration is shown in Fig. 1.4, and discussed further in Section V.

2.3 Definition of Normalized Basis Functions

The normalized basis functions are derived in this section. The starting point for the derivation is the two-dimensional scalar differential equation known as the wave equation. The type of solution desired, determined by the waveguide and type of mode under consideration, determines the boundary conditions which must be enforced in the solution of the differential equation. The geometry of the waveguide in which the electromagnetic fields propagate determines the coordinate system in which the differential operators are expanded, and thus the

actual mathematical functions composing the solution. The treatment following closely follows Reference 4.

The derived normalized basis functions are then used to represent the transverse electromagnetic fields in a transmission line formulation. The formulation represents the transverse electric field and the transverse magnetic field of each mode as the product of an expansion coefficient and a normalized basis function. The total transverse electric and total transverse magnetic fields are then represented as the summation over all modes present. The relationship of the expansion coefficients used herein to transmission line theory and to other current field representation schemes is presented.

The two-dimensional transverse wave equation is

$$\left(\nabla_t^2 + k_{mn}^2\right)\psi_{mn} = 0 \qquad (2.1)$$

where ψ_{mn} is a scalar function with a doubly infinite set of coefficients m and n. k_{mn} is the transverse cutoff constant, and is the eigenvalue associated with ψ_{mn} and a cross section S(z). Because S(z) is a function of z, both ψ_{mn} and k_{mn} are implicit functions of z as well. Variations of S with z will necessarily produce changes in both ψ_{mn} and k_{mn}.

The differential operator ∇_t^2 is defined as the dot product

$$\nabla_t^2 \phi = \vec{\nabla}_t \cdot \left(\vec{\nabla}_t \phi\right) \qquad (2.2)$$

where $\vec{\nabla}_t$ is a part of the operator $\vec{\nabla}$ given by

$$\vec{\nabla}\phi = (\vec{\nabla}_t + \vec{\nabla}_z)\phi \qquad (2.3)$$

and ϕ is a scalar function. Expanding Eq. 2.2 in circular cylindrical coordinates yields

$$\vec{\nabla}\phi = \frac{\partial\phi}{\partial r}\,\hat{r} + \frac{1}{r}\,\frac{\partial\phi}{\partial\theta}\,\hat{\theta} + \frac{\partial\phi}{\partial z}\,\hat{z} \qquad (2.4)$$

The transverse part may be identified as the first two right-hand side terms, so that

$$\vec{\nabla}_t\phi = \left[\frac{\partial\phi}{\partial r}\,\hat{r} + \frac{1}{r}\,\frac{\partial\phi}{\partial\theta}\,\hat{\theta}\right] \qquad (2.5)$$

Substituting Eq. 2.5 into Eq. 2.2, and recalling

$$\frac{\partial\hat{r}}{\partial\theta} = \hat{r}$$

and

$$\frac{\partial\hat{\theta}}{\partial\theta} = -\hat{r}$$

yields

$$\nabla_t^2\phi = \frac{1}{r}\,\frac{\partial}{\partial r}\left(r\,\frac{\partial\phi}{\partial r}\right) + \frac{1}{r^2}\,\frac{\partial^2\phi}{\partial\theta^2} \qquad (2.6)$$

For transverse electric (TE) modes (characterized by $E_z = 0$), the boundary condition is

$$\left.\frac{\partial \psi}{\partial n}\right|_{wall} = 0 \qquad (2.7)$$

and for transverse magnetic (TM) modes (characterized by $H_z = 0$), the boundary condition is

$$\psi\big|_{wall} = 0 \qquad (2.8)$$

The work in this paper deals primarily with a TE right-hand circularly polarized mode. This mode type and Eq. 2.7 yield the following solutions for ψ_{mn},

$$\psi_{mn} = C_{mn} J_m\left(k_{mn} r\right) e^{-jm\theta} \qquad (2.9)$$

where

$$k_{mn} = \frac{x'_{mn}}{r_w(z)} \qquad (2.10)$$

and x'_{mn} is the nth zero of $J'_m(x) = 0$. $r_w(z)$ is the z dependent wall radius, which again shows the implicit dependence of ψ on z. C_{mn} is a normalization constant which will be evaluated below.

The normalized wave functions, $\vec{e}_n(\vec{r})$ and $\vec{h}_n(\vec{r})$, for TE modes are defined[2,16,23]

$$\vec{e}_n(\vec{r}_t) = \vec{e}_n(r,\theta) = -\vec{\nabla}_t \psi_n \times \hat{z} = \vec{h}_n \times \hat{z} \qquad (2.11a)$$

$$\vec{h}_n(\vec{r}_t) = \vec{h}_n(r,\theta) = -\vec{\nabla}_t \psi_n = -\vec{e}_n \times \hat{z} \qquad (2.11b)$$

where the double index, mn, has been reduced to a single index, n, with the doubly infinite sum being understood. With this convention, a particular $\vec{e}_n$ and $\vec{h}_n$ would be associated with a single ψ_{mn}, and a transverse propagation constant written with the form in Eq. 2.10 may be written as k_{tn}.

The normalization chosen has special properties that will be explained below. Normalization may be forced in terms of ψ_{mn}, $\hat{e}_n$, or $\hat{h}_n$. Normalization is achieved by integration of one of these functions over transverse plane S(z), and evaluation of C_{mn} to satisfy

$$\int_{S(z)} \psi_m \psi_n^* \, ds = k_{tn}^{-2} \delta_{mn} \qquad (2.12)$$

or

$$\int_{S(z)} \vec{e}_n \cdot \vec{e}_m^* \, ds = \int_{S(z)} \vec{h}_n \cdot \vec{h}_n^* \, ds = \delta_{mn} \qquad (2.13)$$

where $ds = dr \, r \, d\theta$ in circular cylindrical coordinates, and δ_{mn} is the Dirac delta function defined by

$$\delta_{mn} = \begin{cases} 1 & m = n \\ 0 & m \neq n \end{cases} \qquad (2.14)$$

Substitution of Eq. 2.9 into Eq. 2.12, integration, and algebra yield the following convenient general form for C_{mn}[61,24]

$$C_{mn} = \left\{ \pi \left[p_{mn}^2 J_m'^2\left(p_{mn}\right) - \left(p_{mn}^2 - m^2\right) J_m^2\left(p_{mn}\right) \right] \right\}^{-1/2} \qquad (2.15)$$

where $p_{mn} = x_{mn}'\left(x_{mn}\right)$ for a TE (TM) mode, in which case the term involving $J_m'\left(J_m\right)$ is zero.

The waveguide boundary values expressed in terms of ψ in Eqs. 2.7 and 2.8 may be rewritten in terms of $\hat{e}_n$ and $\hat{h}_n$ as[*]

$$\vec{e}_n \cdot \hat{\ell}\big|_{wall} = \vec{h}_n \cdot \hat{n}\big|_{wall} = 0 \qquad (2.16)$$

and (for TE modes only)

$$\vec{e}_n \cdot \hat{n}\big|_{wall} = \vec{h}_n \cdot \hat{\ell}\big|_{wall} = -\frac{\partial \psi_n}{\partial \ell} \qquad (2.17)$$

These may be explicitly evaluated and verified by use of Eq. 2.11. Equations 2.16 and 2.17 contain exactly the same information as Eqs. 2.7 expressed in terms of normalized basis functions and the tapered waveguide coordinate system shown in Fig. 2.1

With these definitions, the transverse components of the electric and magnetic fields may now be written in the form presented in Section I. The complex phasor forms of these field components are

$$\vec{E}_t(\vec{r}) = \sum_k V_k(z, t) \, \vec{e}_k(r,\theta) \qquad (2.18a)$$

$$\vec{H}_t(\vec{r}) = \sum_k I_k(z, t) \, \vec{h}_k(r,\theta) \qquad (2.18b)$$

V and I, in an analogy to conventional transmission line analysis, may be called the voltage and current coefficients, respectively. Common present practice in the development of equations describing the propagation of electromagnetic fields propagating in a waveguide is the definition of a longitudinal profile function F(z), which is normalized in various ways.[12,24,27,28,31,56,58] There are certain advantages to each approach, although V and I serve essentially the same purpose as F(z). A distinct advantage of the transmission line formulation used herein is found in the method of evaluating the time average RF power in a particular mode.

Given the normalizations in Eqs. 2.13 and 2.17 may, in principle, be solved for the expansion coefficients by evaluation of

$$V_k = \int_S \vec{E}_t(\vec{r}) \cdot \vec{e}_k^*(\vec{r}_t) \, ds \qquad (2.19a)$$

$$I_k = \int_S \vec{H}_t(\vec{r}) \cdot \vec{h}_k^*(\vec{r}_t) \, ds \qquad (2.19b)$$

In practice, this usually is not useful, since V and I are the dependent variables in the transmission line formulation, and $\vec{E}_t$ and $\vec{H}_t$ are defined in terms of V and I.

The real time forms of the transverse fields are completed by choosing a time dependence form, multiplying, and taking the real part,

$$\vec{E}_t(\vec{r}, t) = \text{Re}\left\{ \sum V_k \vec{e}_k \exp(j\omega t) \right\} \qquad (2.20a)$$

$$\vec{H}_t(\vec{r}, t) = \text{Re}\left\{ \sum I_k \vec{h}_k \exp(j\omega t) \right\} \qquad (2.20b)$$

where ω is the RF radian frequency.

The z component of the RF magnetic field, B_z, is found by considering two equations. The first of these is Maxwell's curl equation for the time harmonic $\vec{E}$, given by[37]

$$-j\omega\mu\vec{H} = \vec{\nabla} \times \vec{E} \qquad (2.21)$$

Separating the full curl relation into its longitudinal and transverse parts, we substitute Eq. 2.18 into the longitudinal part to yield

$$-j\omega\mu H_z\hat{z} = \vec{\nabla}_t \times \left(\sum_n V_n \vec{e}_n \right) \qquad (2.22)$$

Using Eq. 2.11a to rewrite the normalized electric field function, and expansion of the result yields

$$-j\omega\mu H_z = \sum_n V_n \nabla_t^2 \psi_n \qquad (2.23)$$

The scalar wave equation, Eq. 2.1, is rearranged to yield

$$\nabla_t^2 \psi_n = -k_{tn}^2 \psi_n \qquad (2.24)$$

which is substituted into Eq. 2.22 to yield

$$H_z = \frac{1}{j\omega\mu} \sum_n V_n k_{tn}^2 \psi_n \qquad (2.25)$$

2.4. Derivation of General Transmission Line Formulation for Electromagnetic Fields

In this section, the expressions describing the changes in V_n and I_n as the wave propagates down the waveguide are derived. The derivation closely follows the work of Baird[4] and Johnson.[37] The equations derived are coupled nonlinear first-order differential equations. The equations of the transmission line formulation are fully capable of dealing with the effects of a general nonideal waveguide, and are coupled to the electron beam by the inclusion of a current source term arising from the curl equation for the magnetic field. The form of the equations also allows consideration of an electromagnetic field composed of more than one mode.

The transmission line equations are derived from Maxwell's curl equations for time-harmonic electric and magnetic fields.[37]

$$\vec{\nabla} \times \vec{E} = -j\omega\mu\vec{H} \qquad (2.26a)$$

$$\vec{\nabla} \times \vec{H} = j\omega\epsilon\vec{E} + \vec{J} \qquad (2.26b)$$

These are separated into longitudinal and transverse parts using Eq. 2.3.

$$\vec{\nabla}_t \times \vec{E}_t = -j\omega\mu\vec{H}_z \tag{2.27}$$

$$\vec{\nabla}_t \times \vec{H}_t = j\omega\epsilon\vec{E}_z + \vec{J}_z \tag{2.28}$$

$$\vec{\nabla}_t \times \vec{E}_z + \vec{\nabla}_z \times \vec{E}_t = -j\omega\mu\vec{H}_t \tag{2.29}$$

$$\vec{\nabla}_t \times \vec{H}_z + \vec{\nabla}_z \times \vec{H}_t = j\omega\epsilon\vec{E}_t + \vec{J}_t \tag{2.30}$$

The transmission line formulation comes from Eqs. 2.29 and 2.30. Comparison of Eq. 2.3 and Eq. 2.4 shows that

$$\vec{\nabla}_z \phi = \frac{\partial\phi}{\partial z}\hat{z} \tag{2.31}$$

Using Eq. 2.31 in Eqs. 2.29 and 2.30 and rearranging yields

$$\hat{z} \times \frac{\partial\vec{E}_t}{\partial z} = -j\omega\mu\vec{H}_t - \vec{\nabla}_t E_z \times \hat{z} \tag{2.32}$$

$$\hat{z} \times \frac{\partial\vec{H}_t}{\partial z} = j\omega\epsilon\vec{E}_t - \vec{\nabla}_t H_z \times \hat{z} + \vec{J}_t \tag{2.33}$$

Premultiplication by $\hat{z}$ and expansion of the resulting triple cross products according to Eq. A.1 yields

$$-\frac{\partial\vec{E}_t}{\partial z} = j\omega\mu(\vec{H}_t \times \hat{z}) - \vec{\nabla}_t E_z \tag{2.34}$$

$$-\frac{\partial\vec{H}_t}{\partial z} = j\omega\epsilon(\hat{z} \times \vec{E}_t) - \vec{\nabla}_t H_z + \hat{z} \times \vec{J}_t \tag{2.35}$$

- 45 -

Dot multiplication of Eq. 2.34 by $\vec{e}_n^*$, and integration over $S(z)$ yields

$$-\int_{S(z)} \overset{(a)}{\frac{\partial \vec{E}_t}{\partial z} \cdot \vec{e}_n^* \, ds} = j\omega\mu \int_{S(z)} \overset{(b)}{(\vec{H}_t \times \hat{z}) \cdot \vec{e}_n^* \, ds} - \int_{S(z)} \overset{(c)}{\vec{\nabla}_t E_z \cdot \vec{e}_n^* \, ds}$$

(2.36)

Dot multiplication of Eq. 2.35 by h_n^*, and integration over $S(z)$ yields

$$- \int \overset{(a)}{\frac{\partial \vec{H}_t}{\partial z} \cdot \vec{h}_n^* \, ds} = j\omega\varepsilon \int_{S(z)} \overset{(b)}{(\hat{z} \times \vec{H}_t) \cdot \vec{h}_n^* \, ds} - \int_{S(z)} \overset{(c)}{\vec{\nabla}_t H_z \cdot \vec{h}_n^* \, ds}$$

$$+ \int_{S(z)} \overset{(d)}{(\hat{z} \times \vec{J}_t) \cdot \vec{h}_n^* \, ds}$$

(2.37)

Each term in Eqs. 2.36 and 2.37 will be considered in detail in the following analysis.

Terms (a) of Eqs. 2.36 and 2.37 are in the form of term (b) of Eq. A.4 (Leibnetz rule for the z derivative of the integral of z dependent variables over z dependent limits). Writing the equivalent terms (a), (c), and (d) of Eq. A.4 yields for term (a) of Eq. 2.36.

$$\int_{S(z)} \overset{(a)}{- \frac{\partial \vec{E}_t}{\partial z} \cdot \vec{e}_n^* \, ds} = - \frac{d}{dz} \int_{S(z)} \overset{(b)}{\vec{E}_t \cdot \vec{e}_n^* \, ds} + \int_{S(z)} \overset{(c)}{\vec{E}_t \cdot \frac{\partial \vec{e}_n^*}{\partial z} \, ds}$$

$$+ \oint_{\ell} \overset{(d)}{\tan \theta_t \, \vec{E}_t \cdot \vec{e}_n^* \, d\ell}$$

(2.38)

The same process applied to term (a) of Eq. 2.37 yields

$$- \int_{S(z)} \frac{\partial \vec{H}_t}{\partial z} \cdot \vec{h}_n^* \, ds = - \frac{d}{dz} \int_{S(z)} \vec{H}_t \cdot \vec{h}_n^* \, ds + \int_{S(z)} \vec{H}_t \cdot \frac{\partial \vec{h}_n^*}{\partial z} \, ds$$

$$+ \oint_{\ell} \tan \theta_T \vec{H}_t \cdot \vec{h}_n^* \, d\ell \qquad (2.39)$$

Terms (b) of Eqs. 2.38 and 2.39 may be rewritten (using Eq. 2.17) as

$$- \frac{d}{dz} \int_{S(z)} \vec{E}_t \cdot \vec{e}_n^* \, ds = - \frac{dV_n}{dz} \qquad (2.40)$$

$$- \frac{d}{dz} \int_{S(z)} \vec{H}_t \cdot \vec{h}_n^* \, ds = - \frac{dI_n}{dz} \qquad (2.41)$$

Term (b) of Eqs. 2.36 and 2.37 may be rewritten (using Eqs. A.2, 2.11, and 2.17) as

$$j\omega\mu \int_{S(z)} (\vec{H}_t \times \hat{z}) \cdot \vec{e}_n^* \, ds = j\omega\mu \int_{S(z)} \vec{H}_t \cdot \hat{z} \times \vec{e}_n^* \, ds$$

$$= j\omega\mu \int_{S(z)} \vec{H}_t \cdot \vec{h}_n^* \, ds$$

$$= j\omega\mu I_n \qquad (2.42)$$

and

$$j\omega\epsilon \int_{S(z)} (\hat{z} \times \vec{E}_t) \cdot \vec{h}_n^* \, ds = -j\omega\epsilon \int_{S(z)} \vec{E}_t \times \hat{z} \cdot \vec{h}_n^* \, ds$$

$$= j\omega\epsilon \int_{S(z)} \vec{E}_t \cdot \vec{e}_n^* \, ds$$

$$= j\omega\epsilon V_n \qquad\qquad (2.43)$$

The first temptation upon consideration of term (c) of Eq. 2.36 is to drop the term because TE modes are being considered, implying E_z is equal to zero. This would indeed be the case for an ideal waveguide. However, for nonideal waveguides, this term is not zero in general, and will be shown to provide for perturbations in the electromagnetic fields due to resistive walls (i.e., walls with non-infinite conductivity values).

The significance of this term may be seen by considering the concept of skin depth. The skin depth, δ, is derived as the depth of penetration by a normally incident plane wave at which the magnitude is $1/|e|$ times the incident magnitude.[37,41] Since all real conductors have conductivity, σ, less than infinity, the fields penetrate into the conductor a short distance. The boundary conditions cited in Eqs. 2.7 and 2.8 are an approximation based on an infinite conductivity. The relationships expressing the exact field forms are quite complicated, and cannot in general be solved in closed form. Lee, Lee, and Chuang[52] have published a numerical technique for calculating the field distribution of RF modes in waveguides coated with dielectric and magnetic materials. Study of their results shows that they are in agreement with Konopinski[41] and Johnson[37] in stating that, at microwave frequencies,

the skin effect due to metallic conductors is minimal but nonzero. For RF modes operating near cutoff, the approximation of the waveguide fields by a plane wave is a good one, as revealed by the bouncing wave picture of wave propagation.[29] As the operating frequency departs from cutoff, the approximation decreases in accuracy, but still adequately represents the loss of power. The power loss may be shown to be proportionate to the magnitude of $|B_z|^2$,[41] which implies that the z component of the RF magnetic field should be carried by the trajectory equations in order to correctly represent the loss to resistive walls.

One of the strengths of the transmission line formulation is in its ability to represent complex waveguides by an expansion of cold ideal waveguide basis functions. This is especially advantageous for microwave tube analysis because practical conductivity values produce very minor changes in the transverse mode pattern; the principle impact of a resistive wall being an energy or amplitude effect as opposed to a mode or distribution pattern effect for the lower order modes used in most devices.[49] The term under consideration represents a perturbation from ideal waveguide conditions due to resistive walls.

As mentioned in Section I, an important application goal for the model presented in this work is the consideration of frequency selective loss configurations and their potential for increasing the oscillation start current in gyrotron traveling-wave amplifiers. Given this objective, the term under consideration is especially significant in this analysis.

This term may be expanded by use of Eqs. 2.11, A.2, and A.11,

$$- \int_{S(z)} \vec{\nabla}_t E_z \cdot \vec{e}_n^* \, ds = - \int_{S(z)} \vec{\nabla}_t E_z \cdot \left(-\vec{\nabla}_t \psi_n^* \times \hat{z} \right) ds$$

$$= \int_S \vec{\nabla}_t E_z \times \vec{\nabla}_t \psi_n^* \cdot \vec{ds}$$

$$= \oint_\ell E_z \vec{\nabla}_t \psi_n^* \cdot \hat{\ell} \, d\ell$$

$$= - \oint_\ell E_z \vec{h}_n^* \cdot \hat{\ell} \, d\ell \qquad (2.44)$$

The integral in Eq. 2.44 is a line integral of $d\ell$, where ℓ is the contour surrounding $S(z)$ (see Fig. 2.2), thus the radial variables are evaluated at the wall radius $r_w(z)$. Under these conditions, Eqs. 2.17 and 2.18 allow this integral to be rewritten as

$$- \int_{S(z)} \vec{\nabla}_t E_z \cdot \vec{e}_n^* \, ds = \oint_\ell E_z \frac{\partial \psi_n^*}{d\ell} \, d\ell$$

$$= - \oint_\ell E_z \left(\vec{e}_n^* \cdot \hat{n} \right) d\ell \qquad (2.45)$$

Term (c) of Eq. 2.37 may be evaluated by replacing $\vec{h}_n^*$ using Eqs. 2.11, and using Green's theorem (Eq. A.6) to expand the result,

$$- \int_{S(z)} \vec{\nabla}_t H_z \cdot \vec{h}_n^* \, ds = - \int_{S(z)} \vec{\nabla}_t H_z \cdot \left(-\vec{\nabla}_t \psi_n^* \right) ds$$

$$= \oint_\ell H_z \frac{\partial \psi_n^*}{\partial n} \, d\ell - \int_{S(z)} H_z \nabla_t^2 \psi_n^* \, ds \qquad (2.46)$$

- 50 -

The first right-hand side term of Eq. 2.46 may be shown to equal zero by use of Eq. 2.17. The second right-hand side term may be rewritten (using Eqs. 2.1, 2.27, and A.2) as

(a)

$$-\int_{S(z)} H_z \nabla_t^2 \psi_n^* \, ds = -\frac{k_{tn}^2}{j\omega\mu} \int_{S(z)} \left(\hat{z} \cdot \vec{\nabla}_t \times \vec{E}_t\right) \psi_n^* \, ds$$

(b) (c)

$$= -\frac{k_{tn}^2}{j\omega\mu} \int_{S(z)} \left(\vec{\nabla}_t \times \psi_n^* \vec{E}_t\right) \cdot \vec{ds} + \frac{k_{tn}^2}{j\omega\mu} \int_{S(z)} \vec{\nabla}_t \psi_n^I \times \vec{E}_t \cdot \vec{ds}$$

(2.47)

Term (b) of Eq. 2.47 may be rewritten (using Stoke's theorem, Eq. A.8) as

$$-\frac{k_{tn}^2}{j\omega\mu} \int_{S(z)} \vec{\nabla}_t \times \psi_n^* \vec{E}_t \cdot ds = -\frac{k_{tn}^2}{j\omega\mu} \oint_{\ell} \psi_n^* \vec{E}_t \cdot \vec{d\ell}$$ (2.48)

Like the analysis of term (b) of Eq. 2.36, comparison of this results with boundary values (Eq. 2.16) could also tempt one to drop this term. Eq. 2.48 is zero for ideal waveguide walls, but is, in general, nonzero for nonideal waveguide walls for the same reasons as stated for term (b) of Eq. 2.36. Consideration of Fig. 2.1 shows that Eq. 2.48 yields a term proportional to E_θ. E_θ is very important in the gyrotron interaction for two reasons. E_θ produces the dominant effect on the electron trajectories, especially for electrons with axis-encircling trajectories, thus any perturbation of E_θ must be considered.[10] Also, the energy stored in the RF field has been shown to be

proportional to E_θ, so that any effect on E_θ is an effect on the primary energy storing component of the RF electromagnetic field.[17]

Term (c) of Eq. 2.47 may be rewritten (using Eqs. 2.11, A.2, 2.18, and 2.19) as

$$\frac{k_{tn}^2}{j\omega\mu} \int_{S(z)} \vec{\nabla}_t \psi_n^* \times \vec{E}_t \cdot \vec{ds} = \frac{k_{tn}^2}{j\omega\mu} \int_{S(z)} \vec{\nabla}_t \psi_n^* \times \vec{E}_t \cdot \hat{z} \, ds$$

$$= \frac{k_{tn}^2}{j\omega\mu} \int_{S(z)} \hat{z} \times \vec{\nabla}_t \psi_n^* \cdot \vec{E}_t \, ds$$

$$= \frac{k_{tn}^2}{j\omega\mu} \int_{S(z)} \vec{e}_n^* \cdot \vec{E}_t \, ds$$

$$= \frac{k_{tn}^2}{j\omega\mu} V_n \qquad (2.49)$$

Thus, term (c) of Eq. 2.37 may be replaced by Eqs. 2.48 and 2.49.

Term (d) of Eq. 2.37 may be rewritten (using Fig. 1 and Eqs. A.2 and 2.11) as

$$\int_{S(z)} \hat{z} \times \vec{J}_t \cdot \vec{h}_n^* \, ds = \int_{S(z)} \vec{h}_n^* \times \hat{z} \cdot \vec{J}_t \, ds$$

$$= \int_{S(z)} \vec{J}_t \cdot \vec{e}_n^* \, ds \qquad (2.50)$$

This term represents the presence of a source producing a vector current density $\vec{J}_t$ in S(z). For gyrotrons (and other microwave tubes as well), this current source is the electron beam, and Eq. 2.50 represents the coupling of the electron beam to the RF electromagnetic fields. It is this term which produces self-consistency in the transmission line

- 52 -

formulation. This term has exactly the same form as found by Johnson[37] and Baird.[4]

Upon collection of Eqs. 2.38, 2.40, 2.42, and 2.45, Eq. 2.36 may be rewritten as

$$-\frac{dV_n}{dz} + \int_{S(z)} E_t \cdot \frac{\partial \vec{e}_n^*}{\partial z} \, ds + \oint_\ell \tan \theta_T \vec{E}_t \cdot \vec{e}_n^* \, d\ell$$

$$= j\omega\mu I_n - \oint_\ell E_z \, \vec{e}_n \cdot \hat{n} \, d\ell \qquad (2.51)$$

Upon collection of Eqs. 2.39, 2.41, 2.43, 2.48, 2.49, and 2.50, Eqs. 2.37 may be rewritten as

$$-\frac{dI_n}{dz} + \int_{S(z)} \vec{H}_t \cdot \frac{\partial \vec{h}_n^*}{dz} \, ds + \oint_\ell \tan \theta_T \vec{H}_t \cdot \vec{h}_n^* \, d\ell$$

$$= j\omega\epsilon V_n - \frac{k_{tn}^2}{j\omega\mu} \oint_\ell \psi_n^* \vec{E}_t \cdot \vec{d\ell} + \frac{k_{tn}^2}{j\omega\mu} V_n + \int_{S(z)} \vec{J}_t \cdot \vec{e}_n^* \, ds \qquad (2.52)$$

Equations 2.51 and 2.52 may be rearranged to give the transmission line equations for the RF electromagnetic fields. First, the longitudinal propagation constant, k_z, is defined as

$$k_z^2 \triangleq \omega^2 \mu\epsilon - k_t^2 = k^2 - k_t^2 \qquad (2.53)$$

Second, the wave impedance, Z_n, is defined for the primary fields $\vec{E}$ and $\vec{H}$ as[4]

- 53 -

$$Z_n = \sqrt{\frac{\mu}{\epsilon}} \frac{k}{k_z} \qquad (2.54)$$

It would be possible to perform exactly the same treatment as presented here using $\vec{E}$ and $\vec{B}$ as the primary fields. This analysis would result in a different value for the expansion coefficients for the magnetic field (the I_n values). Also, since k_{tn} is an implicit function of z, both k_z and Z_n are implicit functions of z as well. The two right-hand side terms of Eq. 2.51 involving V_n may be combined into a single term (using Eqs. 2.52 and 2.53) and written as

$$j\omega\epsilon V_n + \frac{k_{tn}^2}{j\omega\mu} V_n = j\left(\omega\epsilon - \frac{k_{tn}^2}{\omega\mu}\right) V_n$$

$$= j\frac{1}{\omega\mu}\left(\omega^2\mu\epsilon - k_t^2\right) V_n$$

$$= j\frac{k_z}{\omega\mu} V_n \qquad (2.55)$$

The single term of Eq. 2.50 involving I_n may be rewritten by a similar process. With these definitions, Eqs. 2.51 and 2.52 may be rearranged to yield the following general form of the transmission line formulation for the electromagnetic fields,

$$\begin{array}{ccccc} \text{(a)} & \text{(b)} & \text{(c)} & \text{(d)} & \text{(e)} \end{array}$$

$$\frac{dV_n}{dz} = -jk_z Z_n I_n + \int_{S(z)} \vec{E}_t \cdot \frac{\partial \vec{e}_n^*}{\partial z} ds + \oint_\ell \tan\theta_T \vec{E}_t \cdot \vec{e}_n^* d\ell + \oint_\ell E_z(\vec{e}_n \cdot \hat{n}) d\ell$$

$$(2.56)$$

$$\begin{array}{cccc}
\text{(a)} & \text{(b)} & \text{(c)} & \text{(d)}
\end{array}$$

$$\frac{dI_n}{dz} = -j\,\frac{k_z}{Z_n}\,V_n + \int_{S(z)} \vec{H}_t \cdot \frac{\partial h_n^*}{\partial z}\,ds + \oint_\ell \tan\theta_T \vec{H}_t \cdot \vec{h}_n^*\,d\ell$$

$$\begin{array}{cc}
\text{(e)} & \text{(f)}
\end{array}$$

$$+\,\frac{k_{tn}^2}{j\omega\mu}\oint_\ell \psi_n^* \vec{E}_t \cdot d\vec{\ell} - \int_{S(z)} \vec{J}_t \cdot \vec{e}_n^*\,ds \qquad (2.57)$$

Equations 2.56 and 2.57 describe the propagation of a TE mode down a waveguide by providing analytic expressions for the z derivatives of the voltage and current coefficients, V_n and I_n, which may also be thought of as longitudinal profile functions. These general equations will be adapted in the next section to allow simultaneous consideration of resistive and tapered walls in the propagation (and interaction) region.

2.5 Preparation of Transmission Line Equations for Analysis of Tapered Nonideal Waveguides

In this section, the general transmission line equations (Eqs. 2.56 and 2.57) derived in Section 2.4 are adapted to consider tapered nonideal walls. This derivation proceeds in three steps and allows for analytic comparison of the derived equations with previously published results. The derivation proceeds by considering the equations needed for tapered and nonideal walls separately, and then moving to the case where both types of nonuniformity are present in a single cross section of waveguide. As was noted in previous sections, this transmission line type analysis closely follows Baird's work,[4] who expanded on Johnson,[37] Reiter,[63] and Solymar.[71] The beam→field coupling term (term (f), Eq.

2.57) does not change form in this analysis and so will not be carried in this section.

The first case to be considered will be a tapered perfectly conducting (i.e., $\sigma \to \infty$) waveguide. For this case, $E_z = -\tan(\theta_T)E_n$ and $E_\ell = 0$. With these substitution terms, (d) and (e) of Eq. 2.4.31 cancel each other completely. Term (e) of Eq. 2.57 is zero because it involves an integration of E_ℓ.

Term (c) of Eq. 2.4.31 is expanded using Eq. 2.18a and written as

$$\int_{S(z)} \vec{E}_t \cdot \frac{\partial \vec{e}_n^*}{\partial z}\, ds = \int_{S(z)} \sum_k V_k \vec{e}_k \cdot \frac{\partial \vec{e}_n^*}{\partial z}\, ds$$

$$= \sum_k V_k \int_{S(z)} \vec{e}_k \cdot \frac{\partial \vec{e}_n^*}{\partial z}\, ds$$

$$= \sum_k T_{kn} V_k \qquad (2.58)$$

where

$$T_{kn} \stackrel{\Delta}{=} \int_{S(z)} \vec{e}_k \cdot \frac{\partial \vec{e}_n^*}{\partial z}\, ds \qquad (2.59)$$

T_{kn} is a voltage coupling coefficient and represents the coupling of the 7_kth mode to the nth mode due to a waveguide wall taper, θ_T. Each single indice represents a separate mode, and modes may vary from one another in any one (or more) of three ways: (1) boundary condition (mode type), (2) radial variation, and (3) azimuthal variation.

Terms (c) and (d) of Eq. 2.57 may be written as a single term of the form (using Eq. 2.186)

$$\int_{S(z)} \vec{H}_t \cdot \frac{\partial \vec{h}_n^*}{\partial z} \, ds + \oint_{\ell} \tan \theta_T \left(\vec{H}_t \cdot \vec{h}_n^* \right) d\ell$$

$$= \sum_k I_k \left\{ \int_{S(z)} \vec{h}_k \cdot \frac{\partial \vec{h}_n^*}{\partial z} \, ds + \oint_{\ell} \tan \theta_T \left(\vec{h}_k \cdot \vec{h}_n^* \right) d\ell \right\}$$

$$\text{(2.60)}$$

The right-hand side is in the form of the sum of terms (c) and (d) of Eq. A.4 (Leibnetz' rule). Writing the full expression yields

$$\frac{d}{dz} \left[\int_{S(z)} \vec{h}_k \cdot \vec{h}_n^* \, ds \right] = \int_{S(z)} \frac{\partial \vec{h}_k}{\partial z} \cdot \vec{h}_n^* \, ds + \int_{S(z)} \vec{h}_k \cdot \frac{\partial \vec{h}_n^*}{\partial z} \, ds$$

$$+ \oint_{\ell} \tan \theta_T \, \vec{h}_k \cdot \vec{h}_n^* \, d\ell \qquad \text{(2.61)}$$

The left-hand side is the z derivative of Eq. 2.13, which is zero, so that terms (c) and (d) of Eq. 2.57 may be written in a single expression

$$\int_{S(z)} \vec{H}_t \cdot \frac{\partial \vec{h}_n^*}{\partial z} \, ds + \oint_{\ell} \tan \theta_T \left(\vec{H}_t \cdot \vec{h}_n^* \right) d\ell = - \sum_k I_k \int_{S(z)} \frac{\partial \vec{h}_k}{\partial z} \cdot \vec{h}_n^* \, ds$$

$$\text{(2.62)}$$

The right-hand side may be rewritten (using Eqs. 2.11 and A.3) as

$$- \sum_k I_k \int_{S(z)} \frac{\partial \vec{h}_k}{\partial z} \cdot \vec{h}_n^* \, ds = - \sum_k I_k \int_{S(z)} \frac{\partial}{\partial z} \left(\hat{z} \times \vec{e}_k \right) \cdot \left(\hat{z} \times \vec{e}_n^* \right) ds$$

$$= - \sum_k I_k \int_{S(z)} \left(\hat{z} \times \frac{\partial \vec{e}_k}{\partial z} \right) \cdot \left(\hat{z} \times \vec{e}_n^* \right) ds$$

$$= - \sum_k I_k \int_{S(z)} \frac{\partial \vec{e}_k}{\partial z} \cdot \vec{e}_n^* \, ds$$

$$= - \sum T_{nk}^* I_k \qquad (2.63)$$

where

$$T_{nk}^* \overset{\Delta}{=} \int_{S(z)} \frac{\partial \vec{e}_k}{\partial z} \cdot \vec{e}_n^* \, ds \qquad (2.64)$$

T_{nk}^* is a current coupling coefficient and represents the coupling of the kth mode to the nth mode due to a waveguide taper, θ_T. With these results, Eqs. 2.56 and 2.57, when applied to a tapered ideal wall waveguide, may be written as[4,26,62]

$$\frac{dV_n}{dz} = -jk_z Z_n I_n + \sum_k T_{kn} V_n \qquad (2.65)$$

$$\frac{dI_n}{dz} = -j \frac{k_z}{Z_n} V_n - \sum_k T_{nk}^* I_k \qquad (2.66)$$

Solymar showed that T_{kn} and T_{nk}^* could be expressed as line integrals around the contour surrounding $S(z)$. Four cases may be considered for the types of modes involved in the coupling represented by T_{kn} and T_{nk}^*. Following the notation of Baird[4] and Solymar[71] "[ ]" signifies

a TE mode, and "( )" signifies a TM mode. Solymar's results in each
case are:[71]

TM to TE Coupling

$$T_{(k)[n]} = - \oint_{\ell} \tan (\theta_T) \frac{\partial \psi_{(k)}}{\partial \ell} \frac{\partial \psi_{[n]}^*}{\partial \ell} \, d\ell \qquad (2.67)$$

TE to TM Coupling

$$T_{[k][n]} = 0 \qquad (2.68)$$

TE to TE Coupling

$k_{tn} \ne k_{tk}$

$$T_{[k][n]} = \frac{k_{tk}^2}{k_{tn}^2 - k_{tk}^2} \oint_{\ell} \tan (\theta_T) \psi_{[k]} \frac{\partial^2 \psi_{[n]}^*}{\partial n^2} \, d\ell \qquad (2.69)$$

$k_{tn} = k_{tk}$ (self-coupling)

$$T_{[n][n]} = - \frac{1}{2} \oint_{\ell} \tan (\theta_T) \left| \frac{\partial \psi_{[n]}}{\partial \ell} \right|^2 \, d\ell \qquad (2.70)$$

TM to TM Coupling

$k_{tn} \ne k_{tk}$

$$T_{(k)(n)} = \frac{k_{tn}^2}{k_{tk}^2 - k_{tn}^2} \oint_{\ell} \tan (\theta_T) \frac{\partial \psi_{(k)}}{\partial n} \frac{\partial \psi_{(k)}}{\partial n} \, d\ell \qquad (2.71)$$

$k_{tn} = k_{tk}$ (self-coupling)

$$T_{(n)(n)} = -\frac{1}{2} \oint_{\ell} \tan(\theta_T) \left|\frac{\partial \psi_n}{\partial n}\right|^2 d\ell \qquad (2.72)$$

The current coupling coefficients, T_{nk}^*, may be found from Eqs. 2.67-2.72 by interchanging mode indices n and k, and taking the complex conjugate. The use of Eqs. 2.67-2.72 in Eqs. 2.65 and 2.66 allows the calculation of dV_n/dz and dI_n/dz in a tapered ideal waveguide.

The second case to be considered is the nontapered (i.e., $\theta_T = \sin(\theta_T) = \tan(\theta_T) = 0$), nonideal wall waveguide. For this case, all terms proportional to $\tan(\theta_T)$ or $\frac{\partial}{\partial z}$ are zero. This leaves terms (a), (b), and (c) from Eq. 2.56 and terms (a), (b), and (e) from Eq. 2.57. Under these conditions, the transmission line equations may be written as

$$\frac{dV_n}{dz} = -jk_z Z_n I_n + \oint_{\ell} E_z \vec{e}_n^* \cdot \hat{n} \ d\ell \qquad (2.73)$$

$$\frac{dI}{dz} = -j \frac{k_z}{Z_n} V_n + \frac{k_{tn}^2}{j\omega\mu} \oint_{\ell} \psi_n^* E_\ell \ d\ell \qquad (2.74)$$

As noted before, the present analysis deals only with the changes in the voltage and current coefficients of a TE mode.

The coupling terms remaining are exactly those found by Johnson[37] and Baird.[4] The terms are written as line integrals, meaning that the components will be evaluated with radial values of $r_w(z)$. A nonideal wall relationship between the components of E and H parallel to the wall and evaluated at the wall is[37]

$$\vec{E}_p = Z_w(\vec{H}_p \times \hat{n}) \qquad (2.75)$$

where

$$Z_w \overset{\Delta}{=} \frac{1 + j}{\sigma\delta} \qquad (2.76)$$

and

$$\delta \overset{\Delta}{=} \left[\frac{2}{\omega\mu\sigma}\right]^{1/2} \qquad (2.77)$$

Z_w is the wall impedance and has the same function as resistance (except that it is complex) in a dc conductor. Thus, Z_w is a measure of the loss caused by the propagation of electromagnetic fields (in the form of currents) in the waveguide wall. δ is the skin depth, discussed qualitatively in Section 2.4, and σ is the conductivity of the surface material. Subscript "p" signifies the field components parallel to the wall at $r = r_w(z)$. Using Eq. 2.75, the electric field components are written as

$$E_z\hat{z} + E_\ell\hat{\ell} = Z_w\left[\left(H_z\hat{z} + H_\ell\hat{\ell}\right) \times \hat{n}\right]$$

$$= Z_w\left(H_z\hat{\ell} - H_\ell\hat{z}\right) \qquad (2.78)$$

The longitudinal component of E may then be written (using Eq. 2.18) as

$$E_z = -Z_w H_\ell$$

$$= -Z_w \sum_k I_k \vec{h}_k \cdot \hat{\ell} \qquad (2.79)$$

The transverse parallel component of E, E_ℓ, may be written (using Eqs. 2.18 and 2.27) as

$$E_\ell = Z_w H_z$$

$$= - \frac{Z_w}{j\omega\mu} (\hat{z} \cdot \vec{\nabla}_t \times \vec{E}_t)$$

$$= - \frac{Z_w}{j\omega\mu} \sum_k V_k (\hat{z} \cdot \vec{\nabla}_t \times \vec{e}_k) \qquad (2.80)$$

The vector product may be reduced using Eqs. A.1, 2.11, and 2.1, so that Eq. 2.80 may be written as

$$E_\ell = \frac{Z_w}{j\omega\mu} \sum_k V_k k_{tk}^2 \psi_k \qquad (2.81)$$

Equation 2.79 yields a value for E_z, which may be substituted into Eqs. 2.73 to yield

$$\frac{dV_n}{dz} = - jk_z Z_n I_n - \oint_\ell Z_w \left[\sum_k I_k (\vec{h}_k \cdot \hat{\ell}) \right] (\vec{e}_n^* \cdot \hat{n})\, d\ell$$

$$\text{(c)}$$

$$= - jk_z Z_n I_n - \sum_k I_k \oint_\ell Z_w (\vec{h}_k \cdot \hat{\ell})\left(\vec{e}_n^* \cdot \hat{n}\right) d\ell \qquad (2.82)$$

Term (c) of Eq. 2.82 may be rewritten for TE modes (using Eq. 2.17) as

$$\frac{dV_n}{dz} = - jk_z Z_n I_n - \sum_k I_k \oint_\ell Z_w \frac{\partial \psi_k}{\partial \ell} \frac{\partial \psi_n^*}{\partial \ell}\, d\ell \qquad (2.83)$$

- 62 -

Equation 2.81 yields a value of E_ℓ, which may be substituted into Eq. 2.74 to yield

$$\frac{dI_n}{dz} = -j \frac{k_z}{Z_n} V_n + \frac{k_{tn}^2}{j\omega\mu} \oint_\ell \psi_n^* \left[\frac{Z_w}{j\omega\mu} k_{tk}^2 \sum_k V_k \psi_k \right] d\ell$$

or

$$\frac{dI_n}{dz} = -j \frac{k_z}{Z_n} V_n - \frac{k_{tn}^2 k_{tk}^2}{\omega^2 \mu^2} \sum_k V_k \oint_\ell Z_w \psi_n^* \psi_k \, d\ell \qquad (2.84)$$

Two new coupling coefficients are defined as

$$Z_{nk} \triangleq \frac{1}{jk} \oint_\ell Z_w \frac{\partial \psi_k}{\partial \ell} \frac{\partial \psi_n^*}{\partial \ell} \, d\ell \qquad (2.85)$$

and

$$Y_{nk} \triangleq \frac{1}{jk} \frac{k_{tn}^2 k_{tk}^2}{\omega^2 \mu^2} \oint_\ell Z_w \psi_n^* \psi_k \, d\ell \qquad (2.86)$$

Both coefficients are defined in a form similar to but slightly different from those defined by Baird.[4] Equations 2.83 and 2.84 correspond to coupling coefficients of the same name (but again of slightly different form) found by Johnson.[37] The variation from previous definitions was chosen to represent the fact that the Z_w may be a function of azimuthal location on the waveguide wall. Z_{nk} is a current coupling coefficient, and Y_{nk} is a voltage coupling coefficient, where the nature of each is identified by the coefficient (I or V) by which it is multiplied in Eq. 2.84 (2.83). These coefficients represent the strength of

- 63 -

the nonideal wall induced coupling from the mode under consideration, the nth mode, to all other TE modes, represented by the sum over k. Using Eqs. 2.85 and 2.86 in Eqs. 2.83 and 2.84, the transmission line equations for this case are[4,37]

$$\frac{dV_n}{dz} = - jk_z Z_n I_n - \sum_k Z_{nk} I_k \tag{2.87}$$

$$\frac{dI_n}{dz} = - j \frac{k_z}{Z_n} V_n + \sum_k Y_{nk} V_k \tag{2.88}$$

The final case to be considered deals with a tapered nonideal wall waveguide. This analysis produces the final form for the transmission line equations. The geometry remains that is shown in Fig. 2.1, which may be realized by cylindrical geometry (circular waveguide) or rectangular geometry (rectangular waveguide).

Previously, the geometry of the waveguide has been represented in terms of geometry based unit vectors $\hat{n}$, $\hat{\ell}$, and $\hat{z}$, which have apparent relationships to $\hat{r}$, $\hat{\theta}$, and $\hat{z}$, the cylindrical coordinate unit vectors. In this analysis, the explicit relationship, the relationships are expressed via a rotation of angle θ_T about $\hat{\ell}$. It is recognized that this leaves the $\hat{\ell}$, $\hat{\theta}$ relationship unchanged, as well as the respective components of the electromagnetic fields. The rotated coordinates are primed, and the nonrotated coordinates are unprimed and may be represented as[4]

$$\vec{E} = \begin{bmatrix} E_n \\ E_\ell \\ E_z \end{bmatrix} = \begin{bmatrix} \cos\theta_T & 0 & \sin\theta_T \\ 0 & 1 & 0 \\ -\sin\theta_T & 0 & \cos\theta_T \end{bmatrix} \begin{bmatrix} E'_n \\ E'_\ell \\ E'_z \end{bmatrix} \qquad (2.89)$$

and

$$\vec{H} = \begin{bmatrix} H_n \\ H_\ell \\ H_z \end{bmatrix} = \begin{bmatrix} \cos\theta_T & 0 & \sin\theta_T \\ 0 & 1 & 0 \\ -\sin\theta_T & 0 & \cos\theta_T \end{bmatrix} \begin{bmatrix} H'_n \\ H'_\ell \\ H'_z \end{bmatrix} \qquad (2.90)$$

This rotation about $\hat{\ell}$ is shown in Fig. 2.2, which is a modification of Fig. 2.1.

Equation 2.75 may also be used in the prime system to relate $\vec{E}'_p$ and $\vec{H}'_p$,

$$\vec{E}'_p = Z_w(\vec{H}'_p \times \hat{n}) \qquad (2.91)$$

Recalling Eq. 2.1 and using Eq. 2.91 to expand Eq. 2.89 yields (and noting that $H'_\ell = H_\ell$ for a rotation about $\hat{\ell}$),

$$E_n = E'_n \cos\theta_T - Z_w H_\ell \sin\theta_T$$

$$E_\ell = Z_w H'_z$$

$$E_z = - E'_n \sin\theta_T - Z_w H_\ell \cos\theta_T \qquad (2.92)$$

- 65 -
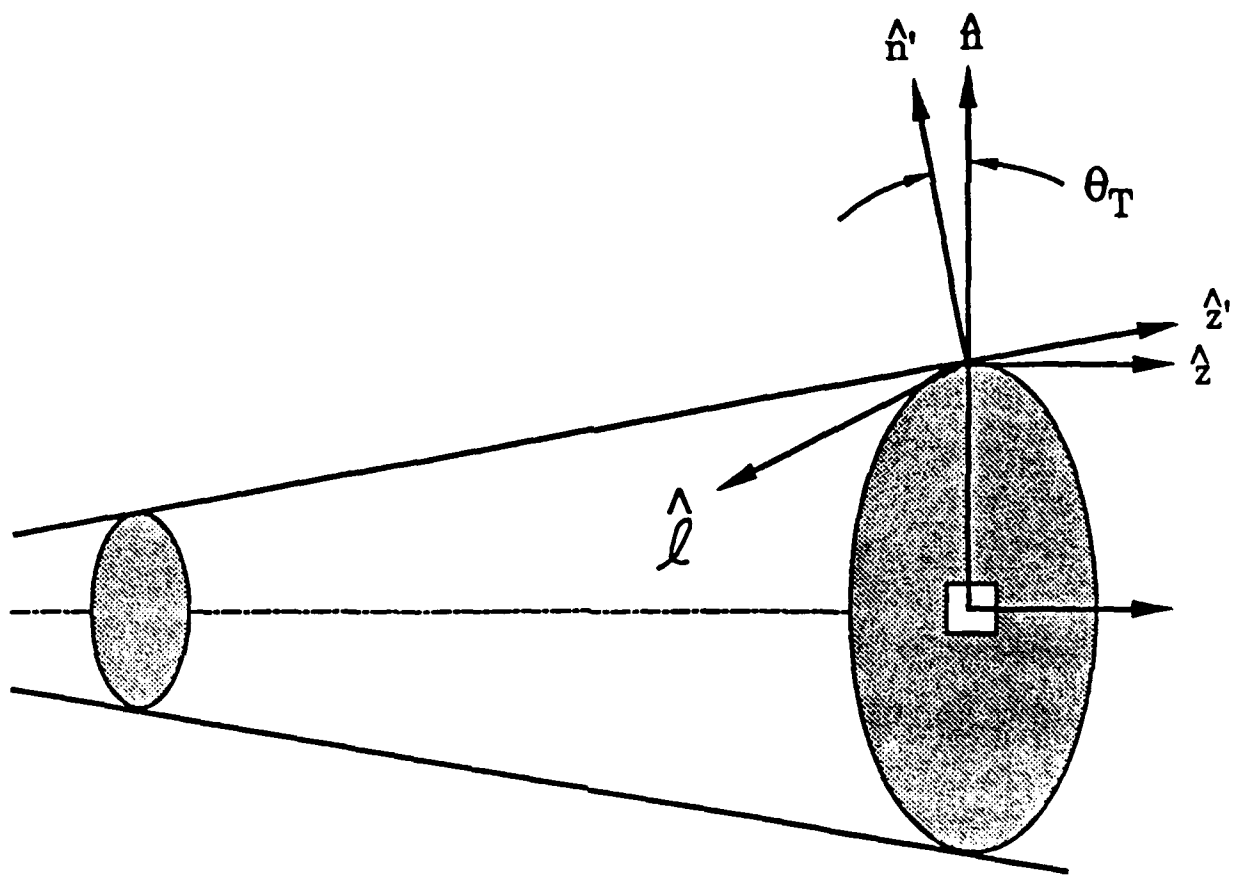
Fig. 2.2.   Diagram of tapered waveguide showing components
resulting from rotation of θ_T radians about ℓ.

Equation 2.92 may be separated into components normal to and in the plane of the waveguide wall. The normal components will be referred to by superscript "i" for "ideal wall," and the parallel components will be referred to as "ni" for "nonideal wall." Equation 2.92 may be written as

$$
\vec{E} = \begin{bmatrix} E_n^i \\ E_\ell^i \\ E_z^i \end{bmatrix} + \begin{bmatrix} E_n^{ni} \\ E_\ell^{ni} \\ E_z^{ni} \end{bmatrix} = \begin{bmatrix} E_n' \cos \theta_T \\ 0 \\ -E_n' \sin \theta_T \end{bmatrix} + \begin{bmatrix} -Z_w H_\ell \sin \theta_T \\ Z_w H_z' \\ -Z_w H_\ell \cos \theta_T \end{bmatrix} \qquad (2.93)
$$

Again using the relation $E_z = -\tan(\theta_T) \, E_n$, terms (d) and (e) of Eq. 2.56 cancel as in the case of the ideal tapered waveguide. Observing from Fig. 2.2 that $\vec{E}_n^i = E_n^i \hat{n}$, it is apparent that term (e) of Eq. 2.57 has no contribution from E^i. Terms (d) and (e) of Eq. 2.57 and term (c) of Eq. 2.56 were reduced to single term expressions dependent only on the transverse structure of $\vec{H}$ or $\vec{E}$. These terms will remain unaltered by the analysis at hand. Equations 2.56 and 2.57 may then be rewritten as

$$
\frac{dV_n}{dz} = -jk_z Z_n I_n + \sum_k T_{kn} I_k + \overset{(d)}{\oint_\ell \tan \theta_T \left(\vec{E}_t^{ni} \cdot \vec{e}_n^* \right) d\ell} + \overset{(e)}{\oint_\ell E_z^{ni} \left(\vec{e}_n^* \cdot \hat{n} \right) d\ell}
$$

$$
(2.94)
$$

$$
\frac{dI_n}{dz} = -j \frac{k_z}{Z_n} V_n - \sum_k T_{nk}^* V_k + \frac{k_{tn}^2}{j\omega\mu} \oint_\ell \psi_n^* \left(\vec{E}_t^{ni} \cdot \hat{\ell} \right) d\ell \qquad (2.95)
$$

The remaining portions of terms (d) and (e) of Eq. 2.94 and term (d) of Eq. 2.95 may be rewritten by expressing the nonideal electric field components in terms of the nonrotated field components given in Eq. 2.93, and expanding the results in terms of the normalized field functions. Terms (d) and (e) of Eq. 2.94 may be rewritten (using Eq. 2.16) as

$$\oint_\ell \left\{ \tan \theta_T \left(\vec{E}_t^{ni} \cdot \vec{e}_n^* \right) + E_z^{ni} \left(\vec{e}_n^* \cdot \hat{n} \right) \right\} d\ell$$

$$= \oint_\ell \left\{ \tan \theta_T \left[\left(E_n^{ni}\hat{n} + E_\ell^{ni}\hat{\ell} \right) \cdot \vec{e}_n^* \right] + E_z^{ni} \left(\vec{e}_n^* \cdot \hat{n} \right) \right\} d\ell$$

$$= \oint_\ell \left\{ \tan \theta_T E_n^{ni} \left(\vec{e}_n^* \cdot \hat{n} \right) + E_z^{ni} \left(\vec{e}_n^* \cdot \hat{n} \right) \right\} d\ell$$

$$= - \oint_\ell Z_w \left\{ \tan \theta_T \sin \theta_T H_\ell + \cos \theta_T H_\ell \right\} \left(\vec{e}_n^* \cdot \hat{n} \right) d\ell$$

$$= - \oint_\ell Z_w \left(\sin \theta_T \tan \theta_T + \cos \theta_T \right) \left(\vec{e}_n^* \cdot \hat{n} \right) H_\ell \, d\ell$$

$$= - \oint_\ell \frac{Z_w}{\cos \theta_T} \left(\vec{e}_n^* \cdot \hat{n} \right) H_\ell \, d\ell$$

$$= - \oint_\ell \frac{Z_w}{\cos \theta_T} \sum_k I_k \left(\vec{h}_k \cdot \hat{\ell} \right) \left(\vec{e}_n^* \cdot \hat{n} \right) d\ell$$

$$= - \sum_k I_k \oint_\ell \frac{Z_w}{\cos \theta_T} \left(\vec{h}_k \cdot \hat{\ell} \right) \left(\vec{h}_n^* \cdot \hat{\ell} \right) d\ell$$

$$= - \sum_k I_k \oint_\ell \frac{Z_w}{\cos \theta_T} \frac{\partial \psi_k}{\partial \ell} \frac{\partial \psi_n^*}{\partial \ell} d\ell$$

$$= jk \sum_k Z_{nk} I_k \tag{2.96}$$

- 68 -

where

$$Z_{nk} \triangleq -\frac{1}{jk} \oint_{\ell} \frac{Z_w}{\cos \theta_T} \frac{\partial \psi_k}{\partial \ell} \cdot \frac{\partial \psi_k^*}{\partial \ell} \, d\ell \qquad (2.97)$$

Equation 2.97 differs from the value derived for the nontapered case (see Eq. 2.85) by the factor $(\cos \theta_T)^{-1}$. Equation 2.97 deals with the general case of current coupling from the kth mode to the nth mode induced by waveguide taper, and thus replaces Eq. 2.85.

The remaining portion of term (d) of Eq. 2.95 may be dealt with in a similar fashion, yielding

$$\oint_{\ell} \frac{k_{tn}^2}{j\omega\mu} \psi_n^* \left(\vec{E}_t^{ni} \cdot \hat{\ell} \right) d\ell = \frac{k_{tn}^2}{j\omega\mu} \oint_{\ell} \psi_n^* E_\ell^{ni} \, d\ell$$

$$= \frac{k_{tn}^2}{j\omega\mu} \oint_{\ell} Z_w \psi_n^* H_z' \, d\ell \qquad (2.98)$$

Equation 2.90 may be inverted, so that the rotated (primed) coordinate system field components are expressed in terms of the nonrotated components. This yields

$$H_z' = H_n \sin \theta_T + H_z \cos \theta_T \qquad (2.99)$$

Substitution of Eq. 2.99 into Eq. 2.98 yields

$$\frac{k_{tn}^2}{j\omega\mu} \oint_{\ell} \psi_n^* \left(\vec{E}_t^{ni} \cdot \hat{\ell} \right) d\ell = \frac{k_{tn}^2}{j\omega\mu} \oint_{\ell} Z_w \psi_n^* \left(\sin \theta_T \, H_n + \cos \theta_T \, H_z \right) d\ell \qquad (2.100)$$

H_n may be expanded using Eq. 2.18, and the resulting line integral can be shown to be zero using Eq. 2.16. Using this result and Eq. 2.25, Eq.

2.100 may be rewritten as

$$\frac{k_{tn}^2}{j\omega\mu} \oint_\ell \psi_n^* \vec{E}_t^{ni} \cdot \hat{\ell}\, d\ell = \frac{k_{tn}^2}{j\omega\mu} \oint_\ell Z_w \psi_n^* \left[\cos\theta_T \sum_k \frac{1}{j\omega\mu} V_k k_{tk}^2 \psi_k\right] d\ell \quad .$$

$$= -\frac{k_{tn}^2 k_{tk}^2}{\omega^2\mu^2} \sum_k V_k \oint_\ell Z_w \cos\theta_T \psi_n^* \psi_k\, d\ell$$

$$= jk \sum_k Y_{nk} V_k \tag{2.101}$$

where

$$Y_{nk} \triangleq \frac{1}{jk} \frac{k_{tn}^2 k_{tk}^2}{\omega^2\mu^2} \oint_\ell Z_w \cos\theta_T \psi_n^* \psi_k\, d\ell \tag{2.102}$$

Y_{nk} as defined by Eq. 2.102 differs from the nontaper case by $\cos(\theta_T)$, and being more general, replaces Eq. 2.86.

The transmission line equations may now be rewritten (using Eqs. 2.56, 2.57, 2.62, 2.63, 2.96, and 2.102) as

$$\frac{dV_n}{dz} = -jk_z Z_n I_n + \sum_k T_{kn} V_k + jk \sum_k Z_{nk} I_k \tag{2.103}$$

(e)

$$\frac{dI_n}{dz} = -j \frac{k_z}{Z_n} V_n - \sum_k T_{nk}^* I_k - jk \sum_k Y_{nk} V_k - \int_{S(z)} \vec{J}_t \cdot \vec{e}_n^* \, ds \tag{2.104}$$

Equations 2.103 and 2.104 are the final general analytic form for the transmission line equations. In this form, the formulation can analyze the effects of nonideal tapered walls. The T_{kn} $\left(T_{nk}^*\right)$ coefficients are defined in Eq. 2.59 (2.63) with Solymar's line integral formulations presented in Eqs. 2.67-2.72. The beam-field coupling term has not changed from the form presented in Section 2.4.

2.6 The Beam-Field Coupling Term

In this section, the beam-field coupling term will be further analyzed, and a method for representation of electrical charge presented. The two methods of gyrotron analysis are considered to determine how the beam is included in the theory derived. The standard method for representing the charge in the beam is presented, and a method for treating the charge as a sum of individual charge carrying points is presented, and the advantages of this technique are discussed.

A brief analysis of the two most used theoretical approaches to gyrotron analysis shows that the two involve the same type calculations for the beam-field coupling mechanism. In each case, a distribution function is calculated or built based on the chosen beam model, and then used in an integral similar to term (e) in Eq. 2.104. The kinetic theory method is based on the linearized Vlasov equation which expresses particle conservation.[5,42] The second method is known as single particle theory, and is based on solution of the Lorentz force equation and the time rate of change of particle energy, which is a product of the application of variational mechanics to the Lagrangian of a charged particle in an RF field.[55] The distribution function usually chosen in both formulations represents the beam as a continuum of charge, though the form of the momentum or velocity dependence may be varied to model the effects of velocity spread. The derived distribution function is then used to represent the beam→field coupling in the solution of a set of linearized Maxwell's equations,[2,5] or a wave equation in E_z or H_z.[2,10,13,17-19,24,37,64] This differential equation is most often

second order, or may be cast, as in the present analysis, in the form of two first-order coupled equations.

The term derived in Section 2.4, restated here for clarity, and represented as E_{bf} (for energy coupled from beam-field) is seen to be one of four driving terms for a differential equation of the form mentioned above.

$$E_{bf} \overset{\Delta}{=} \int_{S(z)} \vec{J}_t \cdot \vec{e}_n^* \, ds \qquad (2.105)$$

The basic purpose of most electron tubes is to arrange an efficient conversion of kinetic energy in the electron to stored energy in the RF fields. E_{bf} measures this transfer of particle energy to the field as a term in a transmission line equation for I_n. The inclusion of such a term is necessary for self-consistency to exist within a theoretical analysis of a device, as it represents the impact of the electrons on the field configuration, just as trajectory equations represent the impact of the trajectories of the electrons. The beam-field coupling term thus provides the final connection between the field and the beam that make the two systems mutually dependent on each other.

The basic method of analyzing a term of this type is outlined by Flyagin,[28] and Ganguly and Ahn,[30] and considered briefly by Konopinski.[41] The form of $\vec{J}_t$ that shows up in Eq. 2.105 is calculated as the fundamental Fourier component of the electron vector current density. $\vec{J}_t$ is often represented as $\vec{J}_t(\vec{r},\omega)$ (frequency domain) or $\vec{J}_t(\vec{r},t)$ (time domain) for this reason. The frequency domain value is calculated as

$$\vec{J}_t(\vec{r}, \omega) = \frac{1}{2\pi} \int_0^{2\pi} \vec{J}_t(\vec{r}, t) \, e^{-j\omega t} \, d(\omega t) \qquad (2.106)$$

Flyagin and Fliflet showed, using slightly different arguments, that the $d(\omega t)$ integration may be replaced by $d(\omega t_0)$.[3,27,28] This physically implies that the electrons in one wavelength of the RF field may be considered as representative of the electron beam. In gyrotrons, the z velocity, v_z, does not change very much from the initial value under conditions specified by Li, Park, and Hirshfield,[53] and met under most operating conditions.[27,24,12] This assumes that the z component of the RF magnetic field, H_z, is sufficiently small that it has a negligible effect on the electron trajectory, as can be seen from Eq. 3.78. Computer analysis shows this is a valid assumption (see Section V). Practically, an electron beam does not consist of the "ring" of electrons used in numerical models. Instead, it is essentially a long distribution of electrons with, ideally, specific spatial and velocity characteristics at the launching point. If the action of the field on a particular electron causes it to drift longitudinally, another electron will drift in such a way so as to compensate for the first electron. Considering this from the point of "rings" of electrons, if one electron in the ring drifts more than one half RF wavelength forward or backward during the interaction period, another electron, from a different ring, would drift into the first ring to replace the first electron. This imposes a limit on the computational model because an electron with too great a drift must be replaced by another drifting electron of the correct velocity and phase with respect to the RF field.

The method of representing the current density is the point at which the various analysis methods diverge significantly. The electron current density found in Eq. 2.106 may be evaluated[64] as

$$\vec{J}_t(\vec{r},t) = -\frac{I_o}{\gamma_o v_{zo}} \gamma \vec{v}_t(\vec{r},t)$$

(2.107)

where I_o is the current in the beam. This treatment models the electron beam as smeared charge, uniformly distributed across the cross section of the beam, though possibly including the effects of velocity spread in the beam. A second method, employed in this report, represents the electron beam as a collection of macroparticles carrying charge and located at specific points in space. Konopinski[41] considered such a model, and Golomb, Goren, Ron, and Hirshfield[31] used it as a basis for their treatment of gyrotron amplifiers. This method also can be used to consider velocity or momentum spread by choice of proper initial conditions for the particles. The charge density in the second method is calculated by evaluating the charge present in a single RF period, τ, where

$$\tau = \left(\frac{\omega}{2\pi}\right)^{-1}$$

(2.108)

The charge per macroparticle is then calculated as

$$\frac{|e|_{eff}}{\tau} = \frac{I_o}{N}$$

(2.109)

where $|e|_{eff}$ is the effective charge in coulombs for each macroparticle,

I_O is the beam current in amps, and N is the number of macroparticles in the ring being used to model the beam. This definition is consistent with the restrictions mentioned above, that is, the physics of the interaction is considered by examining the energy exchange processes within a single RF period.

The charge per particle in units of $|e|$, where $|e|$ is the physical quantity $(1.6008 \times 10^{-19} \text{ C})$, is given by

$$n_{eq} = \frac{|e|_{eff}}{|e|} \qquad (2.110)$$

The factor n_{eq} is used to correct the mass and charge in the trajectory equations so that the macroparticles also obey the Lorentz equations for particles of the charge-to-mass ratio $(n_{eq}|e|)/(n_{eq} m) = |e|/m$. Since the behavior of the macroparticles is identical with that of an electron, $|e|$ and m will be understood to refer to the macroparticles in the remainder of this work.

Localized charge is mathematically represented by the use of a distribution function in phase space, $f(\vec{p},\vec{r},t)$, built of delta functions.[27,36,41] This distribution function is

$$f(\vec{r},\vec{p},t) = \sum_{i=1}^{N} \delta(\vec{r} - \vec{r}_i) \, \delta(\vec{p} - \vec{p}_i) \qquad (2.111)$$

where $\vec{r}_i$ and $\vec{p}_i$ are the spatial location and momentum of the i'th particle at a time not yet specified. The transverse current density, $\vec{J}_t(\vec{r},t)$ then is[2,5,36]

$$\vec{J}_t(\vec{r},t) = -|e| \sum_i \vec{v}_{ti}(t) \, \delta(\vec{r}_t - \vec{r}_{ti}(t)) \, \delta(z - z_i(t)) \qquad (2.112)$$

$\vec{J}_t(\vec{r},t)$ is substituted into Eq. 2.105, and the integral is evaluated using the following technique of evaluating the z delta function in the Fourier integral.[2]

$$\delta(z - z(t_i)) = \frac{\delta(t - t_i)}{\left|\dfrac{dz(t_i)}{dt}\right|} = \frac{\omega \delta(\omega t - \omega t_i)}{v_{zi}} \qquad (2.113)$$

With these results, $\vec{J}(\omega,t)$ may be evaluated as

$$\vec{J}_t(\vec{r},\omega) = -|e| \left(\frac{\omega}{2\pi}\right) \sum_{i=1}^{N} \frac{\vec{v}_{ti}}{v_{zi}\tau} \, \delta(\vec{r}_t - \vec{r}_{ti}(t)) \, e^{-j\omega t_i} \qquad (2.114)$$

where τ is the RF period, and the positions r_{ti} are evaluated at t_i, the time at which the electrons arrive at z. Substituting Eq. 2.114 into Eq. 2.105 yields

$$E_{bf} = -|e| \left(\frac{\omega}{2\pi}\right) \sum_{i=1}^{N} \frac{\vec{v}_{ti}}{v_{zi}} \cdot \vec{e}_n^{\,*}(\vec{r}_{ti}) \, e^{-j\omega t_i} \qquad (2.115)$$

The velocity components, $\vec{v}_{ti}$ and v_z, will be known from the trajectory equations to be derived in the following section. The normalized basis function, $\vec{e}_n^{\,*}$, will be specified by the geometry and mode under consideration.

It was noted earlier that the point of divergence between the two principle techniques lies in the methods used to calculate the current density. Actually, the divergence is present only in theory. Theoretically and numerically, Eq. 2.115 expresses E_{bf} as a summation over

discrete particles. The first approach discussed (see Eq. 2.107) seems theoretically to have the form of an integration over a continuum. Numerically, this still requires discretization, so that the two apparently divergent theories converge when evaluated from the perspective of the actual computation required to evaluate the different analytic forms.

An important aspect of this formulation is found in the fact that the coupling of any given electron within the beam to any given RF mode *may be analyzed. For each RF mode, an equation of the form of Eq. 2.104* would result, and the coupling of the electron to that mode would be expressed by use of the $\vec{e}_n$ representing that mode. Further, this technique allows a minimum number of macroparticles to be used to represent the entire beam and all possible interactions between the beam and the RF field. As a byproduct of the formulation, individual particles may be started in various cyclotron phases and studied for their single particle efficiency, thus identifying the phases that contribute or subtract from the efficiency of the interaction. A discussion of the minimum number of macroparticles required to reach accurate results with this beam formulation may be found in Section 5.4.

2.7. Summary of Transmission Line
Formulation of RF Fields

The geometry of a general cylindrical tapered waveguide was presented in Section 2.2. A coordinate system composed of unit vectors especially suited to consideration of a tapered waveguide is presented. These unit vectors are related to the standard cylindrical
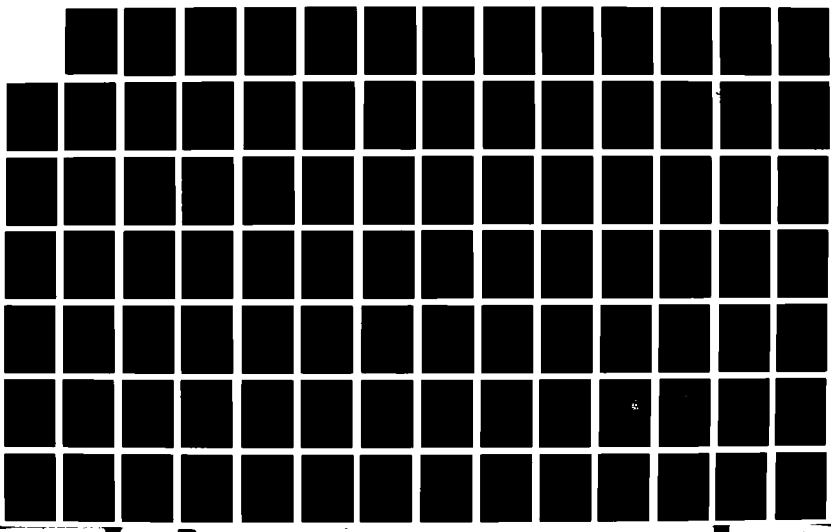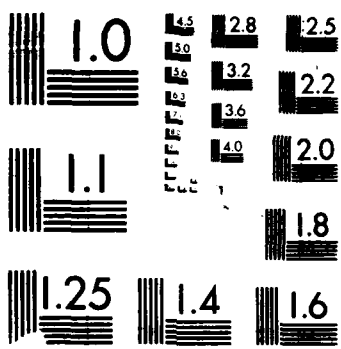
coordinate system unit vectors, and actually equal them for a zero taper case.

The normalized basis functions were presented in Section 2.3. The transmission line analysis allows for electromagnetic wave propagation in a tapered nonideal wall waveguide to be represented as a summation of these basis functions. The complex phasor representation for the transverse electric and magnetic fields for the nth mode is given by the product of V_n by an electric basis function, and by the product of I by a magnetic basis function. The real part is just $Re\{E_{phasor} \exp(j\omega t)\}$. The basis functions are found from solutions to the scalar wave equation for ψ. The longitudinal components for the electromagnetic fields were found from considering the z component of Maxwell's curl equations. The basis functions were normalized in such a way that the time average RF power is simply $0.5 \, RE\{V_n I_n^*\}$ for the nth mode.

The general form of the transmission line formulation was derived in Section 2.4. Maxwell's curl equations were separated into longitudinal and transverse portions, and the transverse portions were analyzed term by term. Terms were recognized that, in ideal waveguides, or in nontapered waveguides, would be zero. The concept of skin depth was considered as an explanation for the nonzero fields at the wall. The wave impedance, Z_n, and the longitudinal propagation constant, k_z, were defined. A set of two coupled first-order nonlinear differential equations were derived for each TE mode propagating in the waveguide in a form suitable for either circular or rectangular waveguides. These transmission line equations are in the form of a derivative on the left-hand side, and several driving terms on the right-hand side, including a

driving term due to the presence of source creating a vector current density, $\vec{J}_t$.

The general transmission line equations were adapted to allow simultaneous consideration of nonideal walls and tapered walls. The process was accomplished in three steps which allowed for verification that the general analytic forms reduced to the proper form in specific cases. Four coupling coefficients were defined, two of which are those previously defined by Solymar.[71] An equivalent wall impedance was defined as a function of the skin depth and conductivity of the wall material. It is shown that the field components present in the tapered system are related to those present in a nontapered system by a very straightforward relation involving the taper angle.

The form of the beam-field coupling term was analyzed in Section 2.6. A technique was presented for the evaluation of the electron beam as though it were comprised of individual charge carriers instead of "smeared" charge. A distribution function describing an ideal beam was used in the evaluation of the coupling term, and it was shown that the integral over $S(z)$ could be completed analytically. By proper choice of other distribution, functions would be possible to describe any reasonable electron beam or the action of any given electron.

The transmission line formulation as presented in Eqs. 2.103 and 2.104 is an exact expression for dV_n/dz and dI_n/dz. No taper terms have been dropped, and the taper angle is unbounded by the derivation technique, although greater taper angles would obviously require a greater number of modes to be considered in the summation terms of these equations. The approach used in the analysis of the terms consists of

integration of the basic terms, avoiding differentiation of the series expansion of the RF fields to insure convergence of the solution.[4,37] The beam-field coupling term as derived provides for a self-consistent (mutually dependent) solution for the propagation of an RF field in the presence of an electron beam within a waveguide. The coupling term is applicable to any form of RF field that may be expanded in terms of normalized basis vectors.

III. TRAJECTORY FORMULATION FOR THE ELECTRON BEAM

3.1 Introduction

The equations describing the behavior of the electrons will be derived in this chapter. The connection between the particles and the RF fields required for self-consistency is expressed in the use of the RF fields derived in Section II as the fields driving the particle motions; i.e., the evolving fields derived in Section II are used to represent the impact of the RF fields on the trajectories and energy of the electrons. The equations derived in this chapter are part of what is known as a single-particle analysis, indicating that each particle is considered independently. Physically, this means that the space-charge effects are neglected. The beam model is introduced in this chapter as well, and the utility of the model is pointed out.

Section 3.2 presents the beam model. The chosen model is that of an annular beam of equally distributed beamlets formed by electrons moving under the influence of the strong, mainly (but not purely) axial, dc magnetic field. The electron beam model is capable of representing both types of beams currently used in research.

The primary slow variable transformation is presented in Section 3.3. The transformation involves the expression of the transverse momentum in terms of a slowly varying magnitude and a phase variable that varies at the cyclotron frequency. The form of the transformation allows the separation of the effects of the RF interaction from the nonperturbed dc motion.

Section 3.4 is an extensive analysis of the nonlinear coupled differential equations required to describe the trajectories of the electrons. Three variables are required to describe the momentum. A slow variable transformation is presented for the momentum phase. The cyclotron harmonics are introduced through the use of a complex adaptation of Graf's addition theorem for Bessel functions. The equations as derived are fully capable of expressing the trajectory effects of a tapered dc magnetic field, and restrictions are presented for operation parameters so as to allow the conservation of electron magnetic moments. An approximation is introduced that allows the straightforward calculation of the dc magnetic field influence on the trajectory of electrons in any form of beam that the general model can be made to represent. The final equations are considered briefly in view of certain approximations made in the literature. The form derived allows analytic comparison of the relative magnitude, and numerical comparison of the cumulative effects of the various terms effected by the approximations. With the exception of the approximations involved in the taper terms, the derived equations are exact.

The equations describing the motion of the guiding center are derived in Section 3.5. These equations are shown to collapse to the dc solution upon substitution of proper values for the operating parameters.

In Section 3.6, the differential equation describing the time rate of change of total energy for the electrons is derived. The final form for the equation is found to be in a form consistent with expected results. The purpose of this equation is to verify the trajectory

equations to insure internal consistency of the solutions. A second form of verification is found to exist between the momentum equations and the energy equation. The effect of certain common approximations is discussed from the perspective of their impact on the energy equation.

Two appendices are included at the rear of this report that pertain specifically to material found in this chapter. Appendix B is a derivation of the mathematical representation chosen for the tapered dc magnetic field. Appendix C is an explanation of Graf's addition theorem for Bessel functions and an application of an adaptation of the theorem to the specific case being studied. The material in these appendices may be omitted, read when referred to, or consulted independently of the main text.

The field analysis presented in Section II was performed using E and H as the basic electromagnetic fields in order to allow for variations in μ, the magnetic permeability parameter. The literature overwhelmingly uses B as the basic magnetic field, with amplitudes given in units of tesla (T) or kilogauss (kG). Therefore, the constitutive relationship $B = \mu H$ will be assumed valid in this report.[30,38] The reader will then interpret the field quantity B according to this relationship, for both dc and RF fields, realizing that the presence of $\mu \neq \mu_o$ material may be accounted for by a simple multiplication by $\mu_r \triangleq \mu/\mu_o$.

3.2 Geometry of Electron Beam

In this section, the general geometry of an electron beam enclosed in a circular waveguide will be described. The beam, in its general form, is a collection of beamlets, each formed by the trajectory of an

- 83 -

individual particle, distributed within the waveguide so as to form an annular beam. It will be assumed in this work that the beamlets are equally distributed in such a way as to form a circular annulus. A dc magnetic field with a strong +z component is assumed present.

Figure 3.1 is a representation of the most general case for a particular beamlet. The vector $\vec{r}$ locates the particle (actually an electron, though numerically modeled as a "macroparticle;" see Section 2.6) as it moves in its RF perturbed orbit. The rectangular axis system is centered in the waveguide, and lies in a transverse plane S(z). Vector $\vec{r}$ is a vector sum of two vectors, $\vec{r}_O$ and $\vec{r}_L$, which locate the guiding center of the electron, and the electron in its cyclotron orbit, respectively. The magnitude of $\vec{r}_L$, $|\vec{r}_L| = r_L$ is the Larmour radius. The wall radius is $r_W(z)$, and the wall is characterized physically by the wall conductivity, σ, as discussed in Section 2.5. If no inter-action occurs between the electron beam and the RF field, the cumulative motion of the electrons when viewed from $\pm z$ would trace a circle of radius r_L centered at r_O. A viewer observing the trajectory of the electrons from off-axis would see a helical path being traced out as a function of time.

Figure 3.2 is an expanded diagram, allowing for better visualiza-tion of the configuration. Angle θ_0 is defined as the angle between $\vec{r}_O$ and $\hat{x}$, where $\hat{x}_L$ is a local unit vector satisfying $\hat{x} \cdot \hat{x}_L = 0$, situated within the Larmour radius of the single electron. Each electron has an $\hat{x}_L$ associated with its trajectory. Angles θ_1 and θ_2 are defined as the angles between $\vec{r}_O$ and $\vec{r}$, and between $\vec{r}_O$ and $\vec{r}_L$, respectively. Initially it will be assumed that r_O, r_L, and r, and angles θ_0, θ_1, and θ_2 all
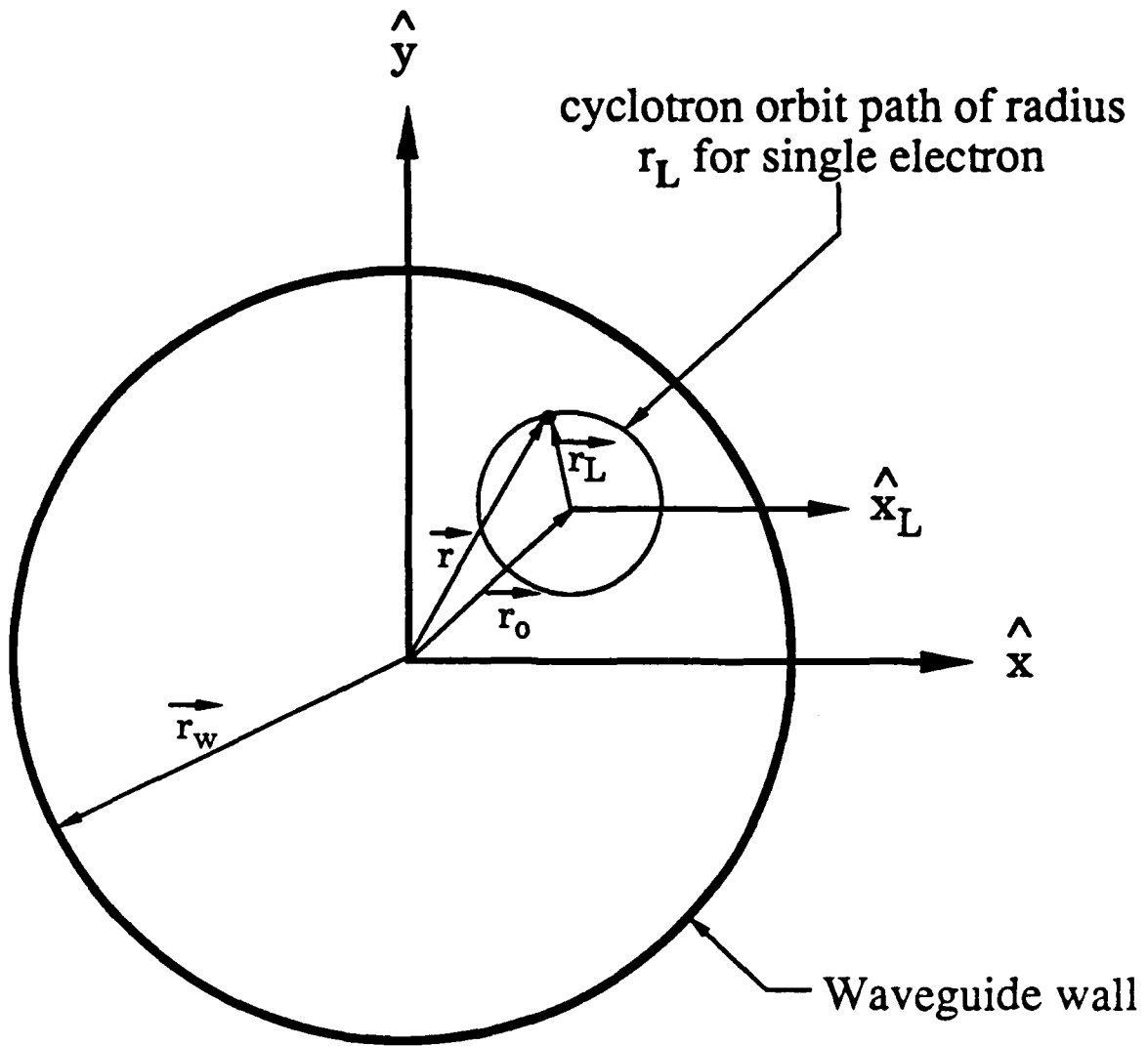
Fig. 3.1. Diagram of electron beam within a circular waveguide, with a single electron and beamlet drawn for clarity. $\hat{x}_L$ is the unit vector in the $\hat{x}$ direction located within the Larmour radius of the electron. The z component of the dc magnetic field points out of the page, and the electron moves counter-clockwise in its orbit.
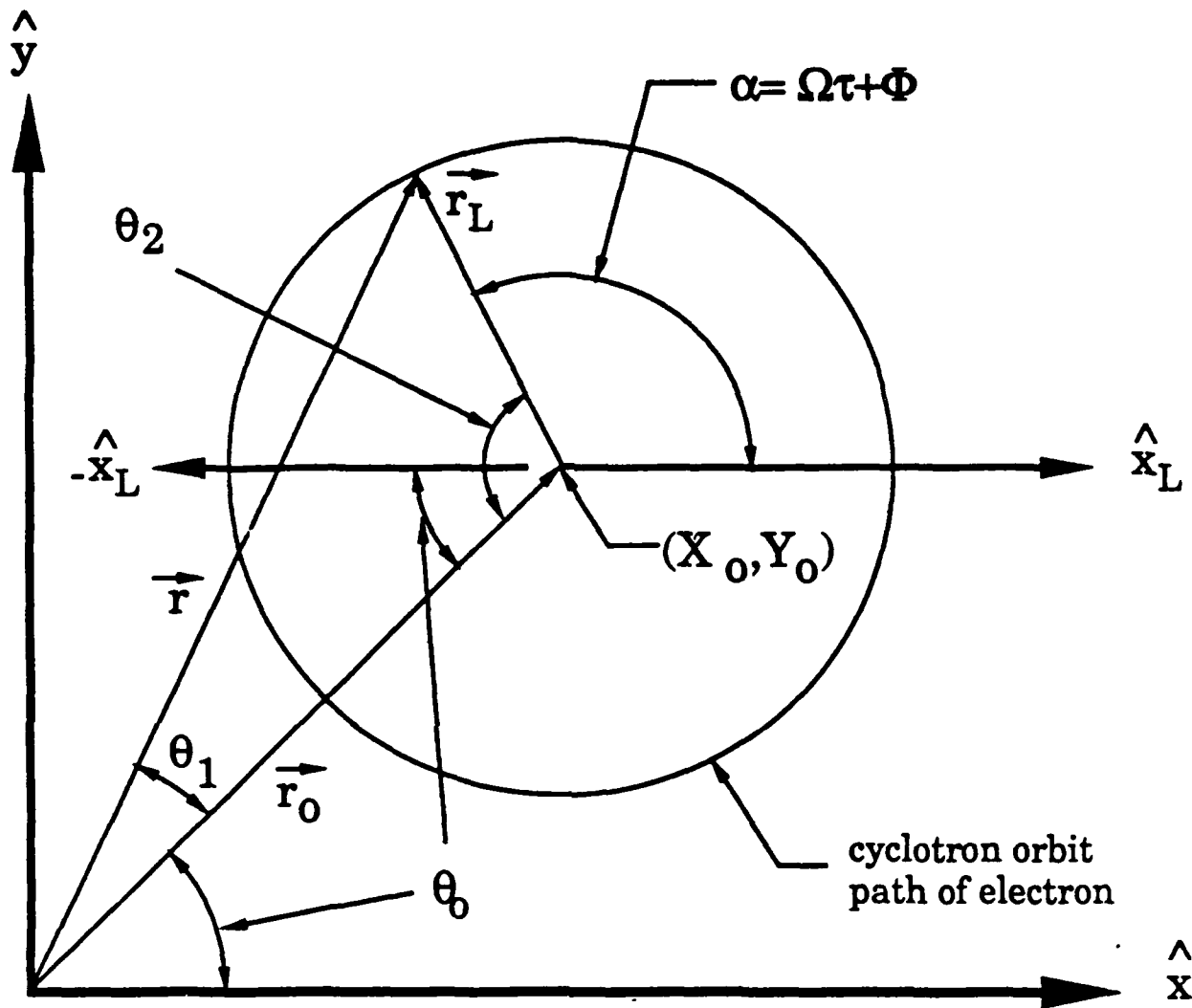
Fig. 3.2. Expanded diagram of an electron beamlet and the associated rectangular coordinate system. The three vectors $\vec{r}_o + \vec{r}_L = \vec{r}$ define the position of the electron as a function of time. (X_o, Y_o) are the rectangular coordinates for the position of the guiding center radius. The magnitude of $\vec{r}_L$ varies linearly with the transverse kinetic energy of the electron. The z component of the dc magnetic field points out of the page.

vary as functions of time. A discussion of this requirement, which is a statement of guiding center drift, will be presented in Section V. Angles θ_0, θ_1, and θ_2 are discussed at length in Appendix C and in Section 3.5. All angles are defined as positive for counterclockwise departure from the x axis. The unit vector $\hat{z}$ points out of the page, toward the reader. A pair of unit vectors, $\hat{r}$ and $\hat{\theta}$, are superimposed on the diagram at the location of the electron.

The angle α is the angle between $\vec{r}_L$ and $\hat{x}$, where the relevant x-y axis system is centered at $\vec{r}_0$. Angle α will be defined in the following section in such a way as to represent the angular component of the cycloidal motion induced by $\vec{B}_0$. Velocities and momenta associated with the electron will be described in Section 3.4.

It may be seen that by proper variation of the initial values of r_0 and r_L, which are the magnitudes of $\vec{r}_0$ and $\vec{r}_L$, respectively, this model may be used to represent any beam configuration being studied. Each particle will be individually initialized, so that the departures from an ideal beam normally considered may be studied using this model. For future reference, it will be noted that $r_0 \neq 0$ is the beam type produced by magnetron injection guns (MIG guns), and $r_0 = 0$ represents a gyrotron configuration known as a large-orbit gyrotron (LOG). Both of these configurations are currently being researched.[2,10,31,51]

3.3 Preliminaries and Slow Time Scale Transformations

The Lorentz force equation is the starting point in the analysis of trajectory equations for electrons. As previously stated, the

presence of a large dc magnetic field is assumed. The trajectory effects related to the dc magnetic field may be separated from those due to the RF field by writing the Lorentz equation as

$$\frac{d\vec{p}}{dt} + \frac{|e|}{\gamma m_o} \vec{p} \times \vec{B}_o = -|e| \left[\vec{E} + \frac{\vec{p}}{\gamma m_o} \times \vec{B} \right] \qquad (3.1)$$

where

$$\vec{p} \overset{\Delta}{=} \gamma m_o \vec{v} \qquad (3.2)$$

and m_o is the "rest mass" of the electron. The relativistic factor, γ, is calculated as

$$\gamma \overset{\Delta}{=} \left[1 - \frac{\vec{v} \cdot \vec{v}}{c^2} \right]^{-1/2} = \left[1 + \frac{\vec{p} \cdot \vec{p}}{\left(m_o c\right)^2} \right]^{1/2} \qquad (3.3)$$

and γ_o is the value of γ based on initial velocity values. Nonsubscripted field quantities, $\vec{E}$ and $\vec{B}$, are the RF fields. The trajectory analysis will use the forms of $\vec{E}$ and $\vec{B}$ derived in Section 2.

An essential element of this analysis is a slow transformation involving velocity or momentum introduced by Rappoport, et al.,[62] and used by Flifl≏t[24] and others.[30,64] The momentum form of this transformation is

$$p_x + j p_y = j p_t \exp \left[j(\Omega \tau + \phi) \right] \qquad (3.4)$$

where each quantity is shown in Fig. 3.3. $\vec{p}_x$ and $\vec{p}_y$ are the momenta in

- 88 -
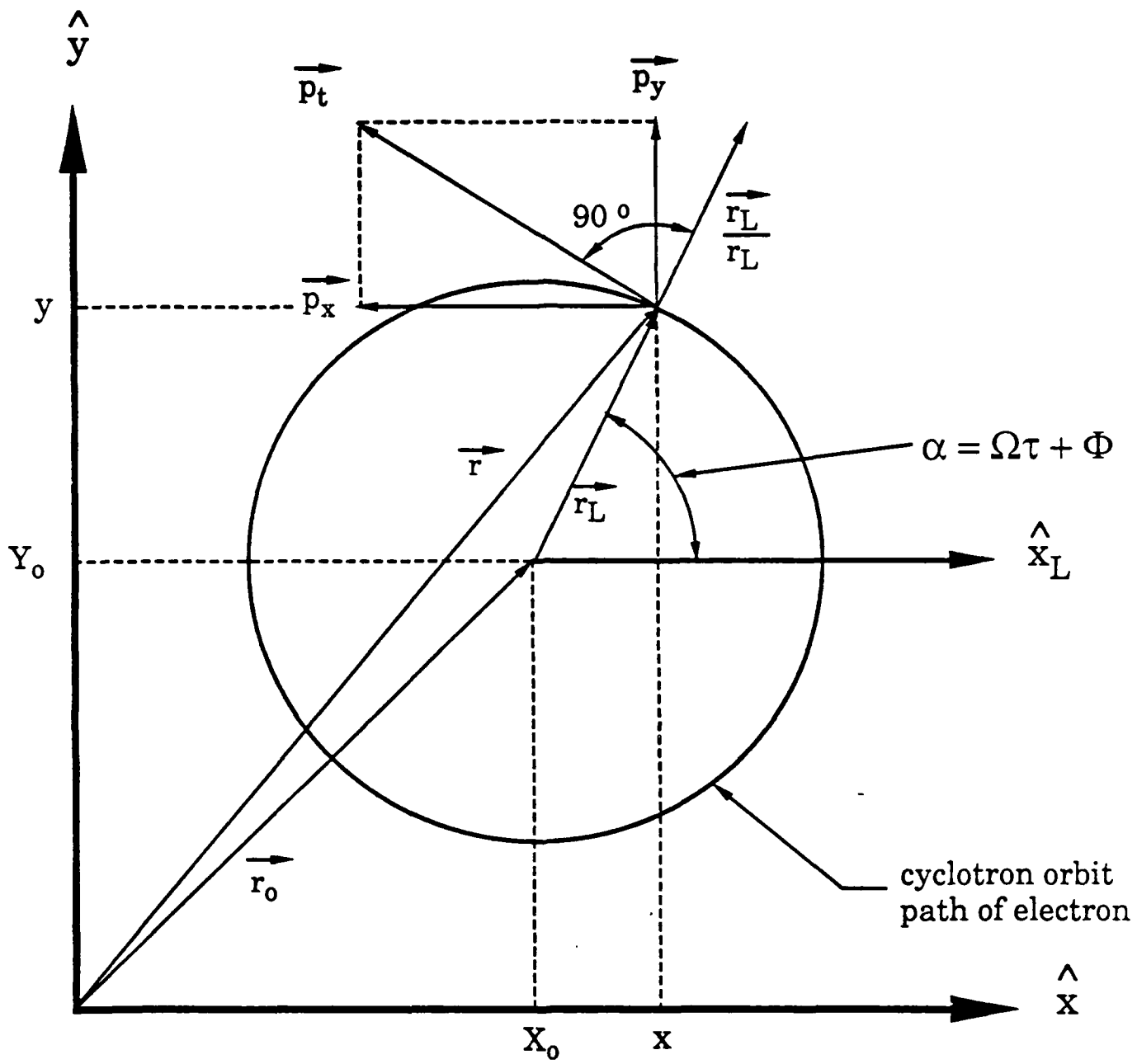
Fig. 3.3. Diagram of the trajectory of a single electron with phase $\alpha = \Omega\tau + \Phi$ and transverse momentum p_t. $\vec{p}_t$ is always at right angles with $\vec{r}_L$, and leads it by 90°. $\hat{x}_L$ is a unit vector in the $\hat{x}$ direction, located in the Larmour radius. Rectangular coordinate points $\left(X_o, Y_o\right)$ and (x, y) are the guiding center and electron positions, respectively.

the $\hat{x}$ and $\hat{y}$ directions, respectively. p_t is the magnitude of the vector sum of $\vec{p}_x + \vec{p}_y$, which is

$$p_t = \left(p_x^2 + p_y^2 \right)^{1/2}$$

Angle α is the azimuthal position of the electron relative to (X_o, Y_o) and $\hat{x}_L$. Ω is defined as[24]

$$\Omega \triangleq \frac{\Omega_o}{\gamma_o} = \frac{|e| \, B_{oz}(z_o)}{\gamma_o m_o} \tag{3.5}$$

Ω is defined as a function of initial conditions, γ_o, m_o, and $B_{oz}(z_o)$, and thus represents the contribution to phase angle α due to dc conditions. The time variable τ is defined as

$$\tau \triangleq t - t_o \tag{3.6}$$

where t_o is the time (corresponding to longitudinal position z_o) at which the electron entered into the interaction region. In a sense, then, τ may be thought of as an elapsed time of interaction. With Eqs. 3.4 and 3.5, it is apparent that the quantity $\Omega\tau$ represents the motion of an electron whose trajectory is unperturbed by interaction with RF fields. An electron moving with an azimuthal variation given by $\exp[j\Omega t]$ would be spinning (cumulative motion viewed in a transverse plane) in a circle, with frequency Ω given by Eq. 3.5. Φ is a time varying quantity, having a value of zero at $t = t_o$. Strictly speaking, $\Phi = \Phi(\tau)$, and Φ evaluated at $\tau = 0$ should be some nonzero value

representing the phase of the electron as it enters the interaction region (i.e., at $z = z_0$). This nonzero value may be eliminated by assuming a different initial phase, backing the electron up in space, so to speak, so that no information is lost and no assumption is made by using

$$\alpha \big|_{\tau=0} = [\Omega\tau + \phi]\big|_{\tau=0} = 0 \qquad (3.7)$$

With these definitions, ϕ may be seen as the variable whose value is the cumulative phase difference between the dc or unperturbed (without RF interaction) and the RF or perturbed (with RF interaction) motion of the electron after some elapsed time τ.

The validity of the slow time transformation may be verified by writing the position of the electron in Fig. 3.3 in rectangular coordinates and assuming dc conditions. Letting (x_t, y_t) represent the total position of the electron, we write

$$x_t = X_0 + x = X_0 + r_L \cos \alpha = X_0 + r_L \cos (\Omega\tau + \phi)$$

$$\qquad (3.8)$$

$$y_t = Y_0 + y = Y_0 + r_L \sin \alpha = Y_0 + r_L \sin (\Omega\tau + \phi)$$

Taking the time derivative yields

$$\frac{dx_t}{dt} = \frac{d}{dt} [r_L \cos (\Omega\tau + \phi)] = -r_L \Omega \sin (\Omega\tau + \phi)$$

$$\qquad (3.9)$$

$$\frac{dy_t}{dt} = \frac{d}{dt} [r_L \sin (\Omega\tau + \phi)] = r_L \Omega \cos (\Omega\tau + \phi)$$

Using

$$r_L \Omega \stackrel{\Delta}{=} v_t \qquad \qquad (3.10)$$

Equations 3.9 may be rewritten as

$$\frac{dx_t}{dt} \stackrel{\Delta}{=} v_x = -v_t \sin (\Omega \tau + \phi) \qquad \qquad (3.11)$$

$$\frac{dy_t}{dt} \stackrel{\Delta}{=} v_y = v_t \cos (\Omega \tau + \phi) \qquad \qquad (3.12)$$

The real and imaginary parts of Eq. 3.4 yield

$$Re\{p_x + jp_y\} = Re\{jp_t \exp[j(\Omega \tau + \phi)]\}$$

$$p_x = -p_t \sin (\Omega \tau + \phi)$$

or

$$v_x = -v_t \sin (\Omega \tau + \phi) \qquad \qquad (3.13)$$

and

$$Im\{p_x + jp_y\} = Im\{jp_t \exp[j(\Omega \tau + \phi)]\}$$

$$p_y = p_t \cos (\Omega \tau + \phi)$$

or

$$v_y = v_t \cos (\Omega \tau + \phi) \qquad \qquad (3.14)$$

Equations 3.11 (3.12) match Eqs. 3.13 (3.14) and the validity of Eq. 3.4 is established. The usefulness of the transformation is seen in the comparison of the rates of change of p_t, p_x, and p_y as a function of time. Under dc conditions, p_t will have a zero time derivative over a 2π phase change. Both p_x and p_y will vary from over a range of magnitude $2|p_t|$ in the same period. Thus, p_t is a slowly varying variable for transverse momentum. A slowly varying phase variable will be introduced in Section 3.4.

The electron beam is assumed to be traveling in a vacuum, characterized by ϵ_o and μ_o, where the speed of light, c, is given by

$$c = \left[\epsilon_o \mu_o\right]^{-1/2}$$

3.4 Derivation of Electron Trajectory Equations

In this section, the equations describing the trajectory of an electron moving in a cylindrical waveguide under the influence of a strong dc magnetic field and an RF electromagnetic field are derived. The trajectory is described in terms of three momentum related variables, p_t and Φ, discussed in the last section, and $p_z \triangleq \gamma m_o v_z$.

The form of the dc magnetic field is chosen to allow for the theory to address the effects of a tapered dc magntic field in conjunction with the tapered wall capability of the field theory derived in Section II. The consideration of a tapered magnetic field produces three additional force terms when compared to analyses assuming the presence of a magnetic field of the form $\vec{B}_o = B_o \hat{z}$.[24,27,44,51,53,77]

Equation 3.1 is rewritten as

$$\frac{d\vec{p}}{dt} = -\vec{F}_o + \vec{a} \tag{3.15}$$

where

$$\vec{F}_o \triangleq F_{ox}\hat{x} + F_{oy}\hat{y} + F_{oz}\hat{z} \tag{3.16}$$

and

$$\left.\begin{matrix} F_{ox} \\ F_{oy} \\ F_{oz} \end{matrix}\right\} = \frac{|e|}{\gamma m_o} \vec{p} \times \vec{B}_o \cdot \left\{\begin{matrix} \hat{x} \\ \hat{y} \\ \hat{z} \end{matrix}\right. \tag{3.17}$$

and where

$$\vec{a} \triangleq -|e|\left[\vec{E} + \frac{\vec{p}}{\gamma m_o} \times \vec{B}\right] \tag{3.18}$$

and the components of $\vec{a}$ may be defined as

$$\left.\begin{matrix} a_x \\ a_y \\ a_z \end{matrix}\right\} = -|e|\left[\vec{E} + \frac{\vec{p}}{\gamma m_o} \times \vec{B}\right] \cdot \left\{\begin{matrix} \hat{x} \\ \hat{y} \\ \hat{z} \end{matrix}\right. \tag{3.19}$$

The notation $\vec{F}_o$ is chosen to represent the fact that Eq. 3.3 represents a force on the electrons due to the presence of a dc magnetic field. Selecting the $\hat{x}$ and $\hat{y}$ components of Eq. 3.15, taking the time derivative

and use of Eq. 3.4, yields

$$\underset{\text{(c)}}{} \qquad \underset{\text{(d)}}{}$$

$$\frac{dp_x}{dt} + j\,\frac{dp_y}{dt} = \frac{d}{dt}\left\{jp_t\,\exp\left[j(\Omega\tau + \phi)\right]\right\} = -F_{ox} - jF_{oy} + a_x + ja_y \qquad (3.20)$$

Term (c) of Eq. 3.20 may be expanded as

$$\frac{d}{dt}\left\{jp_t\,\exp\left[j(\Omega\tau + \phi)\right]\right\} = j\,\exp\left[j(\Omega\tau + \phi)\right]\left(\frac{dp_t}{dt} + jp_t\,\Omega + jp_t\,\frac{d\phi}{dt}\right) \qquad (3.21)$$

Using Eq. 3.21 in Eq. 3.20 yields

$$j\,\exp\left[j(\Omega\tau + \phi)\right]\left(\frac{dp_t}{dt} + jp_t\Omega + jp_t\,\frac{d\phi}{dt}\right) = -F_{ox} - jF_{oy} + a_x + ja_y \qquad (3.22)$$

Rearranging and using the shorthand notation,

$$\alpha = \Omega\tau + \phi \qquad (3.23)$$

introduced earlier yields

$$\frac{dp_t}{dt} = -j\left(p_t\Omega + p_t\,\frac{d\phi}{dt}\right) - j\,e^{-j\alpha}\left(-F_{ox} - jF_{oy} + a_x + ja_y\right) \qquad (3.24)$$

Forming the complex conjugate of Eq. 3.24 and using the complex number identity,

$$\mathrm{Re}\{z\} = \frac{1}{2}\left(z + z^*\right)$$

yields

$$\frac{dp_t}{dt} = \frac{j}{2} \left[\left(-F_{ox} + jF_{oy} \right) e^{j\alpha} + \left(a_x - ja_y \right) e^{j\alpha} \right.$$

$$\left. + \left(F_{ox} + jF_{oy} \right) e^{-j\alpha} - \left(a_x + ja_y \right) e^{j\alpha} \right] \tag{3.25}$$

A value for $d\phi/dt$ may be derived from Eq. 3.22 using the same process. The result is

$$\frac{d\phi}{dt} = - \frac{1}{2p_t} \left[-\left(F_{ox} + jF_{oy} \right) e^{-j\alpha} + \left(a_x + ja_y \right) e^{-j\alpha} \right.$$

$$\left. + \left(-F_{ox} + jF_{oy} \right) e^{j\alpha} + \left(a_x - ja_y \right) e^{j\alpha} \right] - \Omega \tag{3.26}$$

Note that two equations are now derived to represent the transverse momentum, as would be expected. The longitudinal momentum equation is found by taking the dot product of $\hat{z}$ with Eq. 3.15, yielding

$$\frac{dp_z}{dt} = a_z - F_{oz} \tag{3.27}$$

The dc magnetic field is assumed to be of the form

$$\vec{B}_o = B_{oz}\hat{z} + B_{or}\hat{r} \tag{3.28}$$

where $B_{or} \gg B_{oz}$. B_o may also be written as

$$\vec{B}_o = B_{oz}\hat{z} - \frac{r}{2} \frac{\partial B_{oz}}{\partial z} \hat{r} \tag{3.29}$$

Equation 3.29 is derived in Appendix B. Using Eqs. 3.29 and A.13, $\vec{B}_o$ may be expressed in rectangular coordinates as

$$\vec{B}_o = B_{oz}\hat{z} - \frac{r}{2} \frac{\partial B_{oz}}{\partial z} \left[\cos(\theta)\ \hat{x} + \sin(\theta)\ \hat{y}\right] \tag{3.30}$$

Using this form and Eqs. 3.13 and 3.14, the terms involving F_{ox} and F_{oy} are expanded in rectangular coordinates to yield

$$F_{ox} = \frac{|e|}{\gamma m_o} \left[p_t B_{oz} \cos(\alpha) + \frac{rp_z}{2} \frac{\partial B_{oz}}{\partial z} \sin(\theta)\right] \tag{3.31}$$

Similarly,

$$F_{oy} = \frac{|e|}{\gamma m_o} \left[-\frac{rp_z}{2} \frac{\partial B_{oz}}{\partial z} \cos(\theta) + p_t B_{oz} \sin(\alpha)\right] \tag{3.32}$$

F_{oz} is treated by expanding $\vec{p}$, and $\vec{B}_o$ is the cylindrical coordinate (to take advantage of $B_{o\theta} = 0$). This yields

$$F_{oz} = \frac{|e|}{\gamma m_o} \frac{rp_t}{2} \frac{\partial B_{oz}}{\partial z} \cos(\alpha - \theta) \tag{3.33}$$

Equations 3.30 and 3.31 may be combined to produce

$$F_{ox} + jF_{oy} = \frac{|e|}{\gamma m_o} \left(p_t B_{oz}\ e^{j\alpha} - j\frac{rp_z}{2} \frac{\partial B_{oz}}{\partial z}\ e^{j\theta}\right) \tag{3.34}$$

and

$$-F_{ox} + jF_{oy} = \frac{|e|}{\gamma m_o} \left(-p_t B_{oz} e^{-j\alpha} - j \frac{rp_z}{2} \frac{\partial B_{oz}}{\partial z} e^{-j\theta} \right) \qquad (3.35)$$

Using Eqs. 3.34 and 3.35 in the evaluation of terms (a) and (c) of Eqs. 3.26 and 3.27 yields

$$\frac{dp_t}{dt} = \frac{j}{2} \left[(a_x - ja_y) e^{j\alpha} - (a_x + ja_y) e^{-j\alpha} \right] + \overset{(c)}{\frac{|e|}{\gamma m_o} \frac{rp_z}{2} \frac{\partial B_{oz}}{\partial z} \cos{(\alpha - \theta)}}$$

$$(3.36)$$

and

$$\frac{d\Phi}{dt} = -\frac{1}{2p_t} \left[(a_x + ja_y) e^{-j\alpha} + (a_x - ja_y) e^{j\alpha} \right] - \Omega \left(1 - \frac{\gamma_o}{\gamma} \right) \qquad (3.37)$$

Using Eq. 3.33 in Eq. 3.27 yields

$$\frac{dp_z}{dt} = a_z - \frac{|e|}{\gamma m_o} \frac{rp_t}{2} \frac{\partial B_{oz}}{\partial z} \cos{(\alpha - \theta)} \qquad (3.38)$$

Konopinski[*][1] notes that, in the presence of a tapered dc magnetic field, electrons gyrating about an off-axis magnetic field line are subject to additional forces when compared to those gyrating about a field line exactly on the axis. The magnitude of these additional off-axis gyration forces is small when compared to the on-axis forces. Also, the on-axis gyration force terms are small when compared to the other trajectory terms, i.e., the terms of $\vec{a}$. It is therefore reasonable to modify term (c) of Eqs. 3.36 and 3.38 according to the "adiabatic approximation." Consideration of the conservation of electron

magnetic moment identifies three adiabatic invariants, (Br_L), (p_t^2/B), and $(\gamma\mu)$, where an adiabatic invariant quantity is defined as a quantity unchanged during the period of any one Larmour orbit, and μ is the electron magnetic moment.[36,41,42] The most useful of these invariants is the second form, which may be interpreted as

$$\frac{p_t^2(z)}{B_o(z)} = \frac{p_t^2(z_o)}{B_o(z_o)} \tag{3.39}$$

The principle approximation involved in the use of the adiabatic approximation is

$$\frac{r_o}{r_L} \ll 1 \tag{3.40}$$

Under this approximation, $r \approx r_L$, and all transverse momentum is in the $\hat{\theta}$ direction. Under these conditions, kinetic energy is conserved because the force resulting from B_{or} is everywhere perpendicular to the momentum $\vec{p}_\theta$, and the relation

$$\Delta\left(p_t^2\right) = -\Delta\left(p_z^2\right) \tag{3.41}$$

is established. The $\hat{z}$ force term resulting from B_{or} may be written as

$$F_{oz} = -\frac{|e|}{\gamma m_o} p_\theta B_{or} \tag{3.42}$$

Substituting the form for B_{or} given in Eq. 3.29, and applying the adiabatic approximation yields

$$F_{oz} = \frac{|e|}{\gamma m_o} \frac{r_L p_t}{2} \frac{\partial B_{oz}}{\partial z} \qquad (3.43)$$

Writing the Larmour radius, r_L, as

$$r_L = \frac{\gamma v_t}{\Omega_o} \qquad (3.44)$$

yields

$$F_{oz} = \frac{p_t^2}{2\gamma m_o} \frac{1}{B_{oz}} \frac{\partial B_{oz}}{\partial z} \qquad (3.45)$$

Equation 3.45 is the equivalent form of Eq. 3.33 found by using the adiabatic approximation. It should be noted that Eq. 3.33 reduces exactly to the adiabatic form when Eq. 3.40 is applied. Applying the adiabatic approximation to term (c) of Eq. 3.36 yields

$$\frac{|e|}{\gamma m_o} \frac{r p_z}{2} \frac{\partial B_{oz}}{\partial z} \cos (\alpha - \theta) = \frac{p_t p_z}{2\gamma m_o} \frac{1}{B_{oz}} \frac{\partial B_{oz}}{\partial z} \qquad (3.46)$$

Nusinovich[58] derives conditions for the maximum relative magnitude of $(\partial B_{oz}/\partial z)/B_{oz}$ under which the mirroring effect and the guiding center drift induced by the taper may be ignored. The most restrictive of the two conditions is

$$\frac{\left| \frac{\partial B_{oz}}{\partial z} \right|}{B_{oz}} << \frac{\lambda}{r_o} \qquad (3.47)$$

This condition places restrictions on the maximum taper rate in a fashion consistent with the adiabatic approximation.

The electron trajectory equations may be rewritten as

$$\frac{dp_t}{dt} = \frac{j}{2} \left[(a_x - ja_y) e^{j\alpha} - (a_x + ja_y) e^{-j\alpha} \right] + \frac{p_t p_z}{2\gamma m_o} \frac{1}{B_{oz}} \frac{\partial B_{oz}}{\partial z} \qquad (3.48)$$

$$\frac{d\phi}{dt} = - \frac{1}{2p_t} \left[(a_x + ja_y) e^{-j\alpha} + (a_x - ja_y) e^{j\alpha} \right] - \Omega \left(1 - \frac{\gamma_o}{\gamma} \right) \qquad (3.49)$$

$$\frac{dp_z}{dz} = a_z - \frac{p_t^2}{2\gamma m_o} \frac{1}{B_{oz}} \frac{\partial B_{oz}}{\partial z} \qquad (3.50)$$

Equations 3.48, 3.49, and 3.50 are a set of differential equations describing the trajectory of a single electron. The two terms involving $\partial B_{oz}/\partial z$ and the $\Omega \, \gamma_o/\gamma$ term result directly from the presence of a tapered dc magnetic field. The $\partial B_{oz}/\partial z$ terms are not changed in the following analysis, and thus are not carried. They will be added back to the equations when needed.

The components of $\vec{a}$ (defined in Eq. 3.19) may be expanded in rectangular components as

$$a_x = -|e| \left(E_x + v_y B_z - v_z B_y \right) \qquad (3.51a)$$

$$a_y = -|e| \left(E_y + v_z B_x - v_x B_z \right) \qquad (3.51b)$$

$$a_z = -|e| \left(v_x B_y - v_y B_x \right) \qquad (3.51c)$$

where $E_z = 0$ for a TE mode. Using Eqs. 3.11, 3.12, A.16, and Euler's form for angle α, Eqs. 3.51 may be rewritten as

$$a_x = -|e|\left[(E_r \cos(\theta) - E_\theta \sin(\theta)) + \frac{v_t}{2}(e^{j\alpha} + e^{-j\alpha})B_z \right. \tag{3.52a}$$

$$\left. - v_z (B_r \sin(\theta) + B_\theta \cos(\theta))\right]$$

$$a_y = -|e|\left[(E_r \sin(\theta) + E_\theta \cos(\theta)) + v_z(B_r \cos(\theta) - B_\theta \sin(\theta))\right.$$

$$\left. - j\frac{v_t}{2}(e^{j\alpha} - e^{j\alpha})B_z\right] \tag{3.52b}$$

$$a_z = -|e|\frac{v_t}{2}\left[e^{j\alpha}(jB_y - B_x) - e^{-j\alpha}(jB_y + B_x)\right] \tag{3.52c}$$

Equation 3.52c may be rewritten (using Eq. A.18) as

$$a_z = -|e|\frac{v_t}{2}\left[e^{j\alpha}(jB_\theta - B_r)e^{-j\theta} - e^{-j\alpha}(jB_\theta + B_r)e^{j\theta}\right] \tag{3.53}$$

Using Eqs. 3.41 and A.16 allows the quantities $(a_x \pm ja_y)$ to be rewritten as

$$(a_x \pm ja_y) = -|e|\left[(E_r \pm jE_\theta)e^{\pm j\theta} - v_z(B_\theta \pm jB_r)e^{\pm j\theta} + v_tB_z e^{\pm j\alpha}\right] \tag{3.54}$$

Equations 3.53 and 3.54 are the components of the trajectory equations written in a form revealing the dependence of the trajectories on the RF fields. The next step is the derivation of the field

components in a form consistent with Section II. The transverse field components are found by use of Eqs. 2.9, 2.11, and 2.18. The resulting components are

$$E_{rm} = V_m \left(-\frac{1}{r}\frac{\partial}{\partial\theta} \right) \psi_m = j\frac{m}{r} C_{mn} J_m(R) e^{-jm\theta}$$

$$E_{\theta m} = V_m \left(\frac{\partial}{\partial r} \right) \psi_m = C_{mn} k_{tm} J_m'(R) e^{-jm\theta}$$

$$B_{rm} = -I_m \left(\frac{\partial}{\partial r} \right) \psi_m = -C_{mn} I_m k_{bm} J_m'(R) e^{-jm\theta}$$

$$B_{\theta m} = -I_m \left(-\frac{1}{r}\frac{\partial}{\partial\theta} \right) \psi_m = j\frac{m}{r} C_{mn} I_m J_m(R) e^{-jm\theta} \tag{3.55}$$

where

$$R \overset{\Delta}{=} k_{tm} r \tag{3.56}$$

has been used. B_z is given by Eq. 2.25 and written here for convenience.

$$B_{zm} = -\frac{j}{\omega} V_m k_{tm}^2 \psi_m \tag{3.57}$$

Equations 3.55 and 3.57 represent the components of the mth (TE) mode.

Terms (a) and (b) of Eq. 3.54 may be rewritten (using Eq. 3.55b) as

$$E_r \pm jE_\theta = \pm j V_m L_\pm \psi_m e^{\pm j\theta} \tag{3.58}$$

- 103 -

and

$$B_\theta \mp jB_r = \pm jI_m L_{\pm} \psi_m e^{\mp j\theta} \qquad (3.59)$$

where $L_\pm$ is an operator defined as[24]

$$L_\pm \psi_m \triangleq e^{\pm j\theta} \left(\frac{\partial}{\partial r} \pm \frac{j}{r} \frac{\partial}{\partial \theta} \right) \psi_m \qquad (3.60)$$

With these results, Eq. 3.54 may be rewritten as

$$(a_x \pm ja_y) = -|e| \left[\pm j \left(V_m - v_z I_m \right) L_\pm \psi_m + v_t B_z e^{\pm j\alpha} \right] \qquad (3.61)$$

Substituting of Eq. 3.61 into Eqs. 3.36 and 3.37, multiplying by $\exp(j\omega t)$, and taking the real part of the result yields

$$\frac{dp_t}{dt} = \mathrm{Re} \left\{ - \frac{|e|}{2} \left(V_m - v_z I_m \right) \left(L_+ \psi_m e^{-j\alpha} + L_- \psi_m e^{+j\alpha} \right) \exp(j\omega t) \right\} \qquad (3.62)$$

$$\frac{d\phi}{dt} = \mathrm{Re} \left\{ \frac{|e|j}{2p_t} \left[\left(V_m - v_z I_m \right) \left(L_+ \psi_m e^{-j\alpha} - L_- \psi_m e^{j\alpha} \right) \right. \right.$$
$$\left. \left. - 2 \frac{v_t^2 k_{tm}^2}{\omega} V_m \psi_m \right] \exp(j\omega t) \right\} - \Omega \left(1 - \frac{\gamma_o}{\gamma} \right) \qquad (3.63)$$

By a similar process, Eq. 3.38 may be rewritten as

$$\frac{dp_z}{dt} = \mathrm{Re} \left\{ -|e| \frac{v_t}{2} I_m \left[L_- \psi_m e^{j\alpha} + L_+ \psi_m e^{-j\alpha} \right] \exp(j\omega t) \right\} \qquad (3.64)$$

- 104 -

Equations 3.62, 3.63, and 3.64 are general trajectory equations for a single particle. At this stage, the ability to consider cyclotron harmonics is not present. The mathematical scheme used to analyze harmonics involves the application of Graf's addition theorem for Bessel functions.[1] The theorem, the quantities involved, and its application to the present physical model are found in Appendix C. Physically, Graf's theorem allows the formation of expressions for the RF fields at the guiding center of the electrons, thus giving rise to the cyclotron harmonics. Choosing a single mode and a single harmonic to interact with allows the trajectory equations to be written as

$$\frac{dp_t}{dt} = -|e| \, C_{mn} J_{m-s}(R_o) \, \frac{\partial J_s(R_L)}{\partial r_L} \, \text{Re} \left\{ (V_m - v_z I_m) \, e^{j\Gamma} \right\} \qquad (3.65)$$

$$\frac{d\phi}{dt} = \frac{|e|}{p_t} \, C_{mn} J_{m-s}(R_o) \, \frac{s}{r_L} \, J_s(R_L) \text{Re} \left\{ j \left[V_m - v_z I_m - \frac{k_{tm}^2 v_t^2}{s\Omega\omega} \frac{\gamma}{\gamma_o} V_m \right] e^{j\Gamma} \right\}$$
$$- \Omega \left(1 - \frac{\gamma_o}{\gamma} \right) \qquad (3.66)$$

$$\frac{dp_z}{dt} = -|e| \, v_t C_{mn} J_{m-s}(R_o) \, \frac{\partial J_s(R_L)}{\partial r_L} \, \text{Re} \left\{ I_m \, e^{j\Gamma} \right\} \qquad (3.67)$$

where

$$\Gamma \triangleq (\omega - s\Omega)\tau + \omega t_o - s\phi - (m - s)\theta_o \qquad (3.68)$$

and

$$R_o \triangleq k_{tm} r_o \qquad (3.69)$$

and

$$R_L \overset{\Delta}{=} k_{tm} r_L \qquad (3.70)$$

and s is the cyclotron harmonic chosen for interaction. The time derivative of Γ may be expressed as

$$\frac{d\Gamma}{dt} = \frac{d}{dt}\left[(\omega - s\Omega)\tau + \omega t_o - s\phi - (m - s)\theta_o\right] = (\omega - s\Omega) - s\frac{d\phi}{dt} \qquad (3.71)$$

so that a new phase variable Γ may be used in the differential equations in place of ϕ. The new phase equation is

$$\frac{d\Gamma}{dt} = \left(\omega - s\Omega\,\frac{\gamma_o}{\gamma}\right) - \frac{s|e|}{p_t} C_{mn} J_{m-s}(R_o)\,\frac{s}{r_L}\,J_s(R_L)$$

$$\times Re\left\{ j\left[V_m - v_z I_m - \overset{(c)}{\frac{k_{tm}^2 v_t^2}{s\Omega\omega}\,\frac{\gamma}{\gamma_o}\,V_m} \right] e^{j\Gamma} \right\} \qquad (3.72)$$

All components of the RF field present in the waveguide are now present in the trajectory equations. The RF B_z component is represented by term (c) of Eq. 3.72. If the entire RF magnetic field is assumed to exert negligible force on the electrons, the system of equations simplifies considerably, and may be written as

$$\frac{dp_t}{dt} = -|e|\,C_{mn} J_{m-s}(R_o)\,\frac{dJ_s(R_L)}{\partial r_L}\,Re\left\{ V_m\,e^{j\Gamma} \right\} \qquad (3.73)$$

$$\frac{d\Gamma}{dt} = \left(\omega - s\Omega \frac{\gamma_0}{\gamma}\right) - \frac{s|e|}{p_t} C_{mn} J_{m-s}(R_0) \frac{s}{r_L} J_s(R_L) \text{ Re}\left\{jV_m e^{j\Gamma}\right\} \quad (3.74)$$

$$\frac{dp_z}{dt} = 0 \quad (3.75)$$

The full set of equations describing the motion of the electrons, including dc magnetic field taper terms, is

$$\frac{dp_t}{dt} = -|e| \; C_{mn} J_{m-s}(R_0) \frac{\partial J_s(R_L)}{\partial r_L} \text{ Re}\left\{(V_m - v_z I_m) e^{j\Gamma}\right\} + \frac{p_t p_z}{2\gamma m_0} \frac{1}{B_{oz}} \frac{\partial B_{oz}}{\partial z}$$

$$(3.76)$$

$$\frac{d\Gamma}{dt} = \left(\omega - s\Omega \frac{\gamma_0}{\gamma}\right) - \frac{s|e|}{p_t} C_{mn} J_{m-s}(R_0) \frac{s}{r_L} J_s(R_L)$$

$$\times \text{ Re}\left\{j\left[V_m - v_z I_m - \frac{v_t^2 k_{tm}^2}{s\Omega\omega} \frac{\gamma}{\gamma_0} V_m\right] e^{j\Gamma}\right\} \quad (3.77)$$

$$\frac{dp_z}{dt} = -|e| \; v_t C_{mn} J_{m-s}(R_0) \frac{\partial J_s(R_L)}{\partial r_L} \text{ Re}\left\{I_m e^{j\Gamma}\right\} - \frac{p_t^2}{2\gamma m_0} \frac{1}{B_{oz}} \frac{\partial B_{oz}}{\partial z} \quad (3.78)$$

with Γ given by Eq. 3.68.

3.5 Derivation of Guiding Center Motion Equations

In this section, the equations describing the motion of the dc guiding centers are derived. The necessity of these equations is discussed in Section V, where it is found that under some conditions,

motion of the dc guiding centers of the electrons must be considered.

These equations are derived in a manner maintaining the self-consistency mentioned in earlier portions of this work. The derivations begin by writing the time dependent total (sum of dc and RF contributions) position of the electrons. The needed equations were used in Section 3.3, and are rewritten here for convenience,

$$x = X_o + r_L \cos(\Omega\tau + \phi) \tag{3.8}$$

$$y = Y_o + r_L \sin(\Omega\tau + \phi) \tag{3.9}$$

where, as in Fig. 3.3, (x, y) is the location of the electron, and (X_o, Y_o) is the location of the guiding center. The purpose of this section is the derivation of time-varying expressions for the value of (X_o, Y_o). Time derivatives of Eqs. 3.8 and 3.9 are

$$\frac{dx}{dt} = \frac{dX_o}{dt} + \frac{dr_L}{dt} \cos(\Omega\tau + \phi) - r_L \left(\Omega + \frac{d\phi}{dt}\right) \sin(\Omega\tau + \phi) \tag{3.79}$$

$$\frac{dy}{dt} = \frac{dY_o}{dt} + \frac{dr_L}{dt} \sin(\Omega\tau + \phi) + r_L \left(\Omega + \frac{d\phi}{dt}\right) \cos(\Omega\tau + \phi) \tag{3.80}$$

Solving Eq. 3.79 (3.80) for dX_o/dt (dY_o/dt) yields

$$\frac{dX_o}{dt} = \frac{dx}{dt} - \frac{dr_L}{dt} \cos(\Omega\tau + \phi) + r_L \left(\Omega + \frac{d\phi}{dt}\right) \sin(\Omega\tau + \phi) \tag{3.81}$$

$$\frac{dY_o}{dt} = \frac{dy}{dt} - \frac{dr_L}{dt} \sin(\Omega\tau + \phi) - r_L \left(\Omega + \frac{d\phi}{dt}\right) \cos(\Omega\tau + \phi) \tag{3.82}$$

Using Eqs. 3.11 and 3.12 for the velocity terms yields

$$\frac{dX_o}{dt} = \left[-v_t + r_L \left(\Omega + \frac{d\phi}{dt} \right) \right] \sin \left(\Omega \tau + \phi \right) - \frac{dr_L}{dt} \cos \left(\Omega \tau + \phi \right) \quad (3.83)$$

$$\frac{dY_o}{dt} = \left[v_t - r_L \left(\Omega + \frac{d\phi}{dt} \right) \right] \cos \left(\Omega \tau + \phi \right) - \frac{dr_L}{dt} \sin \left(\Omega \tau + \phi \right) \quad (3.84)$$

The Larmour radius is rewritten using the momentum equivalent of Eq. 3.10, and the result is

$$\frac{dX_o}{dt} = \frac{p_t}{m_o \Omega_o} \left[\left(-\frac{\Omega_o}{\gamma} + \Omega + \frac{d\phi}{dt} \right) \sin \left(\Omega \tau + \phi \right) - \frac{dp_t}{dt} \frac{1}{p_t} \cos \left(\Omega \tau + \phi \right) \right] \quad (3.85)$$

$$\frac{dY_o}{dt} = \frac{p_t}{m_o \Omega_o} \left[\left(\frac{\Omega_o}{\gamma} - \Omega - \frac{d\phi}{dt} \right) \cos \left(\Omega \tau + \phi \right) \cdot \frac{dp_t}{dt} \frac{1}{p_t} \sin \left(\Omega \tau + \phi \right) \right] \quad (3.86)$$

These equations are rewritten in terms of Γ, and rearranged to yield

$$\frac{dX_o}{dt} = \frac{p_t \gamma_o}{m_o \Omega} \left\{ \left[-\frac{\Omega_o}{\gamma} + \frac{1}{s} \left(\omega - s \frac{d\Gamma}{dt} \right) \right] \sin \left(\Omega \tau + \phi \right) - \frac{dp_t}{dt} \frac{1}{p_t} \cos \left(\Omega \tau + \phi \right) \right\}$$

$$(3.87)$$

$$\frac{dY_o}{dt} = \frac{p_t \gamma_o}{m_o \Omega} \left\{ \left[\frac{\Omega_o}{\gamma} - \frac{1}{s} \left(\omega - s \frac{d\Gamma}{dt} \right) \right] \cos \left(\Omega \tau + \phi \right) - \frac{dp_t}{dt} \frac{1}{p_t} \sin \left(\Omega \tau + \phi \right) \right\}$$

$$(3.88)$$

As a partial check of the validity of these equations, substitution of dc values of p_t, r_L, γ, Γ, and Ω show that the right-hand side collapses to zero, with the result

$$\frac{dX_o}{dt} = 0 \quad (3.89)$$

- 109 -

$$\frac{dY_o}{dt} = 0 \qquad\qquad (3.90)$$

which is the expected result.

The nonlinearity of this form of guiding center analysis is seen in the presence of (dp_t/dt) and $(d\Gamma/dt)$ on the right-hand side. These in effect state that the RF effects on the guiding center motion are due in part to the change in the RF conditions seen by the electrons as they drift in the waveguide. Graphical analysis of the impact of these terms is presented in Section 5.4.

3.6 Derivation of Differential Description of Particle Energy

Chapter III has been a presentation of the analytic tools needed to model and predict the behavior of the electron beam under the influence of the dc and RF electromagnetic fields assumed present in the waveguide. The topic in this section is not a trajectory equation, but an energy equation. In gyrotron (and peniotron) devices, the goal is to convert kinetic energy of the electron beam into field energy by a particular optimization of the electron cyclotron resonance interaction. The energy equation derived in this section describes the time rate of change of kinetic (actually, the total energy is represented, but only the kinetic part changes) energy for a charged particle, and thus belongs in this section for essentially the same reason that the beam→field coupling term belonged in Section II.

The energy equation comes from the same formulation that may be used to derive the Lorentz force equation that formed the basis for the trajectory analysis of Section 3.3. The Lorentz force equation and the energy equation analyzed in this chapter may both be derived[55,36,41] from the application of Hamilton's principle of least action to the Lagarangian of a charged relativistic particle moving in the presence of external electromagnetic fields.

The energy equation may be cast in terms of the particle momentum as

$$\frac{d(KE)}{dt} = - \frac{|e|}{\gamma m_o} \vec{p} \cdot \vec{E} \tag{3.91}$$

where (KE) is the kinetic energy of the electrons, representing both transverse and longitudinal motion. Specifically, Eq. 3.91 yields the change in kinetic energy; however, since only the kinetic energy is changing, the total change in energy is also given by the same equation. Equation 3.91 may be expanded in rectangular coordinates as

$$\frac{d(KE)}{dt} = - \frac{|e|}{\gamma m_o} \left(p_x E_x + p_y E_y \right) \tag{3.92}$$

where $E_z = 0$ for a TE mode. It is noted that the E_z fields included in Section II were due solely to the presence of nonideal waveguide walls. These E_z fields exist within the wall of the waveguide, having an appreciable value to a single skin depth in the material of the wall. Since all kinetic energy of any electron contacting the wall will immediately be lost to the interaction, these fields are not considered

in the present analysis. Equations 3.13 and 3.14 may be used, along with Euler's form, to rewrite Eq. 3.92 as

$$\frac{d(KE)}{dt} = -\frac{|e|}{\gamma m_o}\frac{p_t}{2}j\left[e^{j\alpha}(E_x - jE_y) - e^{-j\alpha}(E_x + jE_y)\right] \qquad (3.93)$$

where the shorthand notation $\alpha = \Omega\tau + \Phi$ has been used. Equation A.19 is used to transform to cylindrical field expressions, yielding

$$\frac{d(KE)}{dt} = -\frac{|e|}{\gamma m_o}\frac{p_t}{2}j\left[e^{j\alpha}(E_r - jE_\theta)e^{-j\theta} - e^{-j\alpha}(E_r + jE_\theta)e^{j\theta}\right] \qquad (3.94)$$

Now the same process used in Section 3.4 (outlined in Appendix C) is used to yield an expression for d(KE)/dt that extends to cyclotron harmonics. Equation 3.58 is substituted into Eq. 3.94, Graf's theorem is applied, the time factor exp(jωt) is multiplied in, and the real part is taken. This process yields

$$\frac{d(KE)}{dt} = \text{Re}\left\{-\frac{|e|}{\gamma m_o}\frac{p_t}{2}V_m C_{mn}k_{tm}J_{m-s}(R_o)\left[J_{s-1}(R_L) - J_{s+1}(R_L)\right]e^{j\Gamma}\right\} \qquad (3.95)$$

where Eq. 3.68 was used for Γ. Rearranging and making use of the Bessel function identity,[61]

$$B_n'(x) = \frac{1}{2}\left[B_{n-1}(x) - B_{n+1}(x)\right] \qquad (3.96)$$

yields

$$\frac{d(KE)}{dt} = -\frac{|e|}{\gamma m_o} p_t C_{mn} J_{m-s}(R_o) \frac{\partial J_s(R_L)}{\partial r_L} \text{Re} \left\{ V_m e^{j\Gamma} \right\} \qquad (3.97)$$

This result is a differential equation to be used in the calculation of the change of energy of the electrons under the influence of the electromagnetic field. As would be expected for an equation dealing with the gyrotron interaction, the rate of energy loss is proportional to the transverse momentum. This reflects the saturation mechanism that limits the efficiency of the gyrotron interaction for nonfundamental cyclotron harmonic operation.[17,18,72] In a device optimized for the gyrotron interaction, irregardless of the cyclotron harmonic chosen for interaction, the saturation mechanism that limits the interaction is phase trapping, which occurs when an average electron loses enough (transverse) energy that it no longer gyrates at a frequency matching the RF wave frequency.

This equation also presents the clearest picture of the ideal limit of efficiency for a gyrotron device. The available kinetic energy is that which is represented by transverse motion. This result would tend to support the use of the assumption that $dp_z/dt \ll dp_t/dt$.

The principle application in the present work is as a verification of trajectory analysis; i.e., Eq. 3.97 is used to verify that the p_t and p_z values for each particle represent the correct amount of kinetic energy for the particle. It is interesting to note that

$$v_t \frac{dp_t}{dt} + v_z \frac{dp_z}{dt} = \frac{d(KE)}{dt}$$

which may be written as

$$\frac{\vec{p}}{\gamma m} \cdot \frac{d\vec{p}}{dt} = \frac{d(KE)}{dt} \tag{3.98}$$

where the representations in Eqs. 3.76, 3.78, and 3.97 are used and taper terms are dropped. This provides a separate form of verification of both the analytic validity of the equations and of the numerical values calculated using these equations.

IV. NUMERICAL IMPLEMENTATION OF LARGE SIGNAL NONLINEAR THEORY

4.1 Introduction

Sections II and III are analytic in nature. They present an analysis of the gyrotron interaction under a specific set of assumptions and are subject to certain physical laws. In order for the analysis and presentation of the models in these two sections to be useful, the analytical models must be coupled in a single, unified numerical model and implemented on a computer.

Section IV explains the process of collecting the disjointed pieces of work found in previous sections into a single cohesive numerical model. The computer code which implements the model is named AMINUS and is referred to as such for the remainder of this report. The code is written in Fortran, conforming largely to the 1977 ANSI standard for the Fortran language. The nonconforming aspects of the code were included to take advantage of machine specific features available on the Hewlett-Packard 1000 computer used for this work. This computer is maintained by the Department of Electrical Engineering at the University of Utah for research purposes. Due to the use of machine specific features, AMINUS is not portable, although the extensions to the ANSI standard used are "semistandard" extensions found on many computer systems.

Section 4.2 provides a description of the final analytic set of equations. The process of preparing the numerical model necessitates the addition of a new equation. Terms included in the system of equations for convenience are also discussed.

Section 4.3 presents the derivation of the coupling term $\left(E_{bf}\right)$ in a form specific to circular waveguides. This derivation is accomplished via the application of Graf's addition theorem for Bessel functions. Graf's theorem itself is discussed in Appendix C.

Section 4.4 is a flow chart type discussion of the process used to solve the numerical model presented in Sections 4.2 and 4.3. The method of programming used to preserve the advantages of the RF field theory is discussed briefly.

Section 4.5 deals with the choice of the algorithm used to integrate the differential equations in the numerical model. The decision criteria, the evaluation of each of the types of algorithm with respect to the criteria, and the final choice are discussed. The selected algorithm is based on the Gill implementation of the fourth order Runge-Kutta algorithm.

Section 4.6 presents the method used for identification of synchronous frequency parameters. In order for the gyrotron interaction to occur, a specific relationship between the field frequency, the waveguide cutoff frequency, and the electron cyclotron frequency must exist.

Section 4.7 is a discussion of the process of verifying that AMINUS results accurately represent the gyrotron interaction. The verification process was quite extensive, and involved the use of several stages of testing. It was found that excellent agreement existed between AMINUS and results predicted by various methods, including previously published data. It is noted that some error unavoidably exists in the numerical model.

Section 4.8 is a summary of the numerical implementation process and a discussion of AMINUS itself with regard to the analytical model.

4.2 Preparation of Numerical Model

Sections II and III presented the equations required to calculate the derivatives for, respectively, the RF electromagnetic field quantities and the particle related quantities. The combination of these two independent derivations into a unified numerical model is presented in this section. Equations 2.103, 2.104, and 2.105 contain the derivatives of the field quantities in the form we will begin with. Equations 3.76, 3.77, 3.78, 3.87, 3.88, and 3.97 contain the derivatives for the particle quantities for a single particle. These equations are collected and written here for clarity.

$$\frac{dV_n}{dz} = -jk_z Z_n I_n + \sum_k T_{kn} V_k + jk \sum_k Z_{nk} I_k \tag{4.1}$$

$$\frac{dI_n}{dz} = -j \frac{k_z}{Z_n} V_n - \sum_k T_{nk}^* I_k - jk \sum_k Y_{nk} V_k - E_{bf} \tag{4.2}$$

$$\frac{dp_t}{dt} = -|e| C_{mn} J_{m-s}(R_o) \frac{\partial J_s(R_L)}{\partial r_L} \, \text{Re}\left\{ (V_m - v_z I_m) \, e^{j\Gamma} \right\} + \frac{p_t p_z}{2\gamma m_o} \frac{\partial B_{oz}}{\partial z} \tag{4.3}$$

$$\frac{d\Gamma}{dt} = \left(\omega - s\Omega \frac{\gamma_o}{\gamma} \right) - \frac{s|e|}{p_t} C_{mn} J_{m-s}(R_o) \frac{s}{r_L} J_s(R_L)$$

$$\times \, \text{Re}\left\{ j \left[V_m - v_z I_m - \frac{v_t^2 k_{tm}^2}{s\Omega\omega} \frac{\gamma}{\gamma_o} V_m \right] e^{j\Gamma} \right\} \tag{4.4}$$

$$\frac{dp_z}{dt} = -|e| \, v_t C_{mn} J_{m-s}(R_o) \, \frac{\partial J_s(R_L)}{\partial r_L} \, \mathrm{Re}\left\{ I_m \, e^{j\Gamma} \right\} - \frac{p_t^2}{2\gamma m_o} \frac{1}{B_{oz}} \frac{\partial B_{oz}}{\partial z} \qquad (4.5)$$

$$\frac{dX_o}{dt} = \frac{p_t \gamma_o}{m_o \Omega} \left\{ \left[-\frac{\Omega_o}{\gamma} + \frac{1}{s}\left(\omega - s\frac{d\Gamma}{dt} \right) \right] \sin\left(\Omega\tau + \phi\right) - \frac{dp_t}{dt} \frac{1}{p_t} \cos\left(\Omega\tau + \phi\right) \right\}$$

$$(4.6)$$

$$\frac{dY_o}{dt} = \frac{p_t \gamma_o}{m_o \Omega} \left\{ \left[\frac{\Omega_o}{\gamma} - \frac{1}{s}\left(\omega - s\frac{d\Gamma}{dt} \right) \right] \cos\left(\Omega\tau + \phi\right) - \frac{dp_t}{dt} \frac{1}{p_t} \sin\left(\Omega\tau + \phi\right) \right\}$$

$$(4.7)$$

$$\frac{d(KE)}{dt} = -\frac{|e|}{\gamma m_o} \, p_t C_{mn} J_{m-s}(R_o) \, \frac{\partial J_s(R_L)}{\partial r_L} \, \mathrm{Re}\left\{ V_m \, e^{j\Gamma} \right\} \qquad (4.8)$$

It is immediately recognized that, for a model in which N macro-particles are used to represent the electron beam, the system of equations described in Eqs. 4.1 through 4.8 is of the form shown in Fig. 4.1.

Since there are six equations per particle, plus two equations describing the RF fields, the system of equations depicted in Fig. 4.1 is said to be of order 6N + 2, where the order refers to the total number of equations calculated at each new longitudinal position. As written, the system consists of 2 complex equations (for V and I) and 6N real equations (or 6N equations involving only the real part of complex quantities).

For the model to be internally consistent, it is required that a single variable be selected as the independent variable. The derivation of the beam coupling term (see Section 2.6) was predicated on the

- 118 -

$$\frac{dV}{dz}$$

$$\frac{dI}{dz}$$

$$\frac{dp_t}{dt}$$

$$\frac{d\Gamma}{dt}$$

$$\frac{dp_z}{dt}$$

$$\frac{dX_0}{dt}$$

$$\frac{dY_0}{dt}$$

$$\alpha(\Gamma,\tau)$$

$$\gamma(p_t,p_z)$$

$$\frac{d(KE)}{dt}$$

. . . .

$$\frac{dp_t}{dt}$$

$$\frac{d\Gamma}{dt}$$

$$\frac{dp_z}{dt}$$

$$\frac{dX_0}{dt}$$

$$\frac{dY_0}{dt}$$

$$\alpha(\Gamma,\tau)$$

$$\gamma(p_t,p_z)$$

$$\frac{d(KE)}{dt}$$

Equations describing RF electromagnetic fields

Equations describing particle number 1

Equations describing particles 2 through (N_{part} - 1)

Equations describing particle number N_{part}
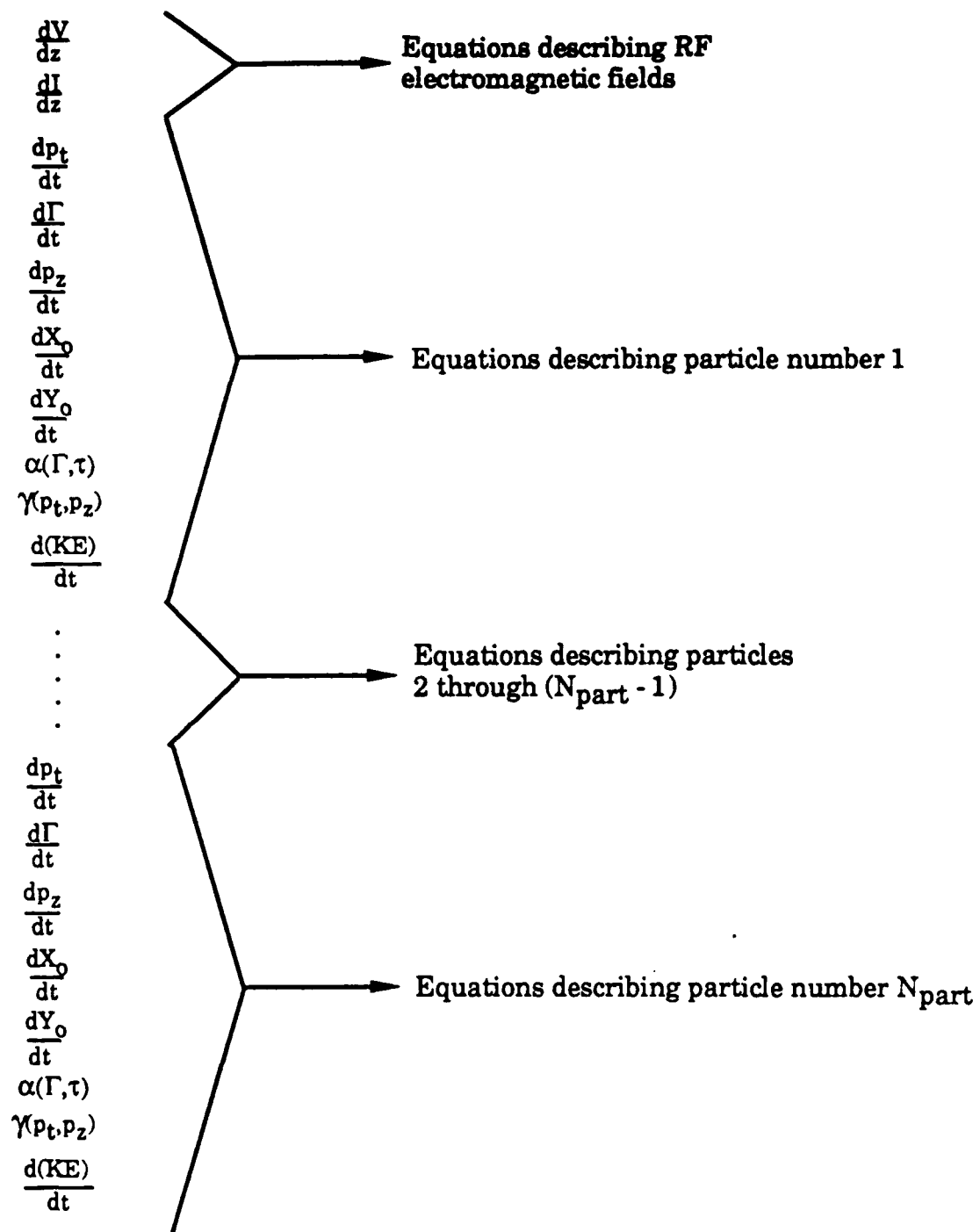
Fig. 4.1. Diagrammatic representation of the system of equations used in the numerical model of an N-particle representation of the electron beam.

selection of z as the independent variable. The transformation

$$\frac{d}{dt} = \frac{dz}{dt}\frac{d}{dz} = v_z\frac{d}{dz} = \frac{p_z}{\gamma m_o}\frac{d}{dz} \tag{4.9}$$

is introduced to allow the particle equations to be calculated as z dependent quantities. Equation 4.9 is rearranged, and when applied to the time derivative of a general function F produces

$$\frac{dF}{dz} = \frac{\gamma m_o}{p_z}\frac{dF}{dt} \tag{4.10}$$

Using Eq. 4.10 as a transformation rule, the previously presented particle equations are now written as

$$\frac{dp_t}{dz} = -|e|\frac{\gamma m_o}{p_z}C_{mn}J_{m-s}(R_o)\frac{\partial J_s(R_L)}{\partial r_L}\,\text{Re}\left\{(V_m - v_z I_m)\,e^{j\Gamma}\right\} + \frac{p_t}{p_z}\frac{1}{B_{oz}}\frac{\partial B_{oz}}{\partial z} \tag{4.11}$$

$$\frac{d\Gamma}{dz} = \frac{\gamma m_o}{p_z}\left(\omega - s\Omega\frac{\gamma_o}{\gamma}\right) - s|e|\frac{\gamma m}{p_z}\frac{C_{mn}}{p_t} \times J_{m-s}(R_o)\frac{s}{r_L}J_s(R_L)$$

$$\times\,\text{Re}\left\{j\left[V_m - v_z I_m - \frac{v_t^2 k_{tm}^2}{s\Omega\omega}\frac{\gamma}{\gamma_o}V_m\right]e^{j\Gamma}\right\} \tag{4.12}$$

$$\frac{dp_z}{dz} = -|e|\,C_{mn}\frac{p_t}{p_z}J_{m-s}(R_o)\frac{\partial J_s(R_L)}{\partial r_L} \times\,\text{Re}\left\{I_m\,e^{j\Gamma}\right\} - \frac{p_t^2}{2p_z}\frac{1}{B_{oz}}\frac{\partial B_{oz}}{\partial z} \tag{4.13}$$

- 120 -

$$\frac{dX_o}{dz} = \frac{p_t \gamma_o}{m_o \Omega} \left\{ \left[\frac{\gamma m_o}{p_z} \left(\frac{\omega}{s} - \Omega \frac{\gamma_o}{\gamma} \right) - \frac{d\Gamma}{dz} \right] \sin \alpha - \frac{1}{p_t} \frac{dp_t}{dz} \cos \alpha \right\} \qquad (4.14)$$

$$\frac{dY_o}{dz} = \frac{p_t \gamma_o}{m_o \Omega} \left\{ \left[- \frac{p_z}{\Gamma m_o} \left(\frac{\omega}{s} - \Omega \frac{\gamma_o}{\gamma} \right) + \frac{d\Gamma}{dz} \right] \cos \left(\Omega \tau + \phi \right) - \frac{1}{p_t} \frac{dP_t}{dz} \sin \left(\Omega \tau + \phi \right) \right\}$$
$$(4.15)$$

$$\frac{d(KE)}{dz} = -|e| \frac{p_t}{p_z} C_{mn} J_{m-s}(R_o) \frac{\partial J_s(R_L)}{\partial r_L} \operatorname{Re} \left\{ V_m \, e^{j\Gamma} \right\} \qquad (4.16)$$

and a new equation is added that calculates the quantity

$$\frac{dt}{dz} = \frac{\gamma m_o}{p_z} \qquad (4.17)$$

for each particle. This allows the particles to move with their own z velocity, $v_z = p_z / (\gamma m_o)$.

The requirement for this transformation, or for the selection of a single independent variable, may be seen from a consideration of the numerical modeling process. First, recall that the present work is focused on the building of a self-consistent model, which was introduced in Section 1 and explained further in Section 2.6. The fundamental principle behind self-consistency is that the RF fields are based on and/or perturbed by the currents in the waveguide, and the particles in the waveguide are subject to the forces resulting from these current based and/or perturbed RF fields. If the fields and particles were not constrained to exist at the same independent variable (z or t), they would be disconnected from each other by not a physical, but a numerical

- 121 -

process, and the self-consistency and physical relevancy of the solution would be destroyed. In effect, the forces on the particles at a time t_1 (or a spatial location z_1) would be calculated based on the fields as they were at some other time t_2 (or spatial location z_2). It is likewise possible to consider problems in terms of the RF fields being perturbed by the particle distribution and energy as occuring at some other temporal or spatial location than the point at which the fields are being evaluated. The selection of a single independent variable forces the model to represent the physical interaction of the RF fields and the particles as they propagate together down the waveguide. Numerically, this requirement has forced the system of equations up in order via the addition of an equation of the form in Eq. 4.17 for each particle. The resulting system is of order 7N + 2.

In addition to the seven derivative equations per particle now calculated each iteration, two more equations per particle have been added in the computer implementation of the analytical model. These equations are added for three reasons: convenience, usefulness in tracing quantities which vary in z but which have no analytic derivative form, and for use in the verification of accuracy. The first of these additional quantities is γ, the relativistic correction factor, which is calculated numerically as

$$\gamma = \left[1 + \frac{p_t^2 + p_z^2}{\left(m_o c \right)^2} \right]^{1/2} \tag{4.18}$$

Calculation of γ each time p_t and p_z are updated (at each new longitudinal position) allows the total power in the electron beam, the

energy in each macroparticle, and the ensemble electronic efficiency to be calculated. The total power and the energy per particle are used in the evaluation of conservation theorems and provide a method of verification which is discussed in Section 4.8. The ensemble electronic efficiency may be calculated directly from knowledge of γ for each particle as

$$\eta_{el} = \frac{\gamma_o - \frac{1}{N} \sum_{j=1}^{N} \gamma_j}{\gamma_o - 1} \qquad (4.19)$$

Equation 4.19 is derived and discussed briefly in Appendix D. There is no derivative equation for γ in this model, rather it is calculated at the top of each computational cycle for use in subsequent calculation of new derivative quantities.

The second nonderivative quantity to be added to the model is $\alpha = \Omega\tau + \Phi$ (see Fig. 3.2), where Φ is the variable storing the phase effects of the RF fields on the particle momentum. α contains this information in a much more accessible form than Γ (as calculated in Eq. 4.12), and so, at each cycle, α is calculated as a function of Γ.

With these two additions, the final system of equations used to numerically model the gyrotron interaction is derived. The system is now of order $9N + 2$, and is shown in Fig. 4.2. A single set of equations (which is also the entire set of equations for a one particle system) is given as

$$\frac{dV_n}{dz} = - jk_z Z_n I_n + \sum_k T_{kn} V_k + jk \sum_k Z_{nk} I_k \qquad (4.20)$$

- 123 -

$$\frac{dV}{dz}$$

$$\frac{dI}{dz}$$

$$\frac{dp_t}{dz}$$

$$\frac{d\Gamma}{dz}$$

$$\frac{dp_z}{dz}$$

$$\frac{dX_0}{dz}$$

$$\frac{dY_0}{dz}$$

$$\alpha(\Gamma,\tau)$$

$$\gamma(p_t,p_z)$$

$$\frac{d(KE)}{dz}$$

$$\frac{dt}{dz}$$

.
.
.
.

$$\frac{dp_t}{dz}$$

$$\frac{d\Gamma}{dz}$$

$$\frac{dp_z}{dz}$$

$$\frac{dX_0}{dz}$$

$$\frac{dY_0}{dz}$$

$$\alpha(\Gamma,\tau)$$

$$\gamma(p_t,p_z)$$

$$\frac{d(KE)}{dz}$$

$$\frac{dt}{dz}$$

Equations describing RF electromagnetic fields

Equations describing particle number 1

Equations describing particles 2 through $(N_{part} - 1)$

Equations describing particle number N_{part}
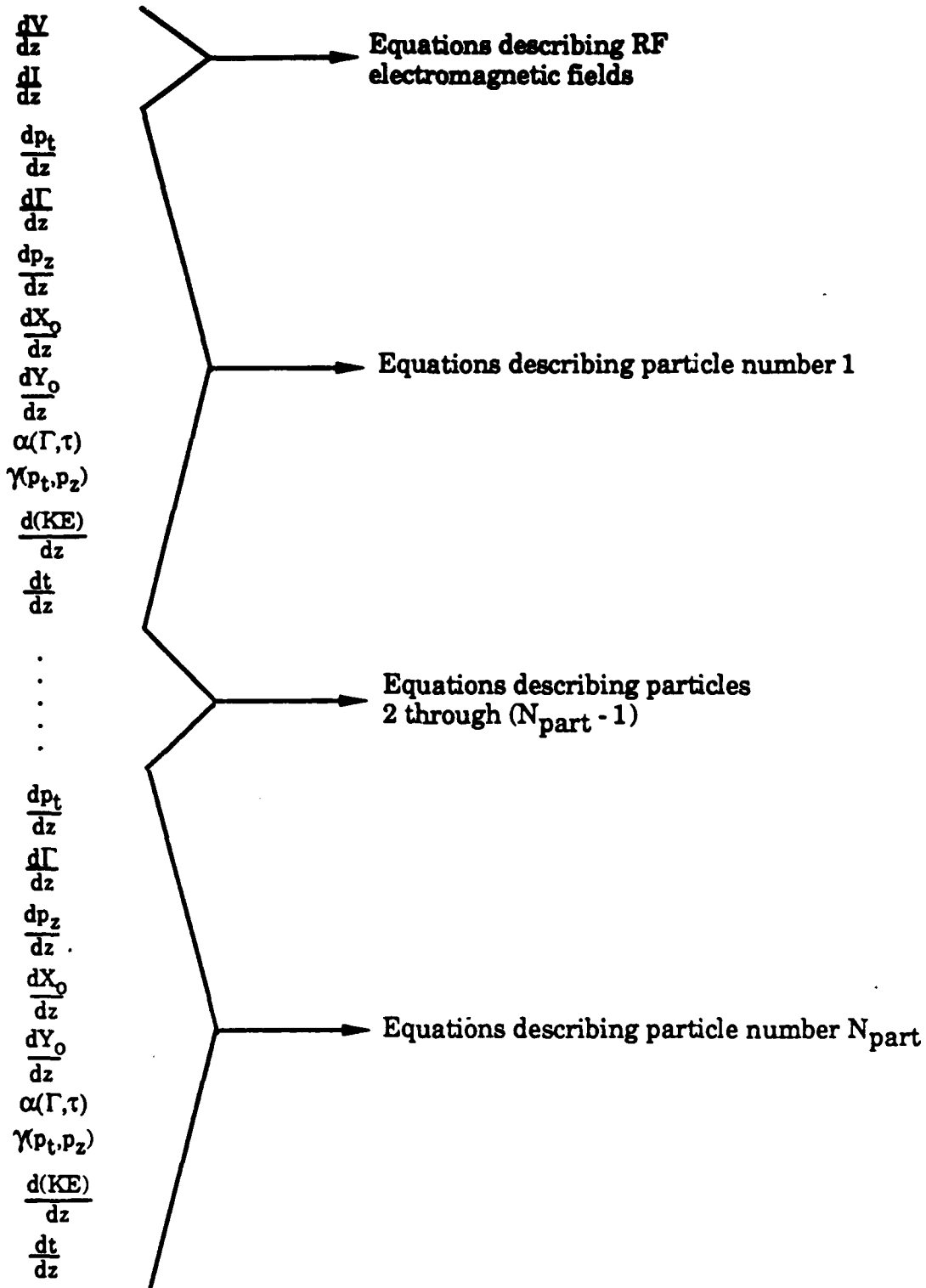
Fig. 4.2. Diagrammatic representation of final system of equations used in the computer implementation of the analytic model. The system is of order 9N + 2.

$$\frac{dI_n}{dz} = -j \frac{k_z}{Z_n} V_n - \sum_k T_{nk}^* I_k - jk \sum_k Y_{nk} V_k - E_{bf} \qquad (4.21)$$

$$\frac{dp_t}{dz} = -|e| \frac{\gamma m}{p_z} C_{mn} J_{m-s}(R_o) \frac{\partial J_s(R_L)}{\partial r_L} \text{Re}\left\{(V_m - v_z I_m) e^{j\Gamma}\right\} + \frac{p_t}{2} \frac{1}{B_{oz}} \frac{\partial B_{oz}}{\partial z}$$

$$(4.22)$$

$$\frac{d\Gamma}{dz} = \frac{\gamma m}{p_z}\left(\omega - s\Omega \frac{\gamma_o}{\gamma}\right) - s|e| \frac{\gamma m_o}{p_z} \frac{C_{mn}}{p_t} \times J_{m-s}(R_o) \frac{s}{r_L} J_s(R_L)$$

$$\times \text{Re}\left\{j\left[V_m - v_z I_m - \frac{v_t^2 k_{tm}^2}{s\Omega\omega} \frac{\gamma}{\gamma_o} V_m\right] e^{j\Gamma}\right\} \qquad (4.23)$$

$$\frac{dp_z}{dz} = -|e| C_{mn} \frac{p_t}{p_z} J_{m-s}(R_o) \frac{\partial J_s(R_L)}{\partial r_L} \times \text{Re}\left\{I_m e^{j\Gamma}\right\} - \frac{p_t^2}{2p_z} \frac{1}{B_{oz}} \frac{\partial B_{oz}}{\partial z} \qquad (4.24)$$

$$\frac{dX_o}{dz} = \frac{p_t \gamma_o}{m_o \Omega}\left\{\left[\frac{\gamma m_o}{p_z}\left(\frac{\omega}{s} - \Omega \frac{\gamma_o}{\gamma}\right) - \frac{d\Gamma}{dz}\right] \sin \alpha - \frac{1}{p_t} \frac{dp_t}{dz} \cos \alpha\right\} \qquad (4.25)$$

$$\frac{dY_o}{dz} = \frac{p_t \gamma_o}{m_o \Omega}\left\{\left[-\frac{\gamma m_o}{p_z}\left(\frac{\omega}{s} - \Omega \frac{\gamma_o}{\gamma}\right) + \frac{d\Gamma}{dz}\right] \cos(\Omega\tau + \phi) - \frac{1}{p_t} \frac{dp_t}{dz}\sin(\Omega\tau + \phi)\right\}$$

$$(4.26)$$

$$\frac{d(KE)}{dz} = -|e| \frac{p_t}{p_z} C_{mn} J_{m-s}(R_o) \frac{\partial J_s(R_L)}{\partial r_L} \text{Re}\left\{V_m e^{j\Gamma}\right\} \qquad (4.27)$$

$$\frac{dt}{dz} = \frac{\gamma m_o}{p_z} \qquad (4.28)$$

$$\gamma = f(p_t, p_z) \qquad (4.29)$$

$$\alpha = f(\Gamma, t) \qquad (4.30)$$

The system of equations in Eqs. 4.20-4.30 is highly nonlinear, as can be seen from the presence of dp_t/dz and $d\Gamma/dz$ in Eqs. 4.25 and 4.26. The nonlinearity of the system was also pointed out when it was shown that the time derivative of the particle energy could be written in terms of the vector product

$$\frac{\vec{p}}{\gamma m} \cdot \frac{d\vec{p}}{dz} = \frac{d(KE)}{dz} \qquad (3.98)$$

4.3 Specific Form of Beam-Field Coupling Coefficient

The final general analytic form for E_{bf} was presented in Section 2.6. The result was given in Eq. 2.115 as

$$E_{bf} = -|e| \frac{\omega}{2\pi} \sum_{i=1}^{N} \frac{\vec{v}_{ti} \cdot \vec{e}_n^*(\vec{r}_{ti})}{v_{zi}} e^{-j\omega t_i} \qquad (4.31)$$

Equation 4.31 is a general form, which, by use of appropriate expressions for $\vec{v}_{ti}$ and $\vec{e}_n^*$, may be used in systems characterized by rectangular or cylindrical geometry. In this section, the needed expressions will be derived for application to a circular waveguide geometry.

The vector transverse velocity may be written as (an extension of Eq. A.17)

$$\vec{v}_t = v_t(j\hat{r} + \hat{\theta}) e^{j(\alpha - \theta)} \qquad (4.32)$$

The recipe for calculating the analytic expressions for $\vec{e}_n^*$ is given in Eq. 2.11a. The scalar wave function ψ_{mn} is given in Eq. 2.9 as

$$\psi_{mn} = C_{mn} J_m(R) e^{-jm\theta} \tag{4.33}$$

$\vec{e}_n^*$ is a function of ψ_{mn}^* and is calculated as

$$\vec{e}_n^* = -\vec{\nabla}_t \psi_{mn}^* \times \hat{z}$$

$$= -(\vec{\nabla}_t \times \hat{z}) \psi_{mn}^*$$

$$= -\left[\left(\frac{\partial}{\partial r}\hat{r} + \frac{1}{r}\frac{\partial}{\partial\theta}\hat{\theta}\right) \times \hat{z}\right] C_{mn} J_m(k_t n) e^{+jm\theta}$$

$$= \left(\frac{\partial}{\partial r}\hat{\theta} - \frac{1}{r}\frac{\partial}{\partial\theta}\hat{r}\right) C_{mn} J_m(k_t n) e^{jm\theta}$$

$$= C_{mn}\left[k_{tn} J_m'(R)\hat{\theta} - j\frac{m}{r} J_m(R)\hat{r}\right] e^{jm\theta}$$

$$= C_{mn} k_{tn}\left[J_m'(R)\hat{\theta} - j\frac{m}{R} J_m(R)\hat{r}\right] e^{jm\theta} \tag{4.34}$$

Equations 4.32 and 4.34 may be used to calculate the dot product term in Eq. 4.31.

$$\vec{v}_t \cdot \vec{e}_n^* = C_{mn} v_t k_{tn}\left[\frac{m}{R} J_m(R) + J_m'(R)\right] e^{j(m-1)\theta} e^{j\alpha}$$

The bracket term may be reduced via use of[23]

$$J_{m-1}(x) = J_m'(x) + \frac{m}{x} J_m(x)$$

where $J_m'(x)$ denotes the derivative of J_m with respect to x. The result is

$$\vec{v}_t \cdot \vec{e}_n^* = C_{mn} v_t k_{tn} J_{m-1}(R) e^{j(m-1)\theta} e^{j\alpha} \qquad (4.35)$$

Equation 4.35 is a function of true geometry coordinates; that is, the spatial variables are expressed in terms of the absolute position relative to the geometric center of the waveguide. The expression as written is not capable of dealing with the presence of cyclotron harmonics. The application of Graf's addition theorem for Bessel functions (see Appendix C) to Eq. 4.35 will transform the expression to one in which the spatial variables are expressed in terms of the guiding center variables discussed in Section 3.5. Further, the resulting expressions will be capable of expressing the effects of the cyclotron harmonics on the coupling term. The portion of Eq. 4.35 dealt with in the application of Graf's theorem is $e^{j(m-1)\theta} J_{m-1}(R)$, for which an expansion is given in Appendix C, Eq. C.16. Substitution of this result into Eq. 4.31 yields

$$E_{bf} = -|e| \, C_{mn} k_{tn} \, \frac{\omega}{2\pi} \sum_{i=1}^{N} \frac{v_{ti}}{v_{zi}} J_{m-s}\left(R_{o_i}\right) J_{s-1}\left(R_{L_i}\right) e^{-j\Gamma_i} \qquad (4.36)$$

where Γ is defined in Eq. 3.68.

Equation 4.36 is the form of E_{bf} implemented in the computer code. It should be noted that a phase term consistent with previous particle calculations has resulted in the present analysis.

4.4 Numerical Solution Flow Chart and Process

This section will describe the steps within the computer code involved in solving the system of equations discussed in Section 4.2. In total, in excess of twenty-five subprograms are involved in the solution of the problem. Some of these calculate Bessel functions and other standard quantities and are not discussed further.

The flow chart in Fig. 4.3 presents a sketch of the computer program. It should be noted that several z-dependent quantities, including B_{oz}, r_w, and Z_w, are calculated in separate subprograms. This arrangement allows a great deal of control over the physical device these quantities model. Wall tapers are modeled by having the wall radius subprogram, RWZ, return a value that corresponds to a chosen waveguide profile. Similarly, dc magnetic field profiles are represented by appropriate values of B_{oz} returned by subprogram BOZ. Subprogram ZWZ serves a similar function, returning a numerical value representing the researcher's choice of electrical characteristics for the waveguide wall. Each of these three program units may return values found by one of three methods. One method would consist of a table of data giving the profile at specific points and the use of an interpolation routine to calculate values for longitudinal positions not specifically included in the table. The second method would be in the form of algebraic relations for each smoothly varying section of the profile, with the profiles calculated as a function of z. Each of these first two methods would be based on input data provided by the researcher before the run began. The third method would be based on an
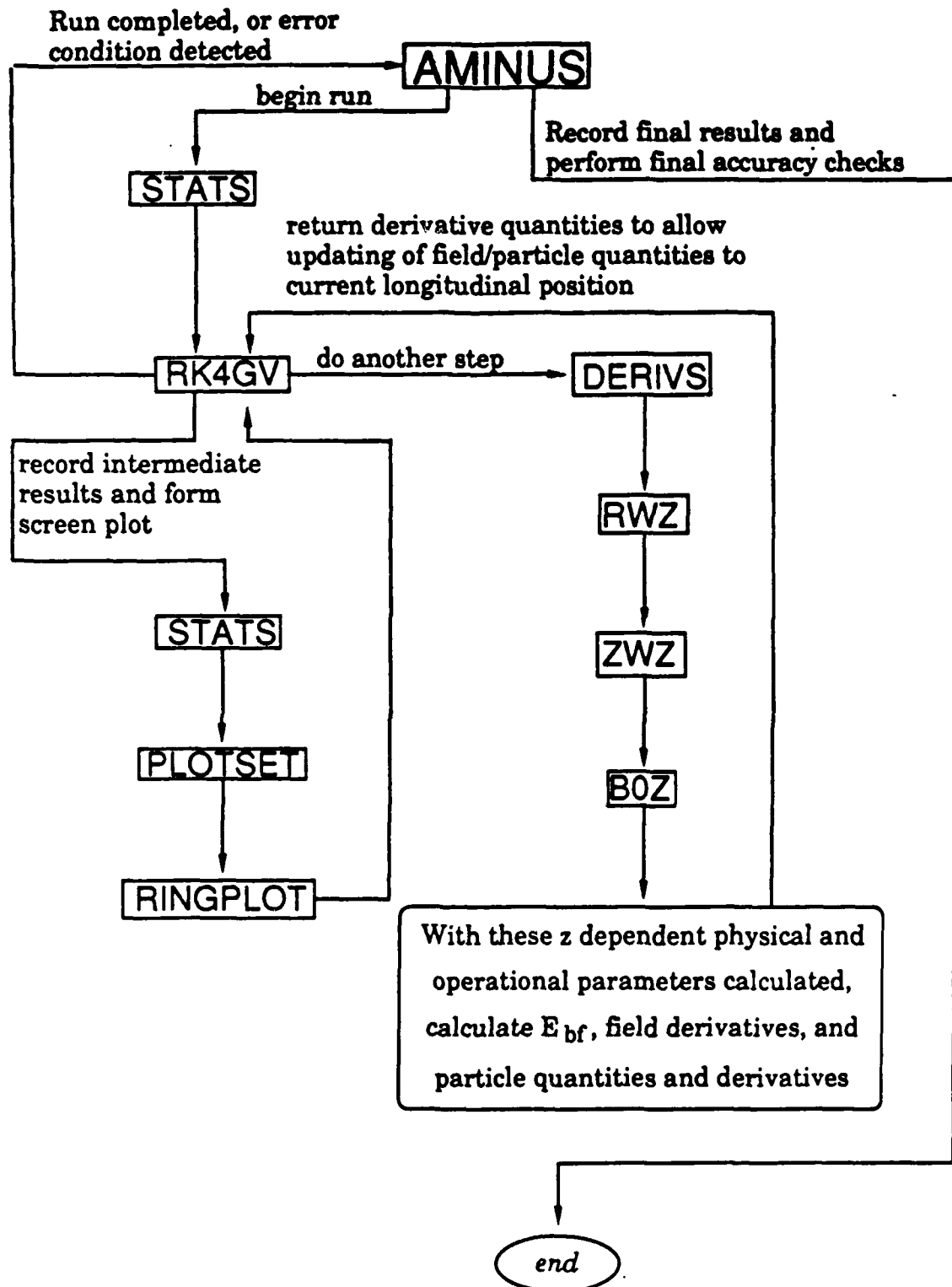
Fig. 4.3. Flow chart for computer simulation of gyrotron interaction as modeled by Eqs. 4.20-4.30 and Eq. 4.36.

optimization scheme in which the profiles are selected in such a way as to optimize with respect to a selection interaction parameter, e.g., RF power, electronic efficiency,[31] or rate of gain.

The physical problem at hand is as follows: Given an injected RF electromagnetic field of known phase/amplitude, and an injected electron beam of known distribution in space/momentum, and derivatives describing the change in each of the known quantities, what will the values of the important quantities be as the interaction takes place? This problem is thus cast as an initial value problem, and is solved by successive evaluation of spatial derivatives, with each evaluation advancing the interaction forward in z. The principal tasks involved in this process are clear. First, the RF field and the electron beam must be initialized with quantities accurately representing the chosen physical characteristics. Initial information should then be stored, and the derivatives are evaluated describing the rate of change with respect to z over the interval $z(t = t_o)$ to $z(t = t_1)$. Intermediate information is stored, internal checks are performed on the accuracy of the results, and the progress of the interaction is checked to determine if continuation is in order. The final z may be chosen prior to the beginning of the computer run, or it may be chosen by the program itself based on some operator chosen criterion. Possible criterion for stopping the run might be based on efficiency, power characteristics, and/or any of a number of internal error conditions in the numerical evaluation mechanism. When the final iteration has been completed, additional data are written to file, and the run is terminated or begun again with different input data.

One of the methods of intermediate evaluation of the interaction used in the present work has been interactive screen plotting of the particle positions at selected intervals. This has allowed the researcher to develop a visual picture of the initial bunching process and the postsaturation debunching process.

4.5 Choice of Integration Routine

This section will describe the process of selection of a numerical integrator routine. Given the solution flow chart of Section 4.4, the integrator algorithm selection is a significant aspect of the work. There are several theoretical alternatives, and for each theoretical alternative, there are several variant forms of implementation.

There were three principal considerations in the selection. First, the algorithm must be robust. Limitations in the algorithm must not limit the applicability of the computer code to physically noninteresting cases. Second, the error inherent in these types of algorithms must not cause unacceptable loss of accuracy. Third, the integrator algorithm should progress from step to step as quickly as possible, which implies that the number of derivative evaluations per step should be as few as possible, where the minimum is limited by the first two considerations as well as the algorithm itself.

The classes of algorithm vary considerably in their robustness. The predictor-corrector (or multistep) methods are the least robust of the three classes,[34] having considerable difficulties with functions that do not vary smoothly.[60] The extrapolation type routines are coupled with either rational function[38,60,73] or polynomial extrapola-

tion.[60,14] Poles and combinations of poles in the extrapolating functions may cause the extrapolation step to fail, and although the algorithm may continue to run, the answers have no significance.[60] It is generally accepted that the rational function extrapolation is superior due to convergence behavior and behavior.[60,38] The Runge-Kutta methods are very robust and capable of dealing with functions with rapid changes or even functions who change rapidly at some values of the independent variable and slowly at others.

The predictor-corrector methods are capable of very good accuracy when they can cope with the demands of the function behavior. The order of accuracy is variable depending on the series expansion of the function, but fourth order accuracy is easily obtainable.[68,38] The extrapolation routines are capable of at least fourth order accuracy and may be extended to sixth order for some "well-behaved" functions.[60] The Runge-Kutta algorithm may be written in orders up to six, although the fourth order algorithm is almost universally used when Runge-Kutta is the class of algorithm of choice.[14]

The consideration of speed is the point at which the algorithms show the greatest differences. In applications where the functions being evaluated are complicated, or where a large system of equations is being integrated for each function call, the number of calls is a good indicator of relative speed[73] because the overhead of the integrator algorithms will not vary much. The extrapolation algorithms typically use the fewest function evaluations per step, and Runge-Kutta the most calls per step. The extrapolation routines can be coupled with less accurate integration methods because of the improvement gained by the

extrapolation, and thus can get by with as few as 1.5 function calls per step.[60] The well-developed predictor corrector methods are coupled with polynomial interpolation, and thus reduce the number of function calls per step to two to three.[68] Each of the classes of routine may be coupled to a step size optimizer, although the predictor corrector methods require a large amount of overhead calculation for such cases,[68] and it is not common for adaptive step size to be used with predictor-corrector methods. In cases of optimization of step size, the extrapolation routines have a clear edge in overall speed for applications in which function calls are expensive.

The actual testing of the various algorithms included versions of some publicly available integration packages. DESOLV, a professionally written PECE (predictor-estimator-corrector-estimator) algorithm was considered.[68] The researcher also wrote and tested several different versions of Runge-Kutta, predictor-corrector and extrapolation routines. The nature of the problem at hand excluded the basis predictor-corrector methods based on robustness. DESOLV was able to handle the equations, but ran very slowly when forced to render the same accuracy as other routines. There are several actual methods for implementing the Runge-Kutta algorithm. The selected basic algorithm was written by the researcher based on an algorithm given by Burden, et al.[14] The framework was used, and the actual calculation process was rewritten to utilize the Gill method.[1] This method was coupled with an adaptive step-size driver routine by Press, et al.[60] for testing. It was found that the problem was well enough behaved that an adaptive step-size driver cost more in overhead than it provided in step-size optimiza-

tion. Thus, the final choice of integrator algorithm was a simple Gill implementation of the fourth order Runge-Kutta method. This final choice of algorithm was then rewritten using the vector instruction set (VIS)[33] available on the HP 1000 on which the simulation work was performed. The VIS commands perform vector instructions very efficiently, and their use sacrificed no accuracy while significantly decreasing the time spent in the integration algorithm during simulation runs.

4.6 Identification of Synchronous Frequency Values

This section will identify the relationships that must exist between the RF field frequency, ω, the electron cyclotron frequency, Ω, and the waveguide cutoff frequency, ω_{co}, in order for synchronism between the field and the particles to exist. Given these synchronous values, detuning parameters may be used to determine actual operating frequencies.

At synchronism, the beam mode (fast cyclotron mode) is characterized by

$$\omega - s\Omega - k_z v_z = 0 \tag{4.37}$$

where s is the cyclotron harmonic number and Ω is given by Eq. 3.5. Also at synchronism, the waveguide mode is given by

$$\omega^2 - k_z^2 c^2 - k_t^2 c^2 = 0 \tag{4.38}$$

These equations may be rearranged to the forms

$$k_z = \frac{1}{v_z} \left(\omega - s\Omega \right) \tag{4.39}$$

$$k_z^2 = \frac{1}{c^2} \left(\omega^2 - \omega_{co}^2 \right) \tag{4.40}$$

where

$$k_t^2 = \frac{\omega_{co}^2}{c^2} \tag{4.41}$$

has been used. The square of the right-hand side of Eq. 4.39 must equal the right-hand side of Eq. 4.40.

$$\frac{1}{v_z^2} \left(\omega - s\Omega \right)^2 = \frac{1}{c^2} \left(\omega^2 - \omega_{co}^2 \right) \tag{4.42}$$

Equation 4.42 may be rewritten as a second order polynomial in ω,

$$\frac{\omega^2}{\gamma_z^2} - 2s\Omega\omega + s^2\Omega^2 + \frac{v_z^2}{c^2} \omega_{co}^2 = 0 \tag{4.43}$$

where

$$\gamma_z \overset{\Delta}{=} \left[1 - \frac{v_z^2}{c^2} \right]^{-1/2} \tag{4.44}$$

has been used. Application of the quadratic rule, and subsequent algebraic manipulation yields

- 136 -

$$\left(s\Omega\right)_{synch} = \frac{1}{\gamma_z} \omega_{co} \tag{4.45}$$

and

$$\omega_{synch} = \gamma_z \omega_{co} \tag{4.46}$$

where the subscript "synch" indicates synchronous values. Selection of the RF mode, beam voltage, waveguide radius, and harmonic number thus determine unique synchronous values for ω and Ω. Within the computer code, two detuning parameters, FDETUN and BDETUN, are used to scale the synchronous values to the desired operating values.

4.7 Verification Tests

This section deals with the process by which it was determined that the numerical values generated by the computer code AMINUS accurately represent the gyrotron interaction for any given set of operating parameters. Several methods of verification are discussed. The discretization of a physically continual process leads to unavoidable error in the form of the integration algorithm, which causes both local error (within one iteration) and cumulative error (summed errors over the entire length of the run). With these errors and the error due to the assumptions discussed in Sections II and III, it is seen that verification does not involve producing perfect results, rather, results that fall within an allowable margin for error. The definition for the "allowable" error is based in the present work on the magnitude of the input quantities and the operating regime, and is discussed further on

the following pages. Results of AMINUS are compared with previously published data.

The natural progression for verification is from simple to complex, from individual pieces to the whole interconnected system of program, subprograms, and etc. The individual pieces of the present model are the electron beam and the RF electromagnetic field. Each has been tested under conditions representing the absence of the other. The testing of the interconnected system is also a multistep process and contains various parameters and results that may be scrutinized for accuracy and consistency.

The testing of the beam with no RF input power is a test of the dc behavior of the electron beam. The total momentum should be unchanged, and the ratio of p_t over p_z at the end of the run should be exactly the same as the input ratio. The guiding centers should not move, and the paths traced out by the orbiting particles should be perfect circles, with each particle traveling the same distance. AMINUS was run under these conditions, with varied beam voltages and α_o values $\left(\alpha_o = p_{to}/p_{zo}\right)$ for extended lengths of up to 100 λ_{cyc}. In all cases, AMINUS passed the dc beam test.

The testing of the RF field in the absence of the beam is known as "cold testing." For this test, the quantities under scrutiny are the phase change of the field, the magnitude of the field, and the conservation of field power. For this test, the conductivity of the wall was set high enough so as to represent a semi-infinite value, thus modeling an electrically perfect wall, i.e., one having no loss. Under these conditions, the field phase should change by 2π every RF wavelength, and

the total power in the RF field should remain unchanged. There are two variations on this test. The first is the true cold test. The second test models the simultaneous presence of both the RF field and the electron beam with the constant amplitude, but with the beam does not influence the RF field. This test is affected by setting $E_{bf} = 0$ for each run. (This second variation also allows the AMINUS to model the interaction in a perfect waveguide.) AMINUS passed both variations of the cold test for a broad range in input power levels and frequencies of operation.

With these two "individual piece" tests accomplished, the next phase of testing is to allow the simplest interaction of the two systems. This test is essentially the second variation of the cold testing phase, with different quantities being considered. This phase of testing allows the checking of the motion of the electron beam under the influence of a constant amplitude RF field. One of the quantities that may be examined for accuracy in this form of test is the electronic efficiency, both in the linear growth regime and at saturation. Results produced by AMINUS were compared to results published by Golomb, et al.[31] and found to match the accuracy of the plotted data.

There are two tests useful for verifying the internal consistency of the code. These are the first tests of the connected systems represented in AMINUS. The first of these involved the conservation of power. The total power in the model initially is the sum of the beam power, given by the product of the beam voltage and current, and the injected RF power, given by $0.5 \times \mathrm{Re}\left(V_n I_n^*\right)$ for the nth mode. If the walls are represented as loss-free by the use of a scaling factor that

forces the conductivity to be very large, the sum of the power at any longitudinal position must equal the initial sum. Physically, this implies the assumption that all power lost by the beam is coupled into the injected mode. For cases in which the injected mode is the dominant mode (TE_{11}), and the frequency is sufficiently far away from the next mode up in frequency space, this is a valid assumption. For cases in which the injected mode is not the TE_{11}, but is instead a higher order mode, the assumption that all the power given up by the beam is coupled into the desired RF mode would require further verification to substantiate the claim. Nusinovich[58] deals with this topic in some depth. The present work embraces this assumption because the parameters chosen for the test preferentially optimize a selected mode, and it is anticipated that once the selected mode has begun growing, it will not allow the significant growth of any parasitic modes. Though the problem of mode interaction and competition is an experimentalist's challenge, it has been possible to operate gyrotron TWA's at nonfundamental mode/harmonic numbers; thus lending experimental evidence to this theoretical assumption.[6,48,74] AMINUS has been tested under a large range of operating conditions for a number of modes (both TE_{mn} and TE_{0n}) and the normalized error in total power (P_T) is always less than 0.85 percent, where the power error between $z = L$ and $z = 0$ is calculated as

$$\%E = \frac{P_T|_L - P_T|_0}{P_T|_0} \times 100\% \qquad (4.47)$$

This test is essential in establishing the validity of the chosen form for E_{bf}, since the coupling of the beam to the RF field is accomplished

by this term. This conservation of power test is, of course, equivalent to a conservation of energy test, and the energy error showed the same tendencies and magnitudes as discussed for the power error. The error present is assumed to be produced by the integration algorithm, since a semi-linear relationship between %E and longitudinal length of interaction exists.

A second internal test involves the energy of the beam particles. There are two methods for finding this value present within AMINUS. The first method uses the hot gamma values, and the relativistic form for the energy of a moving particle is discussed in Appendix D. The second method is the differential equation carried for each particle, an example of which is Eq. 4.27. The disagreement between the final values for these two methods is always less than 0.01 percent. These two internal consistency tests then serve to establish a high degree of accuracy for the calculations within AMINUS.

Extensive verification calculations have been carried out in which the results of AMINUS are compared to two papers reporting work done at the Naval Research Laboratory. Additionally, calculations were carried out to allow comparison with numerical results published recently by Golomb, Goren, Ron, and Hirshfield.[31] These papers[18,19] allow verification of AMINUS results for several GTWA operating modes. The first test was conducted for varying values of BDETUN, the magnetic detuning factor, and P_{in}, the input RF power. The data points were prepared by finding P_{in} such that the saturation efficiency corresponded to a power gain of 20 dB, where

$$P_{out} = P_{in} \times 10^{(G/10)} \qquad (4.48)$$

The data used for this test are listed in Table 4.1 in the form utilized by AMINUS and in the form reported in Reference 18.

Table 4.1. GTWA operating parameters used in comparison of AMINUS with Reference 18, from which these data were drawn.

AMINUS	Reference 12
	$\nu = 2.076 \times 10^{-3}$
$V = 70.82$ keV	$V = 70.82$ keV
$I_O = 9.48$ A	$I_O = 9.48$ A
$B_O = 12.87$ kG	$B_O = 12.87$ kG
FDETUN = 100	$k_z = 1.96$ cm^{-1}
$r_W = 5.37$ mm	$r_W = 5.37$ mm
RONORM = 0.48	$r_O = 2.52$ mm
ALPHA = $\alpha_O = 1.5$	$v_{to}/c = 0.401$
	$v_{zo}/c = 0.268$

Figure 4.4 contains the data drawn from Chu.[18] The published form of the plot was expanded and the values of the plot were extracted for comparison. It is seen that for BDETUN values from 97 to 100, the comparison is very good. Chu predicts the maximum saturated efficiency to occur at BDETUN = 95.7, whereas AMINUS predicts the maximum will occur at 96. Golomb's results[31] show a maximum at 96.8, indicating that 96 is within the range of values found by other researchers. This test checks the performance of AMINUS for fundamental mode, first cyclotron
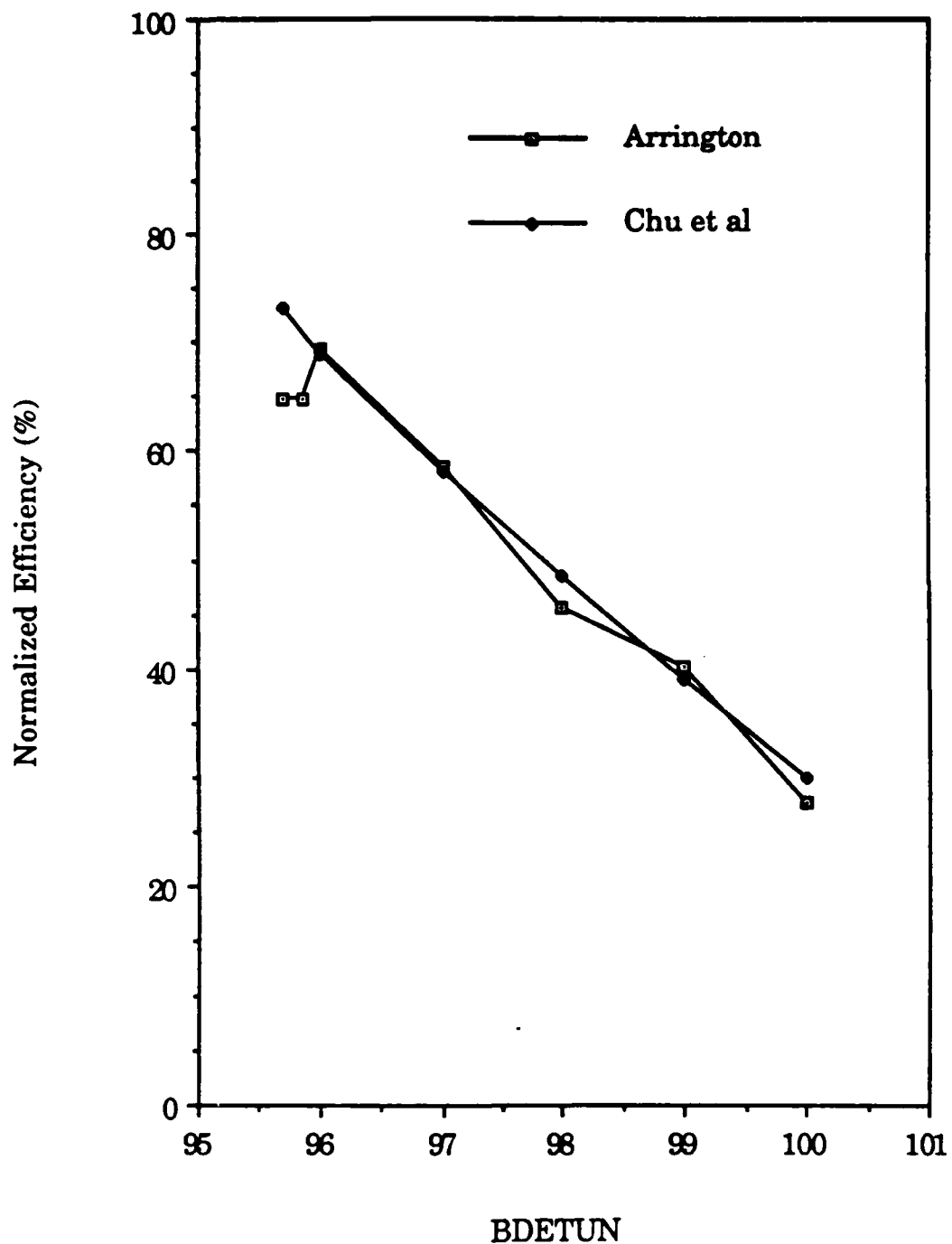
Fig. 4.4. Comparison of AMINUS results with Chu.[18] The plot of saturated efficiency versus BDETUN shows excellent agreement for BDETUN in the range.[96-100] The RF frequency was set to the grazing incidence value predicted by Eq. 4.46. The physical or laboratory frame efficiency is obtained by multiplying the normalized efficiency by 0.73.

harmonic operation. Testing of the performance of AMINUS for operation at higher order modes and higher harmonic operation was done by comparison with results in Reference 19. Comparison was done for $m = 0$, $n = s = 1, 2, 3, 4$, with RONORM $(= r_o/r_w) = 0.48, 0.44, 0.41$, and 0.40 for $n = 1, 2, 3, 4$, respectively. The beam energy level corresponding to $\gamma_o = 1.14$ ($V = 70.82$ keV) was used. With the exception of m, n, and s, the input data in Table 4.1 were used for the present test as well. Chu's results were found by interpolating from an expanded plot. Figure 4.5 shows that the results predicted by the two theories are so close that the error in reading values from the published plots is more significant than the differences seen on the figure. Comparison between Golomb[22] and AMINUS was carried out for values of BDETUN in the range [1, 1.06]. The results of the two theories/codes were indistinguishable to the accuracy of the published plots.

The next verification step was the calculation of linear regime growth rates and comparison of AMINUS results to the results of analytic work published by Fliflet[24] and Chu.[18,19] For the input parameters presented in each of these references, results of AMINUS calculations with the published results were very good.

A single data set was run to check the performance of AMINUS in the CARM regime, which may be characterized by two conditions, given as[12,24]

$$1 - \beta_{ph}^{-2} \ll 1 \qquad (4.49)$$
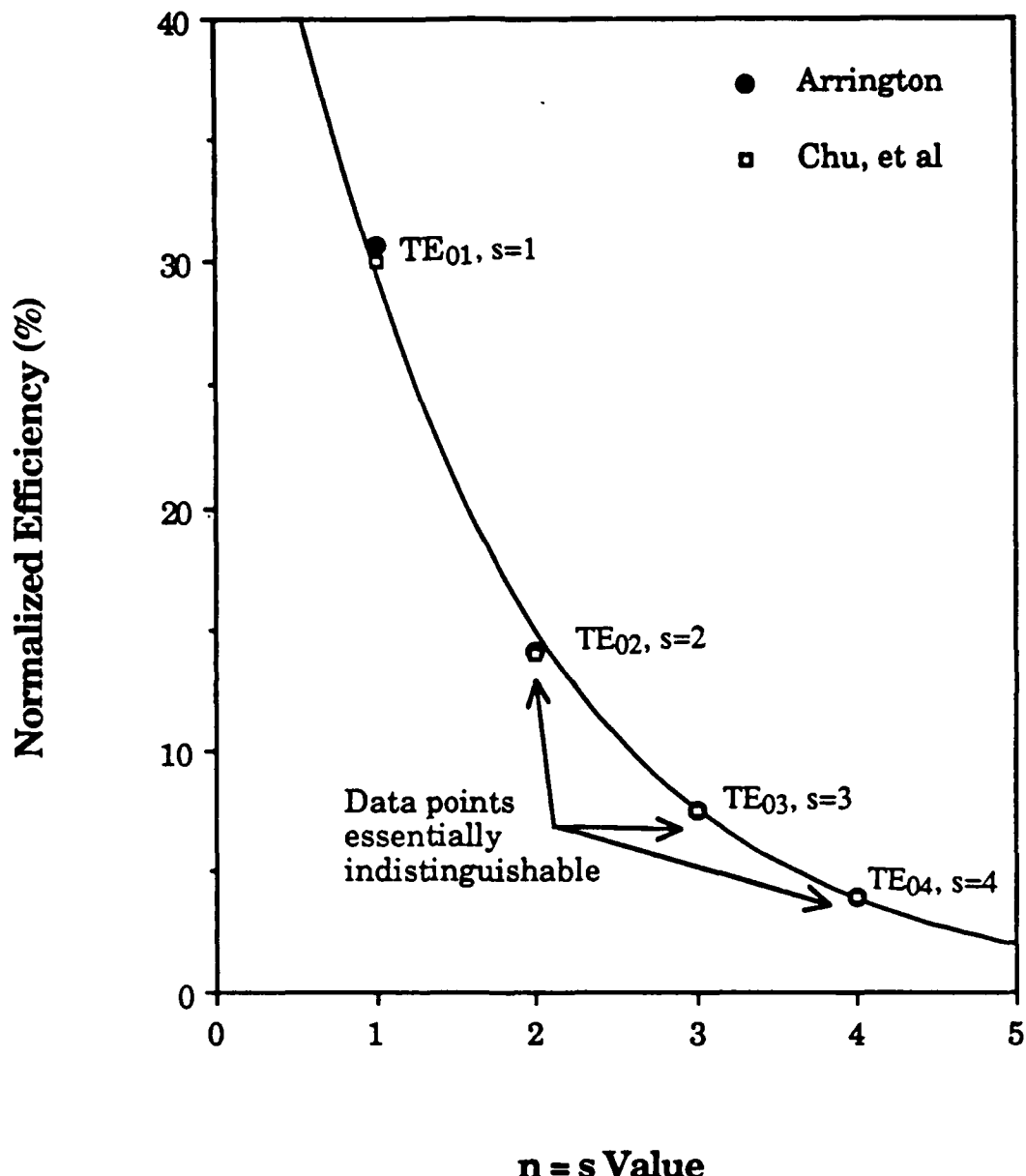
Fig. 4.5. Comparison of AMINUS results with Chu.[18] The plot of efficiency versus mode/harmonic number for TE_{0n} shows excellent agreement for the two theories/codes for, nonnonfundamental mode/harmonic operation. The RF frequency was set to the grazing incidence value predicted by Eq. 4.46.

$$1 - \beta_{ph}^{-2} \ll 1 - \frac{\beta_{zo}}{\beta_{ph}} \qquad (4.50)$$

where β_{ph} is defined as the ratio of v_{ph}/c, and β_{zo} is the ratio of v_{zo}/c. The published values used as input data for the CARM simulation were found in Fliflet,[24] and are listed in Table 4.2.

<div align="center">

Table 4.2. Input data for CARM regime test
case. Drawn from Reference 24.

</div>

$$V \quad = 1 \text{ MeV}$$

$$I_o \quad = 500 \text{ A}$$

$$v_{to} = 0.33 \text{ c}$$

$$v_{zo} = 0.76 \text{ c}$$

$$TE_{11} \text{ mode}$$

$$r_w \quad = 5.4 \text{ mm}$$

$$v_{ph} = 1.015 \text{ c}$$

$$\beta_o \quad = 13.2 \text{ kG}$$

$$\eta_{sat} = 22\% \text{ (laboratory quantity)}$$

$$P_{out} = 110 \text{ MW}$$

Fliflet predicted 50 dB growth for the given parameters, and a saturated efficiency of 22 percent. AMINUS predictions were for 50.4198 dB growth and a saturated efficiency of 22.0297 percent. It is important to realize the magnitude of input data for this run. A total power of 500 MW was contained in the beam alone. The magnitude of these parameters, along with the ~110 MW RF power output, provided a consider-

able test of the internal accuracy of AMINUS. As a result of this simulation run, provisions have been made to allow AMINUS to model devices in which very large levels of RF and dc power are present. The total power error given by Eq. 4.47 was slightly above the 1 percent criteria discussed below, but deemed acceptable in view of the input parameter magnitude.

The verification process consisted of checks on accurate prediction of the behavior of the electron beam and the RF fields in the waveguide, checks on the internal consistency of results, and comparison with previously published results. The main error lies in the conservation of energy/power. The present work has adopted the value of 1 percent error as a maximum acceptable value. The error is greatest for runs in which the linear growth rate is very high (~4 dB/cm). For cases of moderated linear growth rate (~2 dB/cm), the error rarely exceeds 0.4 percent for even low P_{in} and long interaction simulations. This error bound, accompanied by the very close agreement with published data, would seem to establish that both the analytical analysis and model and the computer implementation of that model are accurate.

4.8 Final Discussion of Numerical Implementation

Section 4.8 is a summary discussion of the numerical implementation of the analytic theory. Section IV has presented the process of forcing an analytic theory into a form usable on a computer. The general terms have been broken down into programmable pieces. The process for making calculations based on these pieces has been discussed, along with the numerical tools required for the calculations.

Specifically, an algorithm was selected for use in the integration of the 9N + 2 order system of equations. The process of verification was discussed in the linear fashion in which it was carried out.

Although the system of equations is technically of order 9N + 2, within AMINUS the system is actually of order 9N + 4. The differential equations for V and I are complex (since V and I are complex), and thus would require an integrator capable of integrating complex equations. It is always possible to separate a complex equation into two real equations, one representing the real part of the complex equations, and the other representing the imaginary part. The complex version of the algorithm discussed in Section 4.5 was written to allow comparison of accuracy and speed, as compared to the real version of the algorithm for a system of order 9N + 4. It was found that the most straightforward method was to carry V and I as four real quantities, V_r, V_i, I_r, and I_i, combine them into two complex quantities for the calculation of the differential equation, separate the differential quantity into its real imaginary parts, and then to update the real and imaginary parts of V and I independently.

A prime consideration in the writing of a computer code of the size of AMINUS, which is approximately 2500 hundred lines of Fortran, is speed. The relative speed of the integration algorithm was discussed in Section 4.5, but there are other ways of increasing the running speed of the program. In circular geometry, Bessel functions are utilized to match the boundary conditions for the radial variable, as discussed in Section 2.3. The standard method for achieving high accuracy in the computation of Bessel functions for cases in which the magnitude of the

argument may vary over a large range is based on a reverse summation stability property of the series representation of Bessel functions.[1,60] This is a very time-consuming process, with fully 50 percent of the total run time for AMINUS spent in the Bessel function routine when the normal technique is used. Several authors, e.g., 31, 30, and 1, offer small argument approximations for cases in which the argument of the Bessel function is less than unity. By comparison of the results given by Abramowitz and Stegun,[1] results given by the longer method of calculation, and the results of the small argument approximation, it was concluded that sufficient accuracy was maintained for arguments less than 0.8. Several authors, e.g., 20, 28, 24, 56, and 58, have used these small argument approximations in their work, both in analytic and numerical calculations. The use of this approximate numerical method, along with the speed enhancement discussed in Section 4.5, reduced the run time for AMINUS by a factor of 6.

AMINUS is a reasonably efficient implementation of the numerical model corresponding to the analytic work of Sections II and III. The integrity of the anlytic work has been maintained by a coding style heavily dependent on the use of subprograms. The self-consistency of the theory has been preserved by the calculation of E_{bf} for each new z location and corresponding modulation of the RF fields. The numerical model is a compromise between the requirements of minimum size/run time and the need for maximum accuracy/information.

The calculations in AMINUS are carried out in terms of physical parameters. For this reason, AMINUS results do not require the extensive calculations often necessary to convert the numerically generated

normalized parameters to physical quantities. Numerical values generated by AMINUS may be examined directly for information about the gyrotron interaction, and may be converted directly to physical dimensions or values for use in design of new devices or examination of operating devices. The researcher questions the value of obscuring data by the extensive normalization process often used, when it is not necessary for efficient accurate numerical simulation of GTWA devices.

V. RESULTS OF RESEARCH

5.1 Introduction

To date, the results of this research effort fall into four categories. These categories are:

1. Identification of the problem and generation of device based solutions.

2. Development of the numerical tools needed to implement and predict the behavior of the solution and verification again of the existing related work.

3. Derivation and analysis of beam-field coupling term applicable to nonfundamental cyclotron harmonic operation.

4. Preliminary results from the computer code.

The problem to be considered is twofold. The first problem is the presence of unwanted oscillations in experimental devices. Oscillations have been predicted[48] and experimentally observed.[48,75] The second problem is the limited bandwidth of convention GTWA devices. For radar applications, particularly for ECM/ECCM usage, it is essential that incoming radiation within a known frequency range be amplified in an essentially uniform manner. This has been attempted via the use of a reverse injection configuration first suggested by Lau.[48,6] The second portion of the problem under analysis has been the creation of a method for numerically representing and simulating such a device. The discussion of the first category of results, problem, and model work is discussed in Section 5.2.

The second category of the result involves the design and implementation of a numerical model capable of dealing with the problems identified and modeled inon of the first category of results, problem, and model work is discussed in Section 5.2.

The second category of the result involves the design and implementation of a numerical model capable of dealing with the problems identified and modeled in Section 5.2. This was accomplished by writing two separate but related computer codes. The first, AMINUS, was discussed at some length in Section IV. The second code, TELINGN, was written to predict the linear growth rate for TE modes for given input conditions. These codes and their verification are discussed in Section 5.3. The reader is referred to Section 4.7 for the exhaustive discussion of the verification of AMINUS.

The third category of results involves the identification and testing of a beam-field coupling term. This term was first derived by Baird.[2,4] The term provides a vital link in the self-consistent theory presented in this report.

The final category of results for the present work represents early results of simulation runs by AMINUS, and studies on the limitation of a commonly used analytical approximation (see Eq. 3.47). Variations of efficiency as a function of RF and magnetic detuning are discussed. The variation of gain and saturated efficiency as functions of current are also presented. The simulation results are based on an optimum design calculation performed by Naval Research Laboratory scientists.[19]

5.2 Results Related to Problem and
Solution Identification

This section discussed results achieved and falling in category 1, as explained in Section 4.2. As mentioned in the introduction, the problem under consideration is twofold: dealing with oscillations and the simulation of a wideband GWTA. When the traveling-wave amplifier configuration of the gyrotron was first considered, it was viewed as a simple arrangement capable of producing great amounts of RF power. The circular waveguide is perhaps the simplest waveguide structure, although the rectangular waveguide (also used extensively in experimental efforts) is also a simple structure. Both the circular and the rectangular waveguide are used in experimental work, both were studied early in the development of the GTWA, and predictions were made that lead to the construction of several experimental devices. The shortfall of the numerical models was realized in the presence of undesired oscillations in the devices, at a frequency slightly below the waveguide cutoff frequency.[48] These were explained variously as oscillation induced via coupling to other modes[75] or with significantly more theoretical basis as the onset of an absolute instability.[48,78] Given the fact that RF propagation below cutoff is subject to exponential decay, this discovery proved very problematic for experimentalists.

The theoretical basis for these oscillations was studied in some detail by Lau, et al.,[47-50] in a series of articles published in 1981, and also by Wachtel[79] who identified and discussed the four modes corresponding to the fourth order dispersion relation. It was determined by Lau that the oscillations had two identifiable causes. The

first was due to a feedback process caused by imperfect output couplers. Given the peak output power levels generated in GTWA devices, it may be seen that even a highly efficient output coupler may reflect a significant amount of RF power back into the interaction region. This type of problem was found to be existent in experimental work[74] at Varian Associates. The solution implemented was neither efficient nor elegant. The solution involved coating the interior of the waveguide with a lossy material so as to suppress the growth of the unwanted oscillation by decreasing the effective loop gain to a tolerable level. The problem with this solution is that it reduces the output power, although by a small amount.[50] A second proposed solution is the use of a shortened interaction length. For a desired growth rate, this will impose a new restriction on the power output, as may be seen in Fig. 5.8.

The second type of oscillation is not related to the reflection problems, but rather is related to the strength of coupling between the electron beam and the RF field. This coupling strength is strongly dependent on the magnetic field match.[48,19,24] If the current and magnetic field match are such that the coupling is sufficiently weak, the GTWA will operate as predicted by a basic convective (nonabsolute) instability.[13] For higher current levels and for magnetic field values greater ~~than the~~ synchronous value (see Section 4.6), Lau showed that instabilities always exist and may or may not be absolute.[48] In that work, absolute instability was predicted to set in at current levels substantially below the desired operating level (since efficiency scales approximately as $I_o^{1/3}$, as in conventional traveling-wave tubes[19]).

Further, for values of magnetic field resulting from above synchronous magnetic tuning, the unwanted oscillations set in at even lower currents."[8] Lau, et al., derived linear relations predicting the oscillation start current, I_{st}, for various levels of magnetic detuning. The analytic simulation of the same current levels under conditions of noninfinite wall conductivity predicted increased current levels for which the GTWA can operate according to the convective instability.

The theoretical solution to this problem is based on the use of frequency selective loss mechanisms within, or coupled to, the interaction region.[4] The concept may be represented as in Fig. 5.1. The qualitative loss profiles of the various schemes is represented in Fig. 5.2. (For detailed quantitative analysis, see Reference 52.) The ideal solution would be in the form of frequency selective absorption mechanism with a delta function frequency spectrum of absorption, i.e., Loss(dB) = $f[\delta(\omega - \omega_i)]$, where ω_i is the frequency at which the unwanted oscillations occur. To use the language of delta functional calculus, the loss mechanism would "sift" out the unwanted frequency and absorb the power in that oscillation mode before the mode had grown enough to be carrying a large fractional amount of the total RF power in the guide. One experimental device has been built with the primary waveguide fabricated of graphite in order to deal with this oscillation mechanism.[7] That method was dependent on operation very near cutoff, where the coupled or auxiliary waveguide concept could be constructed to provide loss at an arbitrary frequency. Thus, it is felt that the auxiliary waveguide is a much more palatable solution to this problem.
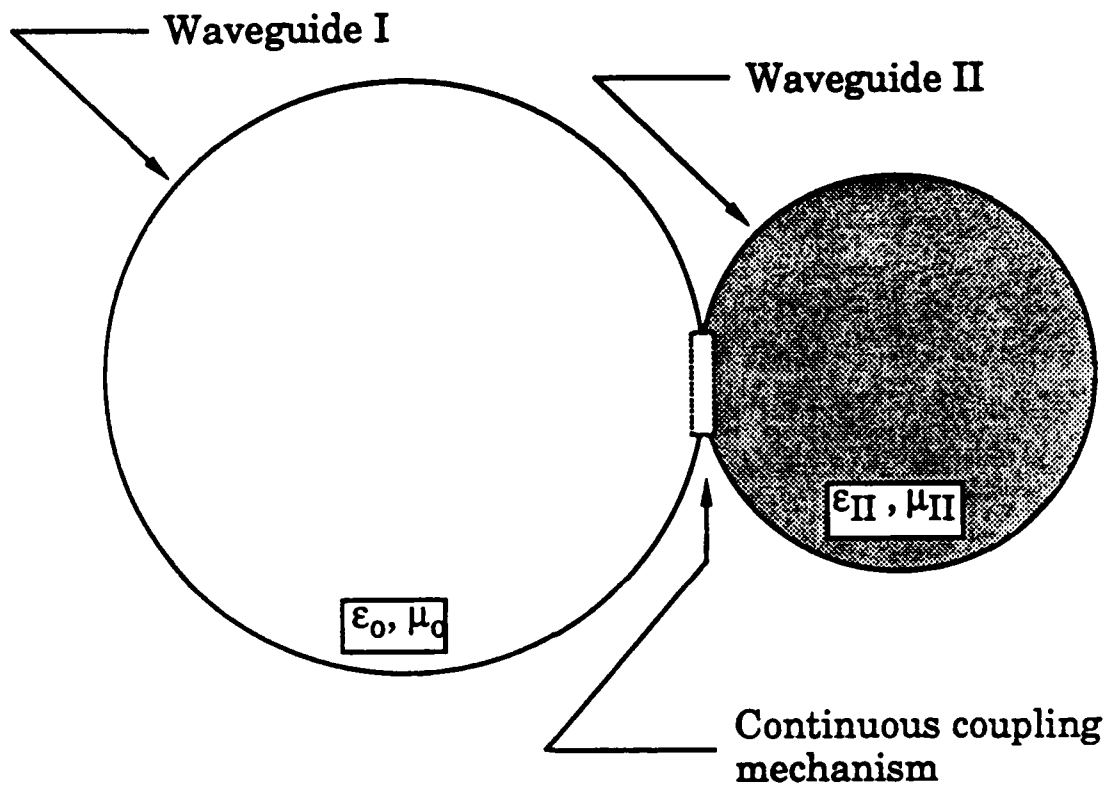
Fig. 5.1.   Schematic representation of continuously coupled auxiliary
           waveguide.   Waveguide I contains the primary interaction
           region.   Waveguide II is filled with a lossy dielectric
           and is geometrically shaped (radius varied) to provide
           loss at the desired frequency (in relation to the cutoff
           frequency in waveguide I) at each longitudinal position.
           (After Reference 6.)
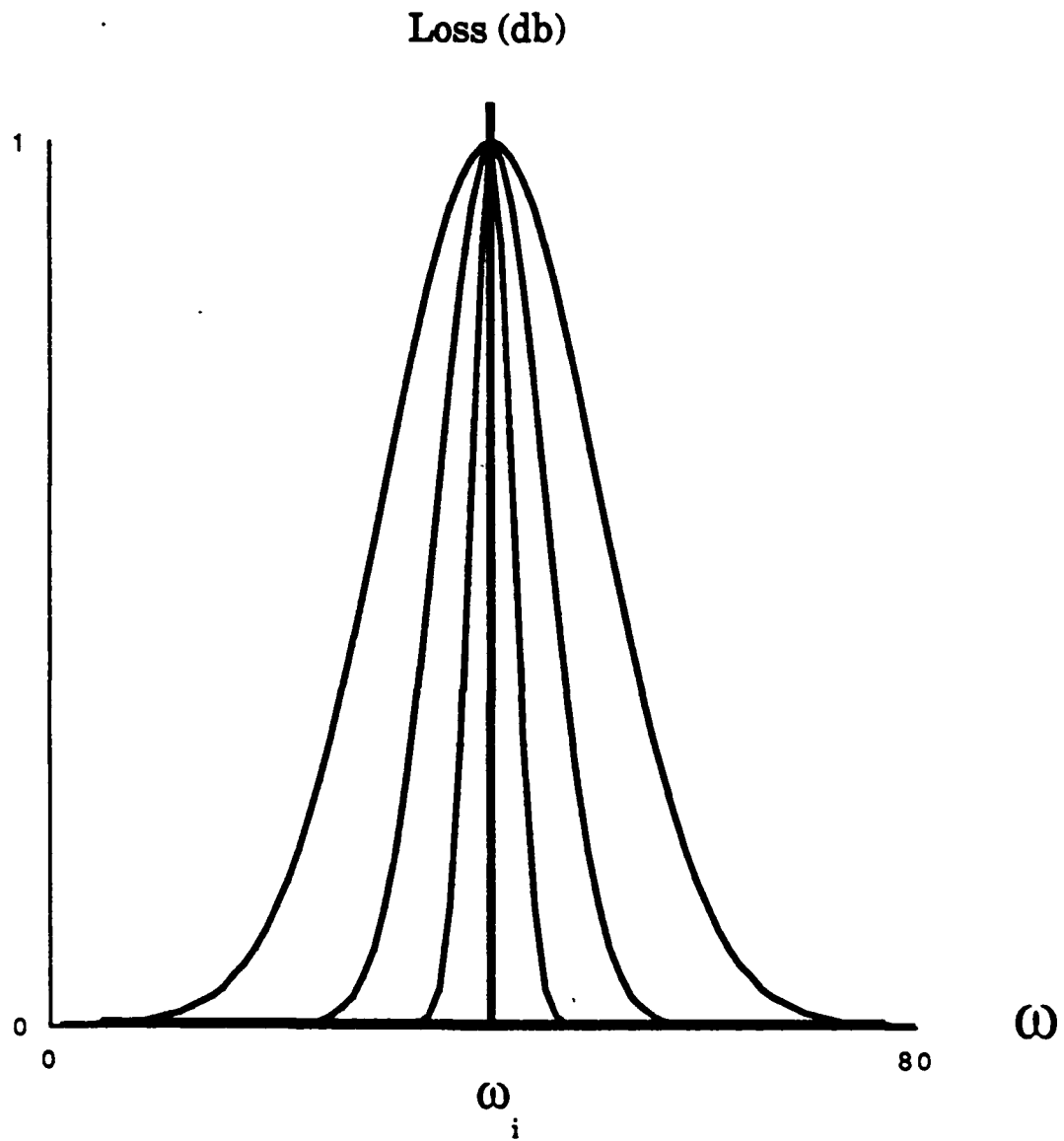
Fig. 5.2. Qualitative diagram of concept of loss profile as a function
of $\Delta\omega \overset{\Delta}{=} \omega - \omega_{co}$. Important concept is the ability to vary
$\Delta\omega$ by appropriate choice of loss mechanism. The peak loss
frequency from the coupled cavity may be selected by proper
choice of cavity dimensions.

The implementation of a simulation for the proposed solution is in the form of a computer code (AMINUS) in which a great deal of control has been retained over the electrical characteristics of the waveguide. The conventional models for the RF fields, which are in the form of a second order differential equation, can not provide the same degree of control. They are thus limited severely in their ability to model application of the theoretical solution. The field model derived in Section 2 is cast in the form of two first order differential equations, Eqs. 2.103 and 2.104. These equations contain terms that permit calculation of the impact of specific forms of loss and taper. The relative magnitude of change induced by any given configuration may be assessed by comparison to the dominant (ideal waveguide) terms in each equation. Earlier researchers, e.g., Rha,[64] were forced by the analytical complexity of loss and taper modeling terms derived under the conventional model to neglect these terms. The concept of auxiliary coupled waveguide cavities is represented in this theory as a loss associated with a specific, researcher specified, area of the waveguide wall. A cavity of known dimension filled with a known dielectric may be easily represented by a wall loss term. It is also anticipated that several regions of very high RF loss will also be representable with AMINUS. It is clear that neglecting these terms is restrictive at least. Thus, the derived transmission line field model gives the researcher a much greater investigative tool than previous models.

The second major problem addressed in this work has been the simulation of a wideband GTWA. It may be noted that a similar effort employing very different methods is under way at the Naval Research

Laboratory.[3] The conventional arrangement of a gyro-amplifier device is for the RF signal to be injected at the end of the tube nearest the electron gun. The field then propagates in the same direction of the beam, and conditions are arranged for the interaction to occur. The reflective mode device, proposed by Lau,[4,7] offers several advantages in terms of bandwidth and ease of signal injection. Figure 5.3 shows a figurative comparison of the two configurations. The longitudinal configuration and gain response are idealized in Fig. 5.4.

A reflective mode, wideband, GTWA has been built, based on data supplied by Lau in Reference 48, with results reported in Reference 6. Values for I_{st} and other performance parameters were close to those predicted by Lau. The problem lies in the fact that, as pictured in Fig. 5.3, a significant portion of the growth of the wave will occur below cutoff. The standard normal mode theories, as mentioned in Section 2, do not allow integration across cutoff, and so are not a satisfactory solution. The proposed solution again lies in the application of transmission line theory, which does not suffer the aforementioned restriction. With the transmission line formulation, any chosen quantity may be expressed as a z dependent quantity, allowing the researcher full control over the waveguide wall configuration, electrically (conductivity/skin depth) and physically (radius).

As pointed out in Section I, the device based problems studied in this report dictated the formulation of a new large signal nonlinear theory of the gyrotron. The new theory is the combination of the transmission line formulation found in Section II, and the single particle ballistic theory found in Section III. These two are fully self-
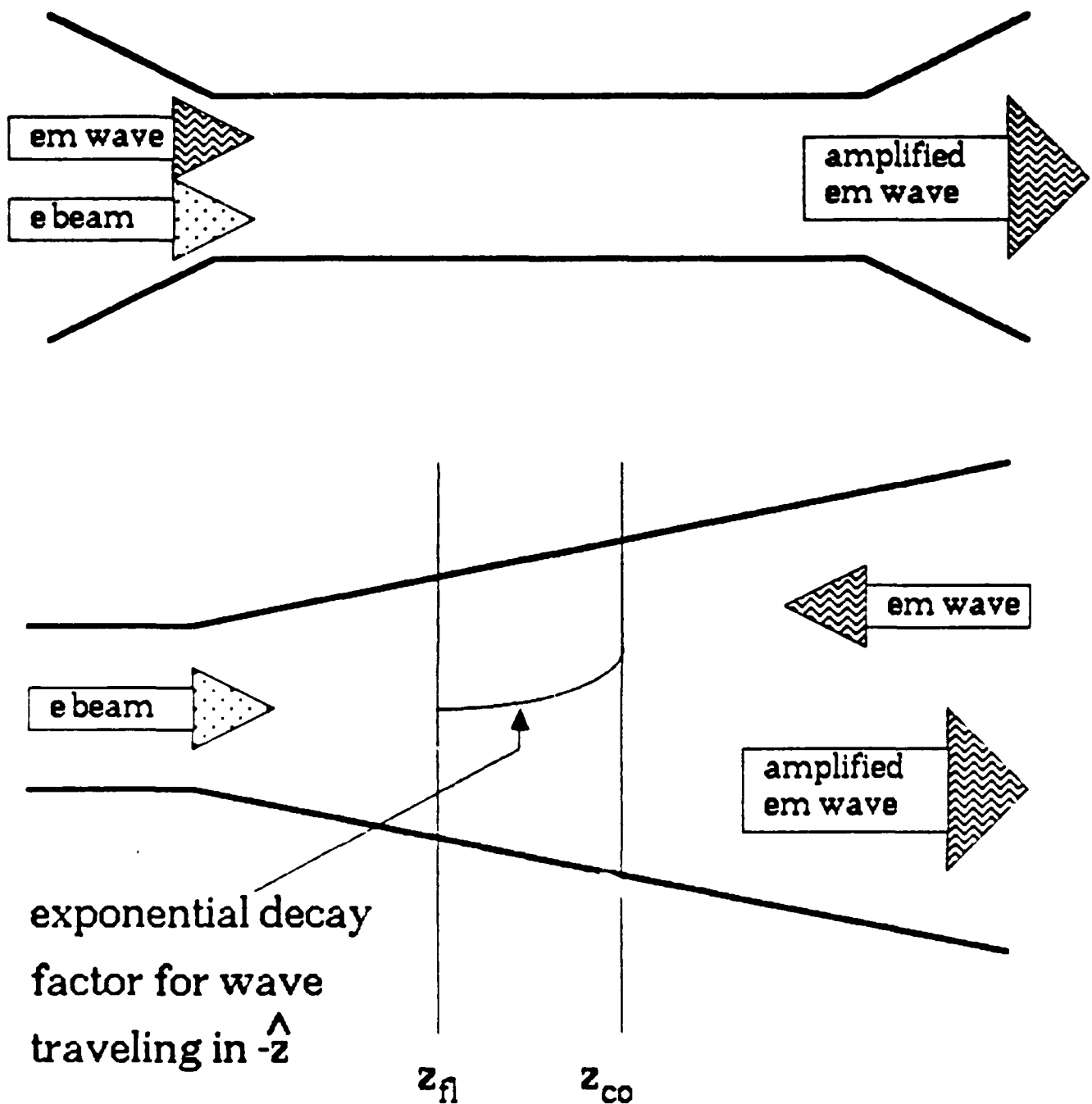
Fig. 5.3. Comparison of conventional GTWA (a) and reflective mode GTWA by symbolic geometries. Note that RF propagation below the cutoff frequency (for z such that $z_{fl} < z < z_{co}$) is subject to exponential decay in the direction of propagation.
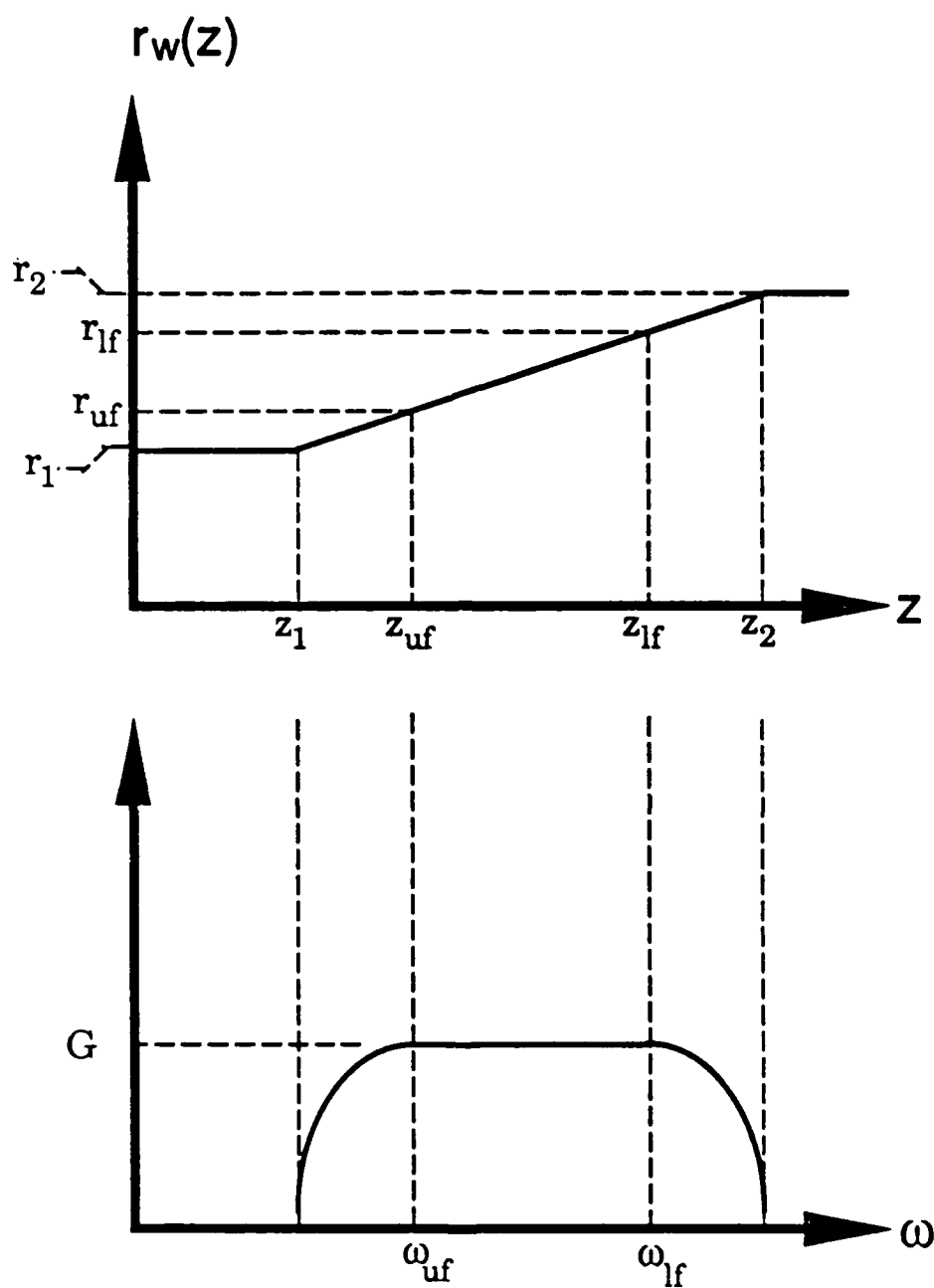
Fig. 5.4. Qualitative diagram of relationship between taper in wall radius and gain over wide bandwidth for the reflective mode GTWA. $\omega_{uf,lf}$ are, respectively, the upper/lower operational frequencies of the device, and are again respectively designed to be a few percent lower/higher than the cutoff frequencies calculated based on z1, z2. (After Lau and Chu.[47])

consistent due to two steps taken during the derivation of the theory. First, the fields are not fixed in amplitude. A coupling term, E_{bf}, was derived that provides an analytical model for the influence of the electrons on the RF fields. The magnitude of the fields is directly influenced by the electron beam, where the influence of the beam is based on the actual location and momentum of each individual charge carrying macroparticle. The second step taken was the use of these beam modulated RF fields in the trajectory equations. The fields are modulated by the beam, and these fields are used in the calculation of the forces on the electrons as they drift down the interaction region of the device. Self-consistency in a theory may be viewed as a closed circle, with each segment of the circle dependent on the other segments. By combining a theory for the RF electromagnetic fields, a theory for the electron beam behavior and a method for allowing the beam to influence the fields and vice versa, the theory is made self-consistent. This claim of self-consistency was verified in Section 4.7. Thus, a substantial portion of the results in this report consists of the generation of a new large signal nonlinear theory of the GTWA, a theory capable of dealing with the specific problems under investigation in this report, as well as the conventional simulation considerations.

5.3 Results Related to Development of Numerical Tools

This section will summarize the results falling in category 2, as noted in Section 5.1. The principal accomplishments in this category have been discussed at some length in Section IV, but will be dealt with

briefly here. The second area of accomplishment in this category has come in the form of programming tasks identified as needed to support AMINUS. Several new routines have been written for various purposes, the most of important of which allows the calculation of the small signal, linear regime growth rate given several input parameters.

AMINUS is a collection of approximately 25 program units. These units serve various purposes, including data acquisition, calculation of synchronous and tuned frequency parameters, automated screen plotting of electron distributions, integration, and calculation of special functions. AMINUS implements a single mode approximation of the transmission line field model and the exact computer equivalent to the particle equations. The set of equations programmed directly into AMINUS is found in Section 4.2.

It is well known that any departure from an idealized electron beam will result in altered (usually degraded) gyrotron performance, implying that a useful research code should be able to represent nonideal electron beams. Each particle is individually initialized in AMINUS, thus allowing the freedom to represent a number of different initial beam conditions. This method seems to be much simpler in implementation than the method proposed by Golomb.[31] The method of treatment of nonideal electron beams is no different from the method for treating ideal beams, save the initialization process. Internal checks are maintained to assure that the longitudinal motion of the particles relative to the plane of the ring is not sufficient to invalidate the model. AMINUS automatically corrects for the energy lost by electrons that intercept the wall, and alerts the operator of the interception.

Also, it will be shown in Section 5.4 that certain combinations of detuning parameters cause the beam to be so far away from synchronism with the RF field that the beam absorbs net energy, rather than giving up net energy. This eventuality is also provided for by an internal check.

The principal support program written for this research effort was TELINGN, which was written in ANSI 77 standard Fortran on a personal computer. The verification process discussed in Section 4.7 was supplemented by the independent calculation of the small-signal linear regime growth rate for TE modes for each set of operating parameters. This provided an independent verification that the calculations within AMINUS did not represent an accelerated or decelerated rate of energy exchange. This program also provides an independent research tool by allowing the gain rate to be predicted without the time and expense of a full scale simulation run.

As has been mentioned throughout this report, one of the primary objectives of this research effort was the generation of a self-consistent large signal simulation code for nonstandard configuration gyro-amplifiers. This task has been accomplished in full. AMINUS incorporates beam modulated RF fields (via E_{bf}), calculates electron trajectories based on these modulated fields, and is thus fully self-consistent. AMINUS is useful for any TE_{mn} mode of arbitrary cyclotron harmonic number.

5.4 Results Related to New-Beam Field Coupling Coefficient

This section will present a brief discussion of the significance of the beam-field coupling term, E_{bf}, as derived in Sections 2.6 and 4.3. The general form found in Section 2.6 is applicable to a wide class of waveguide geometries. The specific term as calculated in Section 4.3 is accurate and simple to calculate.

The final form for E_{bf} (Eq. 2.115) may be used for any waveguide geometry for which solutions to the 2-D scalar wave equation may be found by separation of variables. The process of deriving the pieces is dealt with in some detail in Section 2.6 and will not be discussed further here. It is significant that a term has been derived which is geometry/coordinate system independent. The previous methods have been similar, but have often used some type of approximation to yield a closed form solution, and thus sacrificed accuracy in order to reach a solution. Equation 2.115 is derived without any approximations and yields excellent agreement with other methods of calculating the RF field magnitude (as discussed in Section 4.7).

Equation 4.36 is the form of E_{bf} that results from the evaluation of $\vec{v}_t$ and $\vec{e}_n^*$. Equation 4.36 explicitly includes the effects of operation at nonfundamental harmonics, and is applicable for beams with either axis encircling or nonaxis encircling electron trajectories.

This term is the final required ingredient in a truly self-consistent computer simulation code. It provides the proper connection between the beam and the RF fields by allowing the RF field perturbing contribuiton of each specific charge carrying particle to be explicitly

calculated and summed. The accuracy of this approach is revealed in the accuracy and ease of computation discussed in Section 4.7. The total error in energy/power is seldom greater than 0.5 percent, whereas other recent publications[31] have noted that it was necessary to enforce "the conservation of the total energy of the electron beam and the RF field....every few wave periods." This seems to imply some redistribution of accumulating error, which is not required in AMINUS due to the accuracy of E_{bf} in expressing the coupling of the energy given up by the beam into the RF fields.

5.5 Results Related to Simulation and Analysis of Gyrotraon Traveling-Wave Amplifier

This section presents the results in category 4. These results may be broken down into three subcategories, which are:

1. Results dealing with the development of AMINUS. The concept of a minimum number of particles being required to represent an electron beam is presented, along with the physical parameters found to influence that number. The methods of initializing the macroparticles used to represent a beam according to the beamlet model are presented.

2. Results dealing with guiding center motion are presented.

3. Results of AMINUS simulation runs are presented. Several relationships between input parameters and results are considered.

These results do not represent the limits of AMINUS. Rather, they are the results available at the time of preparation of this report.

The numerical results are primarily based on variations of the Navy Research Laboratory design for a 35 GHz GTWA, as presented in Table 4.1, or on the consideration of a TE_{0n} mode operating under similar input conditions.

Within AMINUS, the electron beam is represented as a collection of macroparticles, each carrying the charge and mass of many electrons. These particles have the same trajectories as electrons under the influence of the RF field because they have the same charge-to-mass ratio $(1.758 \times 10^{11}$ C/kg$)$ as an electron. In order to accurately represent the electron beam, it is necessary to represent all phase relationships between the transverse velocity vector and the RF field vector. It is possible, by using a single particle, to determine the phases of the particles that will be "good" particles, i.e., those particles which give up energy to the RF field, and the phases of the particles that are "bad" particles, i.e., those particles which will absorb energy from the RF field. By finding the phase relationship corresponding to the best of the good particles, it is possible to identify the maximum possible efficiency, which, in the gyrotron interaction, corresponds to the conversion of all kinetic energy associated with the particle's transverse motion to RF field potential energy. With this knowledge, it would be possible to describe the theoretically perfect electron beam. This beam would be composed of particles having this optimum initial phase relationship with the RF field. Research into the formation of this type of beam is currently underway.[3] For general purposes, the interaction of a single particle with the RF field is not an accurate predictor of the interaction of a normal electron beam with the field.

The question at hand is the minimum number of particles required to accurately represent the interaction. The minimum number of particles was determined by choosing a set of input parameters and then varying only the number of particles used to represent the beam. The electronic efficiency was used as the gauge by which the accuracy was evaluated. The number of particles, N, was increased from 4, by single particle increments, and the efficiency was observed to asymptotically approach a value. For $N \leq 12$, the efficiency was constant, showing that 12 particles were required to represent a real electron beam. The minimum value of N, N_{min}, varies with current and current density. Under the assumed beam model, the current density varies inversely as the square of R_L, which is itself a function of the magnetic field strength and the particle kinetic energy, as shown by Eq. 3.44.

$$r_L = \frac{\gamma v_t}{\Omega_o} \quad (3.44)$$

by varying γ, v_t, and Ω (or B_o), the size of r_L is changed. For a given set of parameters, increased current and/or current density increases N_{min}. N_{min} is never less than 12, but is sometimes greater. These findings suggest that one of the first tasks associated with any thorough simulation study should be the determination of N_{min}. Obviously, lower values for N_{min} are desirable, since the time (and cost) of a simulation run will vary directly with the number of particles used to represent the beam.

There are two separate methods for initializing the ring of particles representing the electron beam. The first is to launch the

particles at different times from the same spatial locations. In this method, the particles are distributed in time over a single RF period. The second method, adopted in this report, is to launch the particles at the same time from different spatial locations. In this method, the particles are distributed in space over a single RF wavelength. This concept was discussed briefly in Section 2.6 with regard to the form of the beam→field coupling term. A researcher using the second method has two options for the actual assigning of initial values. The ring of particles may be built with a single guiding center radius value, r_o, a single guiding center angle value, θ_o, and various RF angle values. Consulting Fig. 3.2, it can be seen that this would correspond to a single densely filled beamlet, with initial values of α varied so as to equally distribute the particles around the guiding center. The second option would again assign each particle the same guiding center radius, but would vary θ_o, and assign each particle the same initial value of α. This would correspond, again consulting Fig. 3.2, to one beamlet per particle, with the values of θ_o varied so as to equally distribute the beamlets, and a single initial value of α assigned to each particle. Both representations produce the same results, but they offer the researcher two views of the same physical process. Again, the essential element in the initialization of the electron beam is that the spectrum of phase relationships between the transverse velocity vector and the RF field vector be adequately represented.

The results of subcategory 2 deal with changes in the radial guiding center coordinate, r_o. The magnitude and impact of these changes is not universally agreed upon. As recently as December 1986, a

significant Naval Research Laboratory research effort[24] was published while stating specifically that analytic results were formulated by "neglecting drifts of the electron guiding center due to the RF fields." As recently as June 1988, a paper was published as a study of the saturation processes in gyroamplifiers while neglecting any guiding center drift.[31] On the other side of the coin, papers have been published in which it was deemed necessary to track the motion of the guiding centers, including work by Ganguly[30] and Rha.[64] In view of the results following, it is not surprising that different researchers take differing views on the need for explicitly considering the guiding centers. Figure 5.5 is a plot of normalized guiding center drift for the TE_{0n}, n = s = 1, 2, 3, 4 modes. The input parameters are those for the Naval Research Laboratory design, with BDETUN = 100, and the power input set at a level that produces 20 dB power gain at saturation efficiency.

As can be seen from the figure, the motion can be insignificant (< 0.5 percent) or very significant (~8 percent). The impact of guiding center motion may be evaluated analytically by considering the beam-field coupling coefficient, H_{sm}, identified by Chu,[17] Li and Hirshfield,[52] and Fliflet.[24] H_{sm} is given by

$$H_{sm} = \left[J_{s-m}(R_o) \right]^2 \left[J_s'(R_L) \right]^2 \tag{5.1}$$

For the mode in the figure with the greatest guiding center drift, the TE_{03} (with s = 3), the optimum setting for R_o $(= k_{tn} * r_o)$ is 0.410 * R_w.[19] For the mode under discussion, H_{sm} has the value
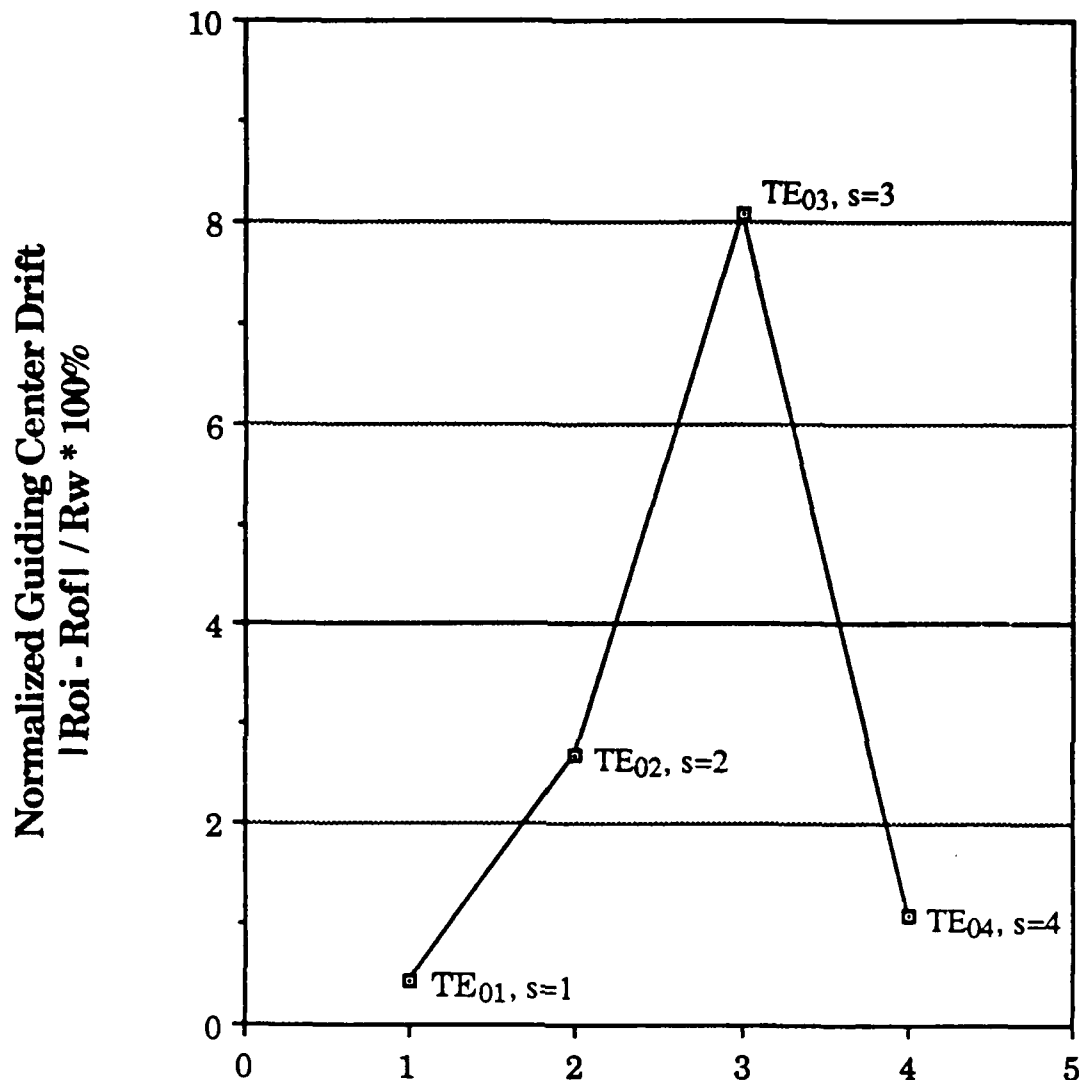
Fig. 5.5. Plot of normalized guiding center motion as a function of mode/harmonic number for the TE_{0n} modes. P_{in} was maintained so as to produce 20 dB power gain at saturation.

$$H_{30} = J_3^2(R_o)J_3^{\prime}(R_L) \qquad\qquad (5.2)$$

For the mode under discussion, a guiding center drift of 8 percent corresponds to a 6 percent decrease in the value of H_{sm} depending on R_o, indicating an important diminution in the coupling of the beam and the RF fields.

Computationally, simulation runs take far less time if the guiding centers are assumed fixed. The reason is simply the number of equations that do not have to be calculated, which, in this report, is two equations per particle per iteration. These results suggest that accuracy demands that simulation results calculated under the assumption of zero guiding center drift must be verified in a run in which the guiding centers are allowed to move.

The final subcategory of results consists of simulation results gathered from AMINUS. Several aspects of these results have been alluded to already in the paragraphs immediately above and in Section 4.7. The first of these results is Fig. 5.6, which is a plot of normalized efficiency as a function of magnetic detuning.

For values of BDETUN greater than 102.54, the synchronism between the beam and the field was so totally destroyed that the beam could not be bunched by the field and acted as an active absorber of RF power. The saturated efficiency decreases monotonically in a nearly linear fashion until BDETUN exceeds 102. For values of BDETUN > 102.54, the gain/efficiency is always less than zero.
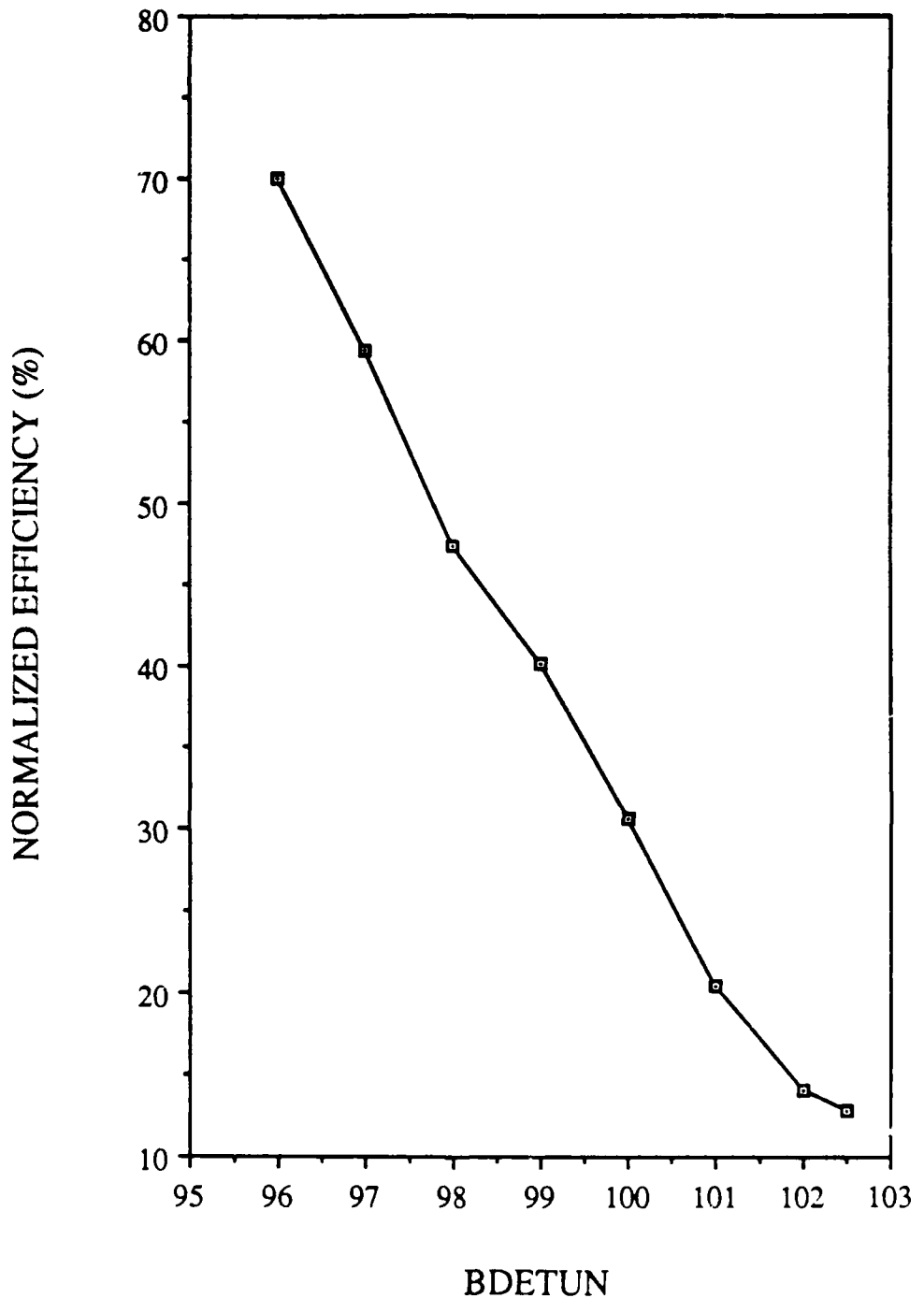
Fig. 5.6. Normalized efficiency as a function of magnetic frequency
(or flux density) detuning for the TE_{01} mode, s = 1.
The operating values, except for BDETUN are those found
in Table 4.1. P_{in} was adjusted to the maximum value for
which 20 dB gain could be attained. BDETUN is the ratio,
in percent, of the operating magnetic field to the syn-
chronous value predicted by Eqs. 4.45 and 3.5.
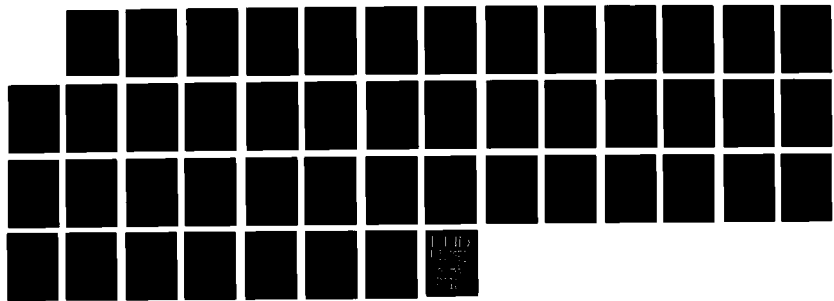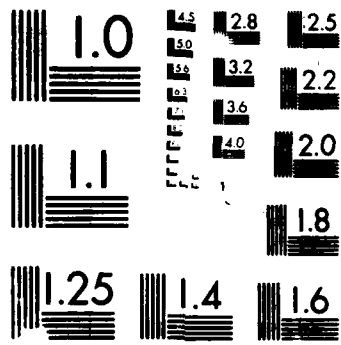
The second type of variation studied was efficiency as a function of RF frequency detuning. FDETUN is the frequency detuning parameter in AMINUS, and is defined as the ratio, in percent, of the RF frequency to the synchronous value predicted by Eq. 4.46. Figure 5.7 contains these results.

The figure shows three features of interest. First, the synchronous frequency offers the lowest efficiency of operation. Second, the curve does not vary monotonically, rather, it is in the form of a parabolic curve, a peak exists at FDETUN = 97, and the efficiency falls off sharply on either side of this local maxima. Third, the efficiency increases sharply as the RF frequency is tuned above the synchronous point.

The first and third of these observations may be explained by considering the dispersion relation for the electron beam, given as

$$\omega = k_z v_z + \frac{s\Omega_0}{\langle\gamma\rangle} \tag{5.3}$$

where $\langle\gamma\rangle$ is defined as an unweighted average of the hot gamma values for the ensemble of electrons or macroparticles. As the electron energy decreases via the interaction with the RF field, $\langle\gamma\rangle$ will decrease, and a frequency set at the synchronous value will soon be too low. Thus, a frequency greater than the synchronous value will cause a favorable exchange of energy for a longer period of time as the average energy of the electrons decreases with the progressing interaction. The second observation is not yet fully explained, but the parabolic shape of the curve may be explained as follows. For FDETUN less than 100, the RF
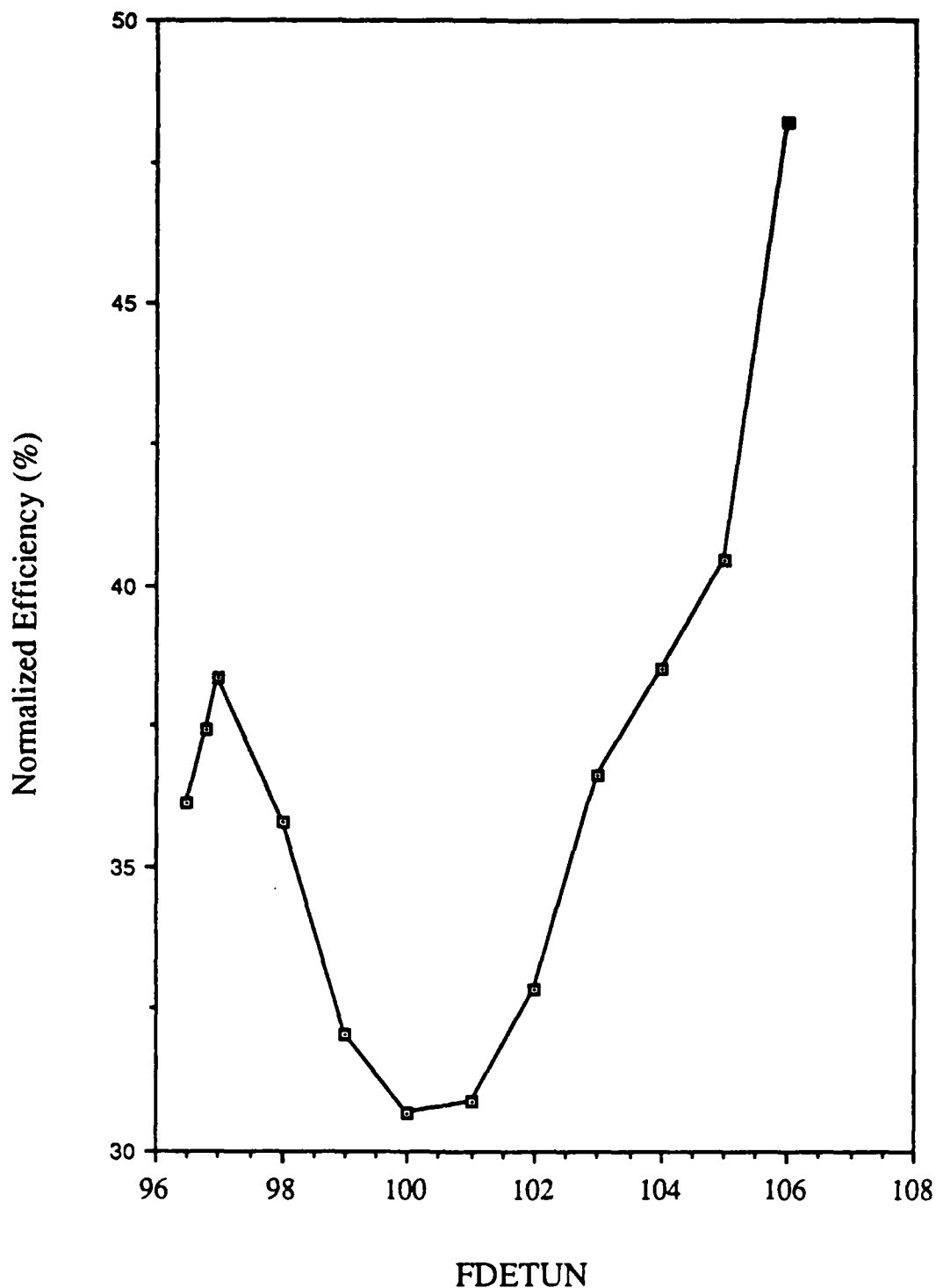
Fig. 5.7. Normalized efficiency as a function of RF frequency detuning for the TE_{01} mode, s = 1. The operating values are as in Table 4.1, with the exception of FDETUN (varied) and BDETUN (= 100, to give synchronous value of magnetic field). Input power level adjusted to yield 20 dB gain at saturation.

field immediately begins pushing the electrons, causing them to give up kinetic energy. FDETUN less than 100 moves the RF frequency closer to the waveguide cutoff, which causes k_z to be smaller. This then causes the RF field and the beam to interact strongly until the decrease in $\langle\gamma\rangle$ causes the frequency mismatch to be too great to achieve a high efficiency. This also corresponds to the high linear regime growth rates predicted by Fliflet[24] as the quantity $(k/k_z - 1) = (v_p/c - 1)$ increases. For FDETUN $=$ 100, the fields are never able to exert as great an influence on the electrons because neither the magnitude of k_z nor the overtuning of the RF frequency aids the interaction.

The third simulation result presented is closely related to the explanation offered for observations discussed above. The variation of interaction length required to reach saturation as a function of RF frequency detuning is shown in Fig. 5.8. The operating parameters and data acquisition process are as in the previous figure.

The monotonic increase in length is related to the time required for the beam to be bunched and phase trapping to occur. For lower values of RF frequency, the field begins pushing the particles immediately, and loses synchronism more quickly as a result. These two factors produce the short interaction length shown in Fig. 5.8, and the lower efficiency shown in Fig. 5.7. Higher frequencies will not interact as effectively with the beam until the net average energy of the beam has been decreased through a relatively inefficient exchange. The field takes longer to bunch the beam so that the net beam energy loss can occur, which produces the longer saturation times. The shape of the
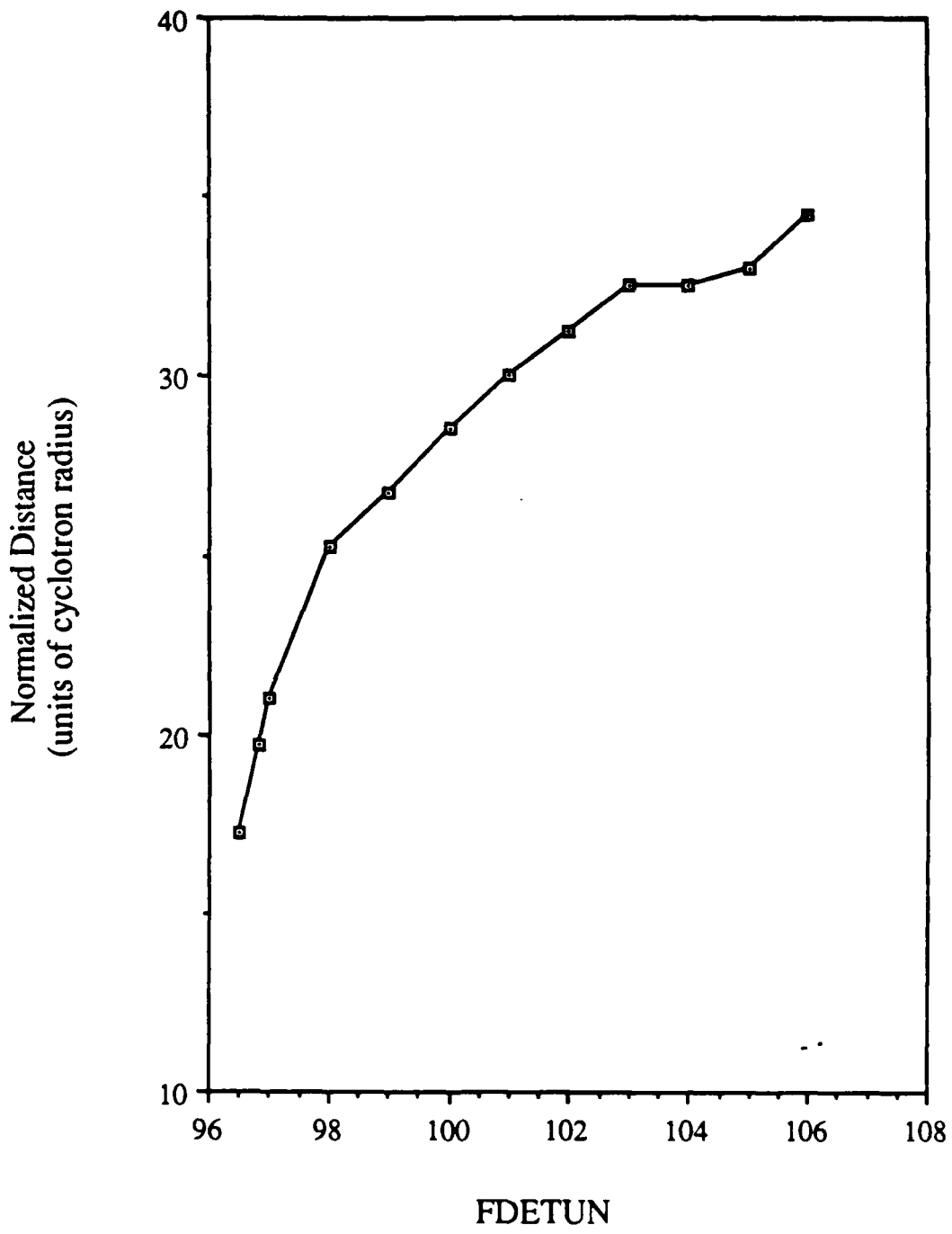
Fig. 5.8. Variation of saturation length,
L_{sat}, with RF frequency detuning.

two RF detuning analysis plots agrees with Golomb[31] (qualitatively, a different case was considered).

The final numerical simulation result to be reported deals with the relationship between RF power in, P_{in}, and saturated efficiency and power gain. Figure 5.9 shows these results. The input data for this plot are as shown in Table 4.1, with the exception of the input power (which was 3.425 kW in the Navy Research Laboratory design).

The efficiency curve monotonically decreases as the input power is increased. This may be explained in part by the fact that the electron bunch is formed slowly $\left(L_{sat} \text{ scales inversely with } P_{in} \right)$ enough that the electrons that are bunched quickly have not slipped out of phase and begun gaining energy before the last electrons to be bunched are giving up their energy. The bunch is formed well, and under the influence of the weaker RF field, the bunch remains in synchronism with the field longer.

The power gain curve is less straightforward to interpret. Neither segment of the gain curve with negative slope produces a situation of increased power in producing decreased power out. The slopes are such that the rate of increase of power out with increased power in is only diminished, not negative. It is possible that the point for P_{in} = 1 kW may be too far below the power level of the beam to be significant (~28 dB down). The points at P_{in} = 9 and 10 kW are also not fully explained either.

These numerical results are samples of the capability of AMINUS. They have displayed the ability of the code to predict the quality of interaction as major input parameters are varied over large ranges.
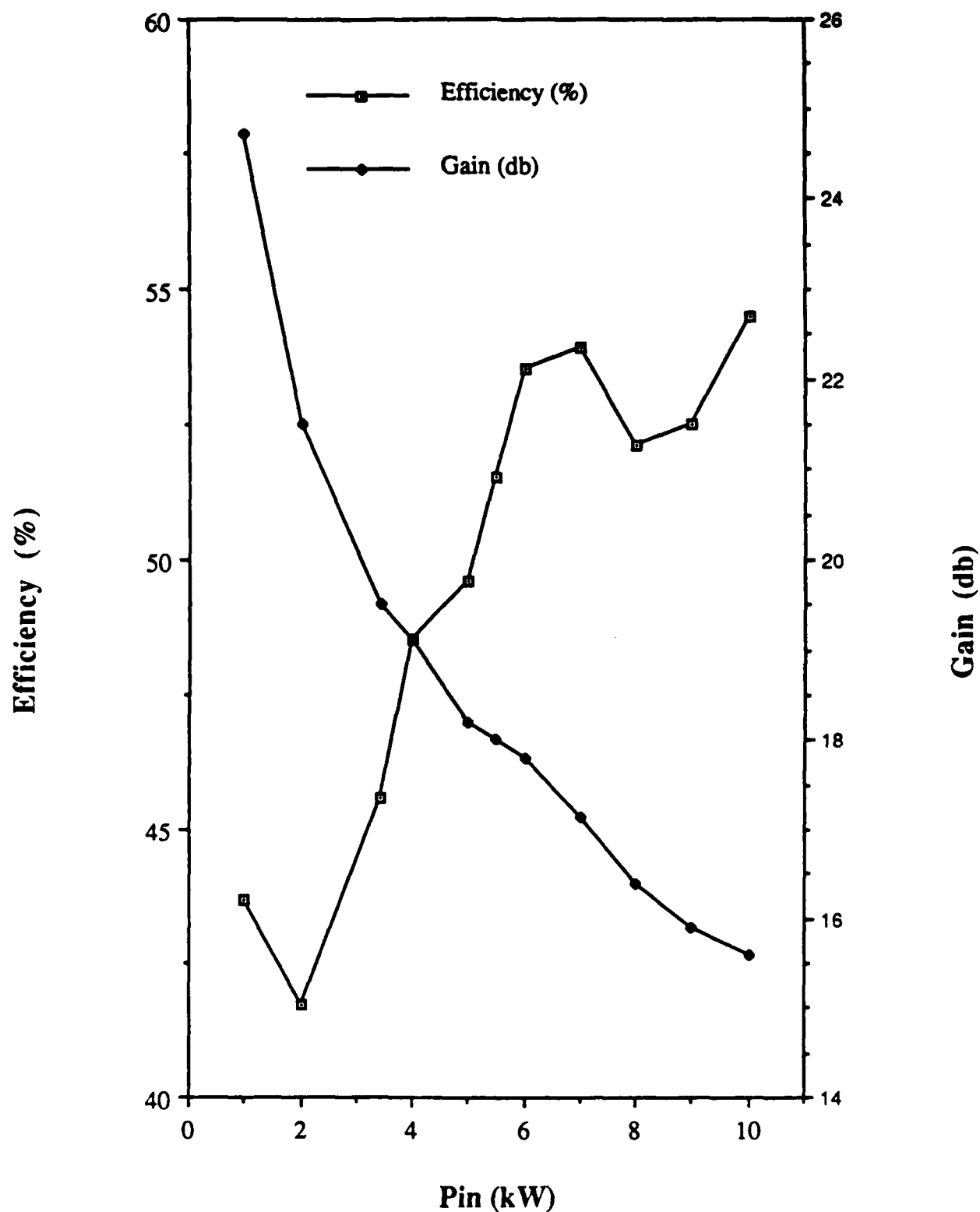
Fig. 5.9. Saturation efficiency and power gain as a function of P_{in}. Efficiency decreases monotonically as P_{in} increases. The power gain curve tends to increase as P_{in} increases.

AMINUS is an effective tool for gaining understanding of the complicated cyclotron maser interaction, and for predicting optimal interaction parameters based on the increased understandings. Based on the extensive verification process discussed in Section 4.7 and the automatic error checking precautions within AMINUS, the reliability of the numerical results is high.

5.6 Summary of Results

The results of this report may be summarized by noting the areas addressed in the previous sections. The GTWA device limitations of unwanted oscillation and narrow bandwidth were studied, and device based solutions were proposed in the form of spatially located frequency selective loss, and a tapered interaction region and dc magnetic field. These proposals pointed out the shortcomings of the available analytic theories and indicated the need for a new large signal nonlinear theory of the GTWA capable of dealing with the proposed configurations. The theory is a combination of a transmission line formulation for the RF fields and a single particle ballistic theory for the electron trajectories. The theory is capable of describing the interaction mechanism for applications in which both taper and nonideal walls are present. The theory is made self-consistent by a beam-field coupling term derived in the context of the transmission line formulation, and by the use of the variable magnitude RF fields in the trajectory calculations. The theory has been implemented in a computer simulation code and verified by a lengthy and rigorous process. The simulation code has been applied to the investigation of the effects of detuning the RF and dc frequency parameters.

VI. CONCLUSIONS AND RECOMMENDATIONS

6.1 Introduction

This final section of the report is devoted to a brief review of the results of the research contained in this report and identification of remaining research objectives related to the present work. For the detailed discussion of the results, both analytic and numerical in nature, the reader is referred to the Table of Contents and Sections I-V.

The actual results are discussed in Section 6.2. These results include device based solutions to actual operational problems with CTWA devices, the derivation of an analytic theory capable of describing the physical configurations arising from the application of the device based solutions, a numerical implementation of the analytic theory, and numerical results drawn from the simulation code.

The conclusions based on the research findings are summarized in Section 6.3. Conclusions regarding the usefulness of the transmission line formulation for the RF electromagnetic fields, the basic form of the beam-field coupling term, the usefulness of the simulation code for modeling, increasing understanding, and design work are drawn and discussed.

Section 6.4 is devoted to recommendations for further work with regard to both analytical and numerical study of the problems identified in Section 1.2. These recommendations deal with the verification of the method for dealing with the RF fields in the region $z_{f1} < z < z_{co}$, the identification of a faster integration algorithm, extensive simulation/ modeling work, and the development of an optimization scheme for the

location of optimal (i.e., higher values of I_{st} and increased operational bandwidth) operating parameters for GTWA devices.

6.2. Summary of Research Accomplishments

This section presents a brief summary of the results obtained and reported in this report. The results in this report may be broken into four distinct categories. The primary results of each category will be summarized in this section. The reader is referred to Sections II and III for the derivation of the analytic theory, Section IV for the discussion concerning the numerical implementation of the analytic theory into a simulation code, and to Section V for the full discussion of the research findings.

The first category of results deals with the device based solutions proposed and developed to circumvent two specific problems that currently limit the usefulness of the GTWA. The first of these problems is the occurrence of unwanted oscillations, which begin at lower than desired current levels, and which occur at a frequency slightly below cutoff and therefore not at the optimum for gain and/or efficiency. The solution proposed for this problem is in the form of a frequency selective loss mechanism that would absorb any power involved in the oscillation at the unwanted frequency. The second problem investigated is the narrow bandwidth of the normal configuration of the GTWA. The proposed solution for this limitation is in the form of a reverse injection configuration coupled with a tapered waveguide and a contoured dc magnetic field.

The research that leads to the next category of results was under-

taken in order to develop the analytic tools needed to study the device based solutions mentioned above. The theories available were not able to adequately address the physical implementation of the solutions, thus indicating the need for the use of a different analytic approach. In particular, the theories available were not suited to address the concept of a spatially located, frequency selective loss mechanism, nor were they suited to address the reverse injection scheme. A largw signal nonlinear theory of the gyrotron traveling-wave amplifier was developed by combining a transmission line formulation for the RF electromagnetic fields with a single-particle ballistic model and theory for the electron trajectory calculations. The transmission line formulation is an excellent tool for the analysis of tapered and/or nonideal wall waveguide interaction regions. The transmission line approach was chosen because it yields terms specifically derived to address each type on nonuniformity in the waveguide, including the case of the simultaneous presence of both types of nonuniformity, and because it is based on a waveguide mode expansion, yielding a profile coefficient for the electric and magnetic fields of each separate mode. A very important aspect of the transmission line formulation is the beam-field coupling term that arises naturally during the derivation. This coupling term is presented in a general term and in a form specific to the circular waveguide configuration being investigated in this report. The selected form for the trajectory equations uses the same type of field representation and allows for the case of a tapered dc magnetic field. The guiding center formulation was also derived in a consistent fashion as well.

Collected together, the individual pieces of analytic work result in a cohesive analytic description of the GTWA interaction, with the capability to deal with a number of complicating, but useful adaptations to the standard configuration. The derived theory is capable of dealing with the conventional GTWA device configurations with the equal or better accuracy as compared to the previously available theories. The significance of this work lies in the fact that nonstandard configurations may be dealt with by use of the theory derived herein. That is, all the information previously available to theoreticians may be found in this theory, as well as information describing the effects of electrically nonideal waveguide walls and/or tapered waveguide walls. Further, the theory is derived in such a fashion so as to allow the analysis of multiple element interaction regions, examples of which would include loss elements used to protect the electron gun, lossy waveguide regions, auxiliary waveguide coupling mechanisms, severs, and other stabilization elements. Thus, the theory derived herein surpasses previously available theories in the generality and realism of physical configurations that may be analyzed.

The next category of results follows again naturally from the previous category. The analytic theory discussed above has been coded into a simulation program, presently called AMINUS. AMINUS retains all the necessary components and capabilites needed to consider the device based solutions discussed as the first category of results. The simulation code has the ability to consider the effects of guiding center motion, or to perform calculations under the assumption that the centers do not move. AMINUS has been time optimized by the use of small

argument approximations where appropriate, and by the use of a machine dependent vector instruction set in the integration algorithm. The code is written to implement the self-consistent theory discussed above, but, for the purpose of run time speed, may be used as a nonself-consistent code for rough results. A rigorous verification scheme was devised and carried out, and the code passed all phases with excellent results. The numerical results of the computer code were shown to agree with the results published previously by Chu[18,19] and Fliflet.[24] The simulation results were compared for gyroamplifier devices operating in both the conventional $(\beta_{ph} \sim 3 - 10)$ CRM region, as well as the CARM regime $(\beta_{ph} \gtrsim 1)$. A supporting code was written to calculate the linear regime small signal gain rate for given input parameters. These two codes, the internal calculations of AMINUS, and all tested published results are in substantial agreement, indicating that AMINUS is an accurate, numerically robust simulation code.

The final category of results deals with the numerical results gained either in the development of the computer simulation code discussed above, or in the use of the code in simulation based studies. The development phase results dealt with the form chosen to represent the electron beam. It was found that a minimum number of particles, namely, $N_{min} \geq 12$, was required to adequately represesnt the range of possible initial phase relationships between the electron motion and the RF field. The simulation studies were done to examine the effects of detuning either the RF field frequency or the dc magnetic field (cyclotron frequency) from the synchronous values. It was found that the synchronous value of the RF frequency corresponded to the lowest value

of saturation efficiency. The variations in efficiency with RF detuning were explained by consideration of the beam dispersion equation. The analysis indicated that the interaction corresponding to below synchronous RF tuning was aided by a small value of k_z, which is characterized by a large linear growth rate, and that above synchronous tuning was aided by the decreasing value of $\langle\gamma\rangle$, which allowed the RF field to remain synchronously coupled to the electron beam long enough to yield a high efficiency value. It was found that the saturated efficiency was peaked at about 0.96 times the synchronous value, and sharply decreased in a linear fashion as the dc magnetic field is adjusted up through the synchronous value. It was found that, for the design considered, a dc magnetic field greater than 1.0254 times the synchronous value created a circumstance in which the RF field could not bunch the electron beam, and the beam became an active energy absorber.

For the parameters tested in detail, the slope of the saturation efficiency versus detuning parameter was approximately 9 percent decrease in saturation efficiency per 1 percent increase in magnetic tuning, and similar findings were observed for other operating conditions. The saturation length was found to increase monotonically for increased RF frequency tuning, with the lowest possible detuning falling just above ω_{synch}/γ_z in the frequency spectrum. It was found that the saturated efficiency/power gain vary approximately monotonically in an inverse/direct way with increased RF power. The guiding center motion was studied as well for various mode and cyclotron harmonic numbers and found to be significant in some cases and insignificant in others,

indicating that care must be used in claiming and/or assuming zero guiding center motion in the analysis of GTWA devices.

6.3 Conclusions Based on Research Accomplishments

This section details some conclusions reached through a consideration of the research findings contained in this report. These conclusions fall into three categories:

1. The validity and usefulness of the transmission line formulation.

2. The validity of the beam-field coupling term.

3. The value of the derived simulation code.

As has been extensively discussed in this report, the device based solutions proposed herein were not adequately dealt with by existing analytic theories of the gyrotron traveling-wave amplifier. It would have been possible to alter those theories to handle at least the tapered waveguide problem, and possibly the nonideal wall problem as well. It was determined, though, that a completely new approach was in order to provide a clear treatment of the two device based solutions. The transmission line theory does not require any assumptions, nor does it require linearization, and so has an exactness about it not found in kinetic theory. Within the report, a single RF mode has been assumed to propagate in the waveguide, and that mode has been represented exactly. It has been possible using the transmission line formulation to derive terms specifically addressing the presence of the two types of waveguide nonuniformity involved in the device based solutions.

Further, earlier work[6,3] that considered only a single type of nonuniformity in the waveguide has been corrected by this approach.[4,3,7] In the case of a single nonuniformity, the equations presented reduce to the proper form. This then leads to the conclusion that the transmission line formulation for the RF electromagnetic fields is a powerful analytic tool. This tool has been exploited in the research reported herein for cases described by a cylindrical coordinate system to a great advantage. This tool could also be applied equally well to devices operating in a geometry best described by a rectangular coordinate system.

The second conclusion deals with the validity of using a distribution function constructed of spatial and velocity delta functions. The concept had been proposed by several authors,[4,36,41] but, to this author's knowledge, has not ever been implemented into a computer simulation code. The implementation has allowed a practical verification of the validity of this simple form for the coupling term. The accuracy of the implementation in this report has been verified by comparison of the amount of energy given up by the beam and the amount of energy gained by the RF fields. The agreement between the two values was found to be so close that the error inherent in the numerical integration process is suspected to be the primary, if not sole, cause of disagreement.

The final conclusion concerns the usefulness of the simulation code, AMINUS, for increasing the understanding of the physical interaction mechanism of the gyrotron interaction in an amplifier configuration. It has been shown that AMINUS is capable of accurately predicting the interaction behavior under a large range of input parameters,

including the interaction that occurs below the classical waveguide cutoff point and the interaction occurring for cases in which the beam and field are so severely detuned that no amplification is possible. The nonlinear behavior of GTWA devices may be modeled using AMINUS under operating conditions simulating various irregular waveguide configurations, including, but not limited to, those proposed in Section 1.3. Several physical explanations have already been made based on the simulation results presented in Section 5.5. It has been concluded that the claim of zero guiding center motion is not always valid, but must be justified on a case by case basis.

The most fundamental conclusion is that the analytic and numerical tools needed for a fuller evaluation and simulation of the operating characteristics of gyrotron traveling-wave amplifier devices are now in place. The tools described in this report allow the simulation of the gyrotron interaction in waveguide interaction regions, which more closely represent the current state-of-the-art experimentation than was possible by use of previously available research tools. The interaction regions may be fully general, including electrically nonideal walls and/or tapered waveguide regions. The presence of these types of uniformities has defeated or severely limited the usefulness of previous theories.

6.4 Recommendations for Further Study

This section will identify several tasks whose successful completion would provide additional insight into the operation and modeling of

GTWA devices and an even more useful computer simulation tool. The recommendations are four in number:

1. Further study of the proper method for representation of the below cutoff properties of the beam-wave interaction.

2. Identification of an integration algorithm requiring fewer function evaluations.

3. Extensive simulation and modeling studies.

4. Design and implementation of an optimization scheme using AMINUS as the function being optimized.

Questions have been raised concerning the appropriateness of the method chosen to represent the electron cyclotron maser interaction when the RF electromagnetic wave has frequency ω less than the local cutoff frequency, $\omega_{co}(z)$, in a tapered waveguide.[3] Within this report, it is assumed, with what is believed to be valid analytical justification, that the RF wave may be modeled as though it were launched or injected from a point labeled z_{f1} in Fig. 5.3 with a very small initial amplitude, even when the launching point has a corresponding waveguide radius less than the cutoff value for the launched mode. The qualitative argument for the model is as follows. Actually, the wave is launched and travels in the $-z$ direction, as shown in Fig. 5.3. The classical cutoff radius occurz at z_{co} at which point the wave coherently reflects and begins to travel in the $+z$ direction. The reflection does not occur in a single plane, though, but may be represented as a wave being exponentially damped as it travels further into the cutoff region, $z_{f1} < z < z_{co}$, until at z_{f1} the wave has been diminished so that it has a very small or infinitesimal magnitude. Viewed as a modeling problem, it is

seen that z_{fl} may be represented as the field launching point, and the wave will grow exponentially in the +z direction (seen by the exponential decay in the -z direction). It is well known that RF waves do not truly propagate, and that no energy can travel down the waveguide for regions in which $\omega < \omega_{co}$.[61,37,32] It is also known that attenuation occurs,[61,37,32] thus validating the physical picture developed here and shown in Fig. 5.3. It is held, then, by the findings in this report, that it is possible, and even necessary, to model the RF field in the cutoff region as explained here. It is known that a significant change occurs in the amplitude of the RF wave in this region,[3] which makes it imperative that this region be subject to numerical simulation. Given the stature of those asking the questions (principal researchers at the Naval Research Laboratory), it is deemed that the questions should be investigated fully.

A discussion of the process used to choose the integration algorithm was presented in Section 4.5. The final choice was a custom written, time optimized implementation of a fourth order Runge-Kutta (RK4) algorithm. The RK4 algorithm is handicapped by the requirement that the function being integrated be evaluated four times per step. For an application in which the function evaluations are expensive, such as is the case in AMINUS, the number of evaluations must be held to a minimum. Reseaarch is currently under way for an algorithm with the same robustness as the presently used algorithm, but which uses fewer function evaluations. Though this may seem like a small point, the simulation code run time (and thus run-time expense) will scale approximately as the number of function calls per step.

No case need be made for the third recommendation, which is an extension of the cases and configurations studied by simulation. Extensive work needs to be done on the design and modeling of the loss mechanisms, as well as optimization of the waveguide and magnetic field contour. The difficulty in experimentally achieving the analytically identified optimal dc magnetic field profile has been documented.[4,6] A scheme for modeling the profile has been noted in a recent work.[31] This scheme would result in a smooth profile, which would presumably be easier to experimentally implement, and which reflects consideration of not only the waveguide taper, but also the changing electron energy. Automation of the process of designing and simulating loss mechanisms, waveguide wall taper, and dc magnetic field taper would provide a helpful simulation tool in the study of complex cavity GTWA devices.

Finally, it is recommended that the present simulation code be configured so that an identifiable result is the power in the backward wave, the amplitude of which is denoted $a^-(z)$, thus giving rise to the name of the present simulation code, AMINUS. The oscillation start conditions may be studied by identifying the current value at which a perfectly matched device breaks into oscillation for $a^-(L)$ is significantly smaller than $a^+(L)$, where $a^+(z)$ is the power in the forward wave at z. Ideally, a^- would be zero, but a sufficient and more practical condition would be to require that a^- be 20 to 30 dB down from a^+. At that point, the device would make the transition from an amplifier to an oscillator, and the current would be identified as I_{st}. The optimization would be in the form of an optimization of a real function of two real variables, i.e., $\mathrm{MIN}\{a^-(\omega, I_o)\}$. The values of a^- corresponding

to (ω, I_o) points could be thought of as contours in a three-dimensional space, where the surface so constructed would represent the start oscillation conditions for a GTWA device. The objective of this recommendation would be to raise the entire surface and/or to locate the local and absolute maxima on the surface.

Research on each of these recommendations, by this researcher, is currently underway at the University of Utah. Results on the first and second recommendations are considered imminent. Work on recommendations three and four is underway, and results are anticipated, but due to the nature of the work, will take longer to achieve.

APPENDIX A

VECTOR AND SCALAR RELATIONSHIPS

Several vector and scalar relationships and theorems are listed in this appendix. These relationships are used in various parts of the report and are collected here for convenience.

$\hat{x}$, $\hat{y}$, and $\hat{z}$ are unit vectors in the rectangular coordinate system. $\hat{r}$, $\hat{\theta}$, and $\hat{z}$ are the unit vectors in the circular coordinate system. The circular coordinate system is actually a subset of the set of coordinate systems strictly called cylindrical coordinate systems.[35] For purposes of brevity within this report, cylindrical coordinates will be understood to refer specifically to the circular cylindrical coordinate system. Quantities $\vec{A}$, $\vec{B}$, and $\vec{C}$ are vectors which may be formulated in either of the two coordinate systems mentioned above. Quantities ϕ and ρ are scalars and also may be formulated in either of the two coordinate systems.

The triple cross product may be expanded as[35]

$$\vec{A} \times (\vec{B} \times \vec{C}) = (\vec{A} \cdot \vec{C})\vec{B} - (\vec{A} \cdot \vec{B})\vec{C} \qquad (A.1)$$

The scalar quantity given by $\vec{A} \cdot \vec{B} \times \vec{C}$ may also be evaluated in any of the following forms given by[35]

$$\vec{A} \cdot \vec{B} \times \vec{C} = [\vec{A}\vec{B}\vec{C}] = [\vec{B}\vec{C}\vec{A}] = [\vec{C}\vec{A}\vec{B}] \qquad (A.2)$$

The chain rule for differentiation of the product of a scalar and a vector is[35]

$$\vec{\nabla} \times \phi\vec{A} = \phi\vec{\nabla} \times \vec{A} + \vec{\nabla}\phi \times \vec{A} \qquad (A.3)$$

The two-dimensional Leibnetz rule for the integration of the dot product of two vectors is[4]

$$\overset{(a)}{} \qquad \overset{(b)}{} \qquad \overset{(c)}{} \qquad \overset{(d)}{}$$

$$\frac{d}{dz} \int_{S(z)} \vec{A} \cdot \vec{B} \, ds = \int_{S(z)} \frac{\partial\vec{A}}{\partial z} \cdot \vec{B} \, ds + \int_{S(z)} \vec{A} \cdot \frac{\partial\vec{B}}{\partial z} \, ds + \oint_{\ell} \frac{\partial n_b}{\partial z} \vec{A} \cdot \vec{B} \, d\ell$$

$$(A.4)$$

The quantity n_b is the value of the outward normal variable at the boundary of $S(z)$. Examination of Fig. 2.1 reveals that $\partial n_b/\partial z$ is just the slope of the boundary in the n - z plane. Therefore, $\partial n_b/\partial z = \tan(\theta_T)$.

Two forms of the two-dimensional Green's theorem for scalar functions are used herein. These two forms may be written as[4]

$$\overset{(a)}{} \qquad \overset{(b)}{} \qquad \overset{(c)}{}$$

$$\int_{S(z)} \phi\nabla_t^2\rho \, ds + \int_{S(z)} \vec{\nabla}_t\phi \cdot \vec{\nabla}_t\rho \, ds = \oint_{\ell} \phi \frac{\partial\rho}{\partial n} \, d\ell \qquad (A.5)$$

$$\overset{(a)}{} \qquad\qquad \overset{(b)}{}$$

$$\int_{S(z)} \phi\nabla_t^2\rho - \rho\nabla_t^2\phi \, ds = \oint_{\ell} \phi \frac{\partial\rho}{\partial n} - \rho \frac{\partial\phi}{\partial n} \, d\ell \qquad (A.6)$$

where ℓ is the closed countour around $S(z)$, and n is the outward normal. Stoke's theorem may be written as[35]

$$\int_{S(z)} (\vec{\nabla} \times \vec{A}) \cdot \vec{ds} = \oint_{\ell} \vec{A} \cdot \vec{d\ell}$$

The transmission line formulation always uses $\vec{ds} = \hat{z}\,ds$, as in Fig. 2.1, so that Stoke's theorem may also be written as

$$\int_{S(z)} (\vec{\nabla} \times \vec{A}) \cdot \hat{z}\,ds = \oint_{\ell} \vec{A} \cdot \vec{d\ell} \qquad (A.7)$$

The manner in which this theorem is used involves a vector of the form,

$$\vec{A} = \rho\vec{\nabla}_t\phi \qquad (A.8)$$

With this form for A, two forms result,[*]

$$\int_{S(z)} (\vec{\nabla}_t\rho \times \vec{\nabla}_t\phi) \cdot \vec{ds} = \oint_{\ell} \rho\vec{\nabla}_t\phi \cdot \vec{d\ell} \qquad (A.9)$$

and

$$\int_{S(z)} (\vec{\nabla}_t\rho \times \vec{\nabla}_t\phi) \cdot \vec{ds} = - \oint_{\ell} \phi\vec{\nabla}_t\rho \cdot \vec{d\ell} \qquad (A.10)$$

The components of $\vec{C}$ may be expressed in rectangular coordinates as

$$\vec{C} = C_x\hat{x} + C_y\hat{y} + C_z\hat{z} \qquad (A.11)$$

$$C_r = C_x \cos\theta + C_y \sin\theta \qquad (A.12)$$

$$C_\theta = -C_x \sin\theta + C_y \cos\theta \qquad (A.13)$$

The vector, C, may be expressed in cylidnrical coordinates as

$$\vec{C} = C_r \hat{r} + C_\theta \hat{\theta} + C_z \hat{z} \qquad (A.14)$$

and transformed into the equivalent rectangular terms by using the relationships[35]

$$C_x = C_r \cos \theta - C_\theta \sin \theta \qquad (A.15)$$

$$C_y = C_r \sin \theta + C_\theta \cos \theta \qquad (A.16)$$

Using Eqs. A.15 and A.16, a relationship is derived between a combination of transverse unit vectors in the two coordinate systems.

$$\hat{x} + j\hat{y} = (\hat{r} \cos \theta - \hat{\theta} \sin \theta) \pm j(\hat{r} \sin \theta + \hat{\theta} \cos \theta)$$

$$= \hat{r}(\cos \theta \pm j \sin \theta) + j\hat{\theta}(j \sin \theta \pm \cos \theta)$$

$$= \hat{r}(\cos \theta \pm j \sin \theta) \pm j\hat{\theta}(\cos \theta \pm j \sin \theta)$$

so that

$$\hat{x} \pm j\hat{y} = (\hat{r} \pm j\hat{\theta}) e^{\pm j\theta} \qquad (A.17)$$

Equation A.17 also holds for the conversion of the components of vector quantities from one coordinate system to the other. This may be verified by dot multiplying the left-hand side of Eq. A.17 into the vector expressed in rectangular form, and the right-hand side of Eq. A.16 into the vector expressed in circular cylindrical form.

APPENDIX B

EXPRESSION OF B_{or} IN TERMS OF MAGNETIC FIELD TAPER

The dc magnetic field is assumed to have the form

$$\vec{B}_o = B_{oz}\hat{z} + B_{or}\hat{r} \tag{B.1}$$

where

$$B_{oz} \gg B_{or}$$

Taking the divergence of $\vec{B}_o$, and using Maxwell's divergence relationship for $\vec{B}$ yields

$$\vec{\nabla} \cdot \vec{B}_o = \frac{1}{r}\frac{\partial}{\partial r}\left(r\, B_{or}\right) + \frac{\partial B_{oz}}{\partial z} = 0$$

or

$$\frac{1}{r}\frac{\partial}{\partial r}\left(rB_{or}\right) = -\frac{\partial B_{oz}}{\partial z}$$

$$\int \partial\left(rB_{or}\right) = -\frac{\partial B_{oz}}{\partial z}\int r\,\partial r$$

$$rB_{or} = -\frac{1}{2}r^2\frac{\partial B_{oz}}{\partial z}$$

$$B_{or} = -\frac{1}{2}r\frac{\partial B_{oz}}{\partial z} \tag{B.2}$$

Equation B.2 allows B_{or} to be expressed in terms of the taper of B_{oz}, and is the transformation used in Eq. 3.46.[36]

APPENDIX C

EXPLANATION AND APPLICATION OF GRAF'S ADDITION
THEOREM FOR BESSEL FUNCTIONS

The basic reference for this appendix is Abramowitz and Stegun, _Handbook_ _of_ _Mathematical_ _Functions_, p. 363.[1] The formulation is also used and applied in articles by Chu,[17] Fliflet,[24] and other researchers, though without any elaboration. Graf's theroem as stated[1] is

$$B_\nu(w) \frac{\cos}{\sin} (\nu b) = \sum_{k=-\infty}^{\infty} B_{\nu+k}(u) J_k(v) \frac{\cos}{\sin} (k\alpha) \qquad (C.1)$$

subject to the condition

$$|v \, e^{\pm j a}| < |u| \qquad (C.2)$$

where B represents a Bessel function of the first or second kind, or a complex sum or difference of the two.

Figure C.1 shows the geometry used in Graf's theorem. The function served by Graf's theorem, geometrically, is the expression of a triangle in the form of two sides and an included angle as opposed to a single side and an adjacent angle. Physically, the theorem allows the expansion of the RF fields at the guiding center of the electron orbits. This process identifies the strength of the field detected by the electron itself, and reveals the utility of the beam model chosen in Section IV.
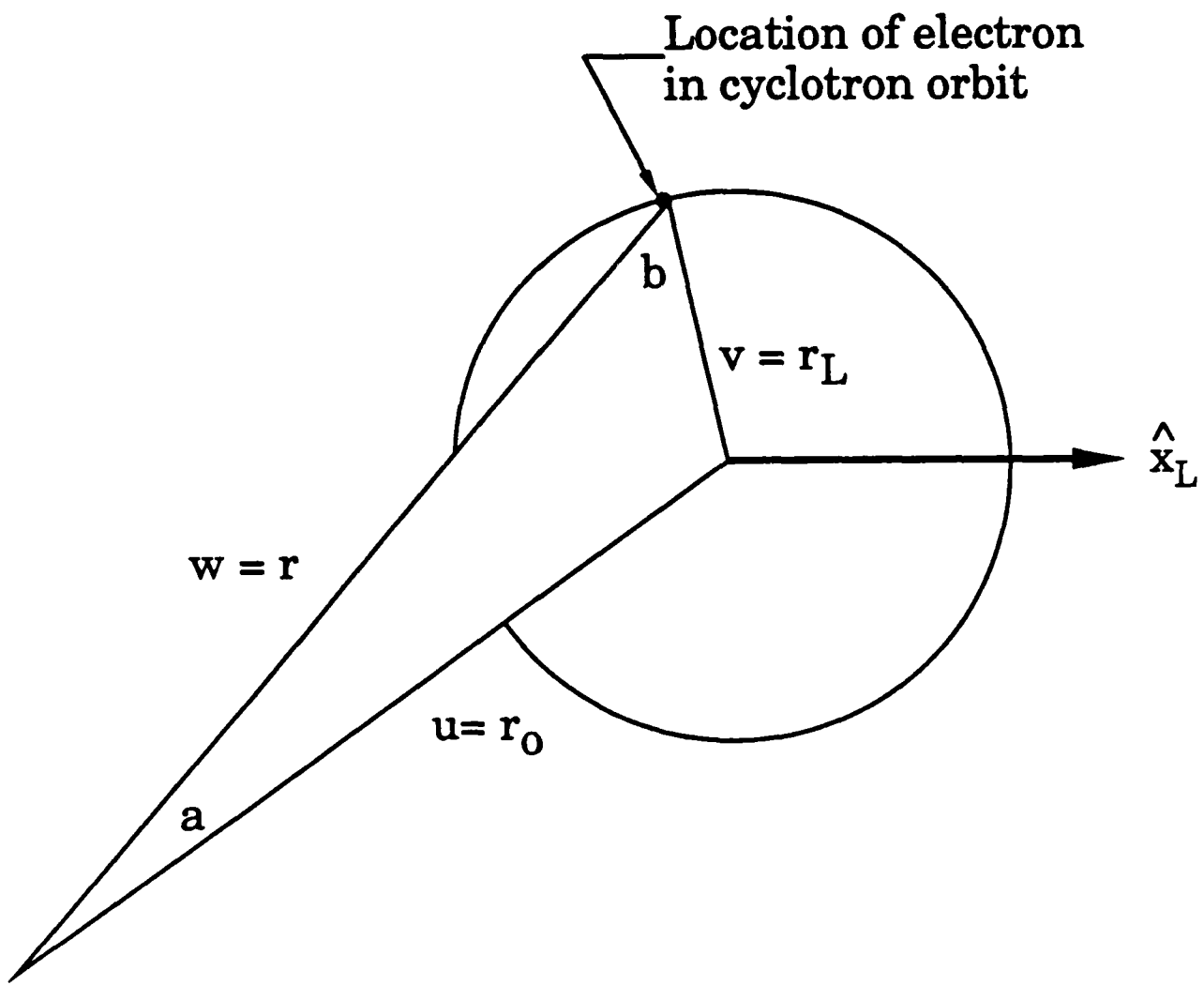
Fig. C.1. Geometry used for Graf's addition theorem for Bessel functions, overlaid on a single beamlet cross section to identify the use of the theorem's variables.

The form of Eq. C.1 used in the present work is found by adding the cosine portion of Eq. C.1 to $(-j)$ times the sine portion. The resulting expression is in a form useful for expressions involving exponential functions of angle.

$$B_\nu(w) \ e^{-j\nu b} = \sum_k B_{\nu+k}(u) J_k(v) \ e^{-jk\alpha} \qquad (C.3)$$

The expressions found in Section III that were modified by application of Graf's theorem were (from Eq. 3.60)

$$L_\pm \psi_m \ e^{\mp j\alpha} = \pm C_{mn} k_{tm} J_{m\mp 1}(R) \ e^{-j(m\mp 1)\theta} \ e^{\mp j\alpha} \qquad (C.4)$$

The values for the radial variables are clear from Fig. C.1, but the angular values require further consideration. Figures C.2 and C.3 (a copy of Fig. 3.2) are diagrams of a beamlet with additional angles labeled for convenience. From a comparison of Figs. C.1 and C.2, the values of the angles a and b are

$$a = \theta_1$$

$$(C.5)$$

$$b = \theta_2$$

For the case pictured in Fig. C.2, in which $\vec{r}_o$ lies exactly on $\hat{x}$, the relation

$$\theta_2 + (\Omega\tau + \phi) = \pi \qquad (C.6)$$
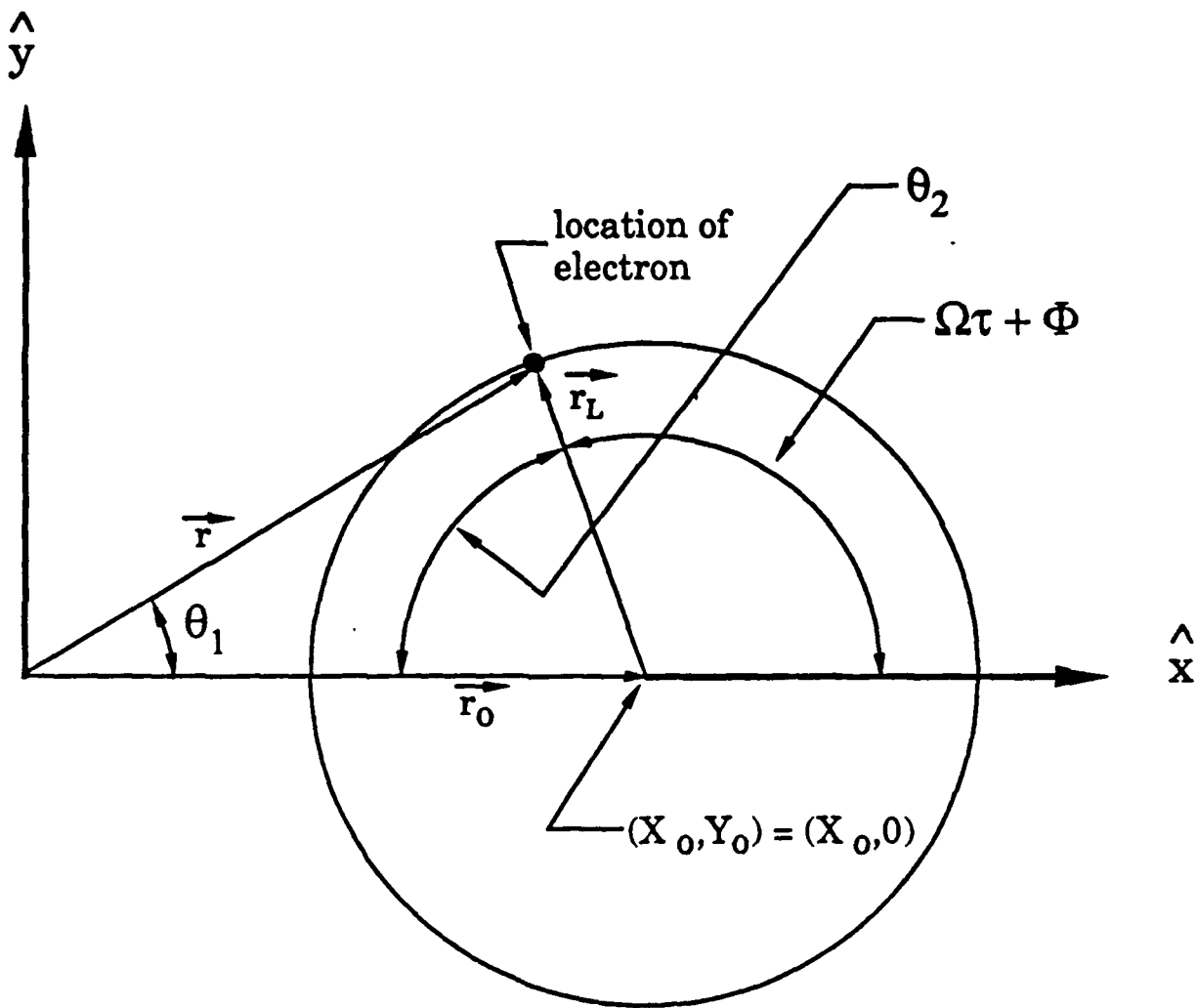
Fig. C.2. Beamlet geometry for the special case when $\vec{r}_o \cdot \hat{x} = r_o$.
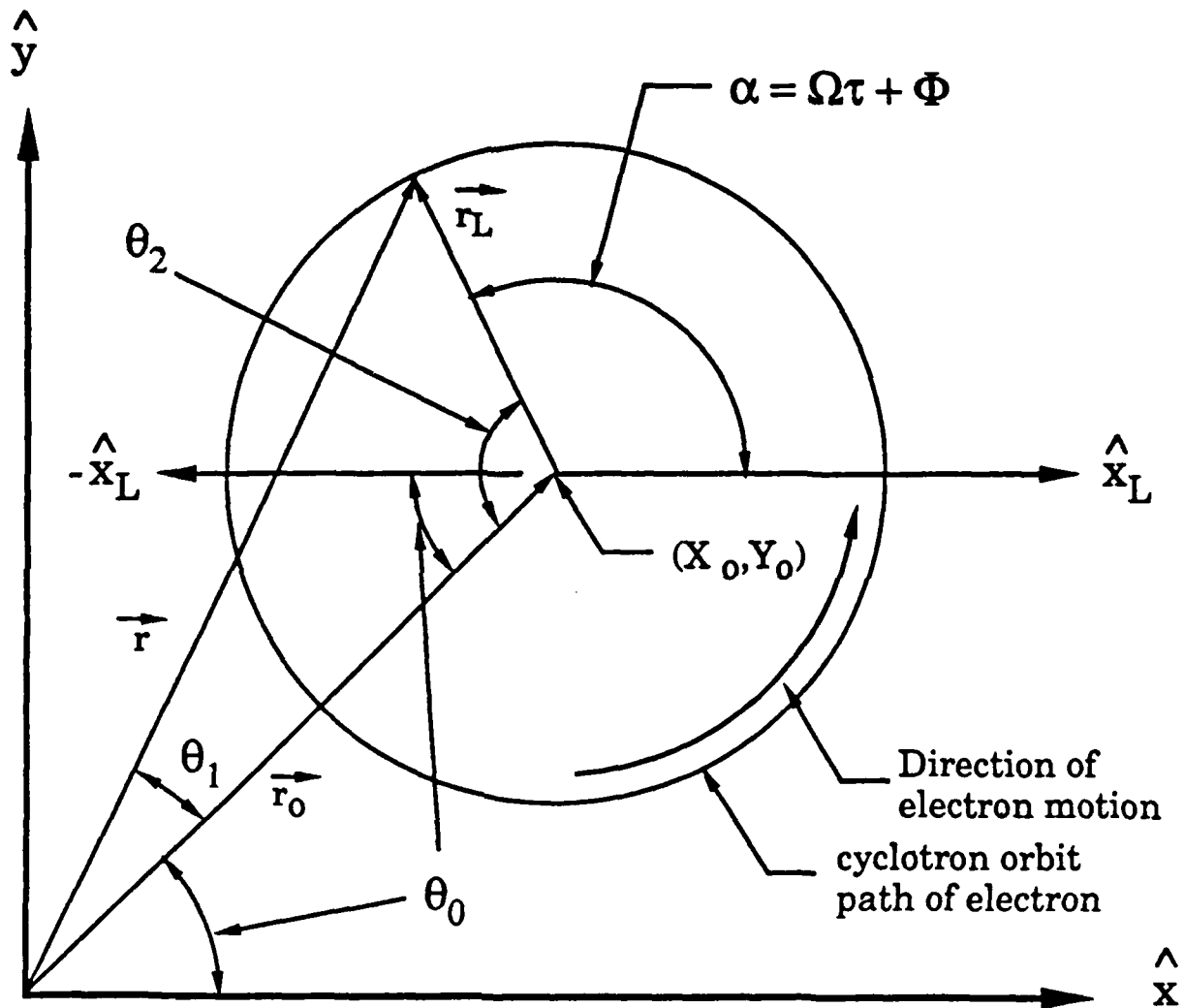
Fig. C.3. General beamlet geometry. The guiding center
has been rotated azimuthally by angle θ_o.

- 203 -

may be observed. Figure C.3 may be thought of as the same beamlet with the guiding center azimuthally displaced by an angle θ_o. Figure C.3 is the general case, and the standard case would involve a beam composed of beamlets with an equal distribution of initial θ_o values. For the beamlet in Fig. C.3, the relationship equivalent to Eq. C.6 is

$$\theta_2 - \theta_0 + (\Omega\tau + \Phi) = \pi \qquad (C.7)$$

or

$$\theta_2 = \pi + \theta_0 - (\Omega\tau + \Phi) \qquad (C.8)$$

The value for θ_1 is obtained simply as

$$\theta_1 = \theta - \theta_0 \qquad (C.9)$$

Substitution of Eqs. C.8 and C.9 into Eq. C.4 yields

$$L_\pm \psi_m \, e^{\mp j\alpha} = \pm C_{mn} k_{tm} \, e^{-j[(m\mp 1)\theta_0 \pm (\Omega\tau + \Phi)]} \, J_{m\mp 1}(R) \, e^{-j(m\mp 1)\theta_1} \qquad (C.10)$$

The scalar wave function is transformed using Graf's theorem in Section 3.6. It may be written in a form similar to Eq. C.10 as

$$\psi_m = C_{mn} J_{m-s}(R_o) J_s(R_L) \, e^{-j[(m-s)\theta_0 - s(\Omega\tau + \Phi)]} \qquad (C.11)$$

The substitution $\ell = m \mp 1$ is made in Eq. C.10, and the result is

- 204 -

substituted into Graf's theorem in the form given in Eq. C.4. This yields

$$L_{\pm}\psi_m \, e^{\mp j\alpha} = \pm C_{mn}k_{tm} \, e^{-j[\ell\theta_0 \pm (\Omega\tau + \Phi)]} \sum_{k=-\infty}^{\infty} J_{k+\ell}(R_o)J_k(R_L) \, e^{-jk\theta_2}$$

$$= \pm C_{mn}k_{tm} \sum_{k} J_{k+m\mp 1}(R_o)J_k(R_L)e^{-jk[\pi+\theta_0-(\Omega\tau+\Phi)]} e^{-j[(m\mp 1)\theta_0+(\Omega\tau+\Phi)]}$$

$$= \pm C_{mn}k_{tm} \sum_{k} J_{m+k\mp 1}(R_o)J_{-k}(R_L) \, e^{-j[(m+k\mp 1)\theta_0-(k\mp 1)(\Omega\tau+\Phi)]}$$

The summation indices are shifted according to

$$-q = k \mp 1 \tag{C.12}$$

so that

$$k = -q \pm 1$$

and

$$-k = q \mp 1$$

which yields

$$L_{\pm}\psi_m \, e^{\mp j\alpha} = \pm C_{mn}k_{tm} \sum_{q=-\infty}^{\infty} J_{m=q}(R_o)J_{q\mp 1}(R_L) \, e^{-j[(m-q)\theta_0+s(\Omega\tau+\Phi)]} \tag{C.13}$$

Now a single harmonic, the sth harmonic, is selected by taking the sth term in the summation. This yields

$$L_{\pm}\psi_m \, e^{\mp j\alpha} \stackrel{\sim}{=} \pm C_{mn} k_{tm} J_{m-s}(R_o) J_{s\mp 1}(R_L) \, e^{j[(m-s)\theta_0 + s(\Omega\tau+\Phi)]} \qquad (C.14)$$

By a similar process, ψ_m may be expanded from Eq. C.11 to yield

$$\psi_m \stackrel{\sim}{=} C_{mn} J_{m-s}(R_o) J_s(R_L) \, e^{-j[(m-s)\theta_0 - s(\Omega\tau+\Phi)]} \qquad (C.15)$$

The expansion of $e^{j(m-1)\theta} J_{m-1}(R)$ is needed in Section IV. Use of an index substitution similar to Eq. C.12 allows the straightforward application of the theorem. The result is

$$e^{j(m-1)\theta} J_{m-1}(R) \stackrel{\sim}{=} J_{m-s}(R_o) J_{s-1}(R_L) \, e^{-j(s-1)(\theta_0 - \alpha)} \qquad (C.16)$$

Equation C.14 is substituted into Eqs. 3.62, 3.63, and 3.64, the result multiplied by exp(jωt), and the real (physical) part is taken. This process yields Eqs. 3.65, 3.66, and 3.67. Also used in the process is the Bessel function identity in Eq. 3.96. The value of Γ, defined in Eq. 3.68, follows directly from this process. Eq. C.15 is substituted into Eq. 3.58 and the result into Eq. 3.94. The same process described above is then used to find Eq. 3.95.

It is interesting to note that the condition placed on the use of Graf's theorem in Eq. C.2 is always met in the present application. Consideration of the effects of diminishing r_o on angle a reveals that the limiting case of r_o = 0, which produces r = r_L, produces a value of a = 0, so that Eq. C.2 is always satisfied in the physical situations dealt with in the assumed beam model.

APPENDIX D

DERIVATION OF ELECTRONIC EFFICIENCY RELATIONSHIP

The total energy (TE) of a relativistic particle of mass m_0 and velocity v is given by[55]

$$TE = \gamma m_0 c^2 \qquad (D.1)$$

where

$$\gamma = \left[1 - \frac{\vec{v} \cdot \vec{v}}{c^2} \right]^{-1/2} \qquad (D.2)$$

and TE(0) is the initial total energy. We define γ_0 as the value of Eq. D.2 based on the initial velocity. In our case, this is the velocity of the particle prior to any interaction of the particle with the RF fields. The energy associated with this value is

$$(0) = \gamma_0 m_0 c^2 \qquad (D.3)$$

With this formulation, the kinetic energy (KE) of the particle may be written as[55]

$$KE = \left(\gamma - 1 \right) m_0 c^2 \qquad (D.4)$$

We then define a normalized electronic efficiency for exchange of kinetic energy as

$$\eta_{e\ell} \triangleq \frac{KE(0) - KE(Z)}{KE(0)} \qquad (D.5)$$

Using Eq. D.4, the most general form of Eq. D.5 for an ensemble of N particles would be

$$n_{el} = \frac{m_o c^2 \left[\left(\frac{1}{N}\sum_{p=1}^{N}\gamma_{o,p}\right) - 1\right] - m_o c^2 \left[\left(\frac{1}{N}\sum_{p=1}^{}\gamma_p\right) - 1\right]}{m_o c^2 \left[\left(\frac{1}{N}\sum_{p=1}^{N}\gamma_{o,p}\right) - 1\right]} \qquad (D.6)$$

where the possibility of an initial spread in velocity or momentum has been assumed. If we assume an initially mono-energetic electron beam, with kinetic energy given by γ_o, we may write as

$$n_{el} = \frac{m_o c^2 \left[\gamma_o - 1 - \left(\frac{1}{N}\sum_{p=1}^{N}\gamma_p\right) - 1\right]}{m_o c^2 \left(\gamma_o - 1\right)}$$

or

$$n_{el} = \frac{\gamma_o - \frac{1}{N}\sum_{p=1}^{N}\gamma_p}{\gamma_o - 1} \qquad (D.7)$$

Equation D.7 yields the electronic efficiency of an ensemble of electrons by measuirng the change in kinetic energy for the ensemble, including "good" and "bad" electrons.

APPENDIX E

DERIVATION OF A CYLINDRICAL COORDINATE EXPRESSION
FOR TRANSVERSE VELOCITY

The general expression for the transverse velocity in cylindrical coordinates is

$$\vec{v}_t = v_r \hat{r} + v_\theta \hat{\theta} \tag{E.1}$$

Equations 3.13 and 3.14 may be substituted into Eqs. A.12 and A.13 to yield

$$v_r = -v_t \sin(\alpha) \cos(\theta) + v_t \cos(\alpha) \sin(\theta)$$

$$= v_t \left[\cos(\alpha) \sin(\theta) - \sin(\alpha) \cos(\theta) \right] \tag{E.2}$$

and

$$v_\theta = v_t \sin(\alpha) \sin(\theta) + v_t \cos(\alpha) \cos(\theta)$$

$$= v_t \left[\sin(\alpha) \sin(\theta) + \cos(\alpha) \cos(\theta) \right] \tag{E.3}$$

The products of trigonometric functions may be reduced to a single expression to yield

$$v_r = -v_t \sin(\alpha - \theta) \tag{E.4}$$

$$v_\theta = v_t \cos(\alpha - \theta) \qquad\qquad (E.5)$$

Substitution of Eqs. E.4 and E.5 into Eq. E.1 yields

$$\vec{v}_t = v_t[-\sin(\alpha - \theta)\hat{r} + \cos(\alpha - \theta)\hat{\theta}] \qquad (E.6)$$

Equation E.6 is Eq. 4.33 in the text. Equation E.6 applies to both axis-encircling and nonaxis-encircling electron orbits.

A similar expression for $\vec{v}_t$ may be written using Eq. A.16. This expression offers certain advantages and is used in Section IV in the process of manipulating E_{bf} into its simplest form.

$$\vec{v}_t = v_t(\hat{r} + j\hat{\theta}) e^{+j\theta} \qquad\qquad (E.7)$$

APPENDIX F

DISPERSION RELATIONS FOR VARIOUS BEAM AND WAVEGUIDE CONFIGURATIONS

This appendix presents the dispersion relations derived by Lau, et al., in References 48 and 50. These dispersion relations were derived as approximations and adjustments to Eq. 1.6 of the text, which is repeated here for clarity.

For a cold beam, with no velocity or energy spread, and an ideal wall waveguide, the normalized dispersion relation was found to be

$$\left(\bar{\omega}^2 - \bar{k}^2 - 1\right)\left(\bar{\omega} - \bar{k}\beta_z - b\right)^2 = -\varepsilon_c \tag{F.1}$$

where

$$\omega_{co} \triangleq \text{RF cutoff frequency}$$

$$\bar{\omega} \triangleq \frac{\omega}{\omega_{co}}$$

$$\bar{k} \triangleq \frac{k_z}{k_{mn}}$$

$$\beta_z = \frac{v_{zo}}{c}$$

$$\beta_{to} = \frac{v_{to}}{c}$$

$$b \triangleq \frac{s\Omega_c}{\omega_{co}}$$

$$\varepsilon_c \triangleq \frac{4vc^2\beta_{to}^2 H_{sm}}{\gamma_o r_\omega^2 k_{mn}^2 \omega_{co}^2}$$

- 211 -

and H_{sm} is defined in Eq. 1.4

For a warm beam, i.e., one having velocity spread and/or total energy spread and a lossless waveguide, the dispersion relation is

$$(\bar{\omega}^2 - \bar{k}^2 - 1) \left[(\bar{\omega} - \bar{k}\beta_z - b)^2 - \left\{ \bar{k}\beta_z \frac{\langle \Delta v_z \rangle}{v_{zo}} \right\}^2 - \left\{ \omega \frac{\langle \Delta \gamma \rangle}{\gamma_o} \right\}^2 \right] = -\varepsilon_c \quad (F.2)$$

where

$$\langle \Delta v_z \rangle \overset{\Delta}{=} \frac{\int_{-\infty}^{\infty} f(\Delta v_z) f(\vec{r}, \vec{p}, t) \, d^3 p}{\int_{\infty}^{-\infty} f(\vec{r}, \vec{p}, t) \, d^3 p}$$

represents a spread in z velocity and

$$\langle \Delta \gamma \rangle \overset{\Delta}{=} \frac{\int_{-\infty}^{\infty} f(\Delta \delta) f(\vec{r}, \vec{p}, t) \, d^3 p}{\int_{-\infty}^{\infty} f(\vec{r}, \vec{p}, t) \, d^3 p}$$

represents a spread in the total energy of the electrons in the beam.

For a cold beam and a lossy waveguide, the dispersion relation is

$$\left\{ \omega^2 - k^2 - \left[1 - \frac{\delta}{r_w} (j - 1) \right] \right\} - (\omega - k\beta_z - b)^2 = -\varepsilon_c \quad (F.3)$$

where δ is the skin depth of the waveguide wall, defined in Eq. 2.77, and it was assumed that $\delta/r_w \ll 1$.

BIBLIOGRAPHY

1. M. Abramowitz and I. A. Stegun, Handbook of Mathematical Functions, Dover Publications, Inc., New York, 1972.

2. J. M. Baird, "Gyrotron Theory," High Power Microwave Sources, V. L. Granatstein and I. Alexeff, Editors, Artech House, Inc., Boston, Massachusetts, Chapter 4, 1987.

3. J. M. Baird, private communication, August 1988.

4. J. M. Baird, "Study of Input Couplers for Tapered Interaction Gyrotron Amplifiers," Final Technical Report on Naval Research Laboratory Contract No. N00014-82-K-2053, Microwave Device and Physical Electronics Laboratory, Department of Electrical Engineering, University of Utah, Salt Lake City, Utah, June 1985.

5. D. E. Baldwin, I. B. Bernstein, and M. P. H. Weenink, "Kinetic Theory of Plasma Waves in a Magnetic Field," Advances in Plasma Physics, Vol. 3, Edited by A. Simon and W. B. Thompson, John Wiley and Sons, Inc., New York, 1969.

6. L. R. Barnett, Y. Y. Liu, K. R. Chu, and V. L. Granatstein, "An Experimental Wide-Band Gyrotron Traveling-Wave Amplifier," IEEE Transactions on Electron Devices, Vol. ED-28, No. 7, 1981, pp. 872-875.

7. L. R. Barnett, J. M. Baird, Y. Y. Lau, K. R. Chu, and V. L. Granatstein, "A High Gain Single Stage Gyrotron Traveling-Wave Amplifier," IEEE International Electron Device Meeting (IEDM) Journal, 1980, pp. 314-317.

8. L. R. Barnett, K. R. Chu, J. M. Baird, V. L. Granatstein, and A. T. Drobot, "Gain, Saturation, and Bandwidth Measurements of the NRL Gyrotron Traveling-Wave Amplifier," IEEE International Electron Device Meeting (IEDM] Journal, 1979, pp. 164-167.

9. L. R. Barnett, private communication, July 1987.

10. H. P. Bleum, P. E. Latham, W. G. Lawson, and C. D. Striffler, "Single Particle Motion in a Large-Orbit Gyrotron," IEEE Transactions on Microwave Theory and Techniques, Vol. MTT-35, No. 11, 1987, pp. 946-955.

11. D. L. Bobroff, "Independent Space Variables for Small Signal Electron Beam Analysis," IEEE Transactions on Electron Devices, Vol. ED-6, January 1959, pp. 68-78.

12. V. L. Bratman, N. S. Ginzburg, G. S. Nusinovich, M. I. Petelin, and P. S. Strelkov, "Relativistic Gyrotrons and Cyclotron Autoresonance Masers," *International Journal of Electronics*, Vol. 51, No. 4, 1981, pp. 541-567.

13. R. J. Briggs, *Electron-Stream Interaction with Plasmas*, MIT Press, Cambridge, Massachusetts, 1964.

14. R. L. Burden and J. D. Faires, *Numerical Analysis*, Third Edition, Prindle, Weber & Schmidt Publishers, Boston, Massachusetts, 1985.

15. E. Butkov, *Mathematical Physics*, Addison-Wesley Publishing Company, Reading, Massachusetts, 1968.

16. R. Chou and A. Lee, "Modal Attenuation in Multilayered Coated Waveguides," *IEEE Transactions on Microwave Theory and Techniques*, Vol. 36, No. 7, 1988, pp. 1167-1176.

17. K. R. Chu, "Theory of Electron Cyclotron Maser in a Cavity at the Harmonic Frequencies," *Physics of Fluids*, Vol. 21, No. 12, 1978, pp. 2354-2364.

18. K. R. Chu, A. T. Drobot, V. L. Granatstein, and J. L. Seftor, "Characteristics and Optimum Operating Parameters of a Gyrotron Traveling-Wave Amplifier," *IEEE Transactions on Microwave Theory and Techniques*, Vol. MTT-27, No. 2, 1979, pp. 178-187.

19. K. R. Chu, A. T. Drobot, H. H. Szu, and P. Sprangle, "Theory and Simulation of the Gyrotron Traveling-Wave Amplifier Operation at Cyclotron Harmonics," *IEEE Transactions on Microwave Theory and Techniques*, Vol. MTT-28, No. 4, 1980, pp. 313-317.

20. K. R. Chu and J. L. Hirshfield, "Comparative Study of the Axial and Azimuthal Bunching Mechanisms in Electron Cyclotron Instabilities," *Physics of Fluids*, Vol. 21, No. 3, 1978, pp. 461-466.

21. K. R. Chu, Y. Y. Lau, L. R. Barnett, and V. L. Granatstein, "Theory of a Wide-Band Distributed Gyrotron Traveling-Wave Amplifier," *IEEE Transactions on Electron Devices*, Vol. ED-28, No. 7, 1981, pp. 866-871.

22. G. Dohler and W. Friz, "Coupling Impedances in Synchronous Fast-Wave Devices," *International Journal of Electronics*, Vol. 55, No. 4, 1983, pp. 523-532.

23. J. J. Dongarra, C. B. Moler, J. R. Bunch, and G. W. Stewart, *Linpack User's Guide*, Society for Industrial and Applied Mathematics, Philadelphia, Pennsylvania, 1979.

24. A. W. Fliflet, "Linear and Nonlinear Theory of the Doppler-Shifted Cyclotron Resonance Maser Based on TE and TM Waveguide Modes," International Journal of Electronics, Vol. 61, No. 6, 1986, pp. 1049-1080.

25. A. W. Fliflet, private communication, April 1988.

26. A. W. Fliflet and M. E. Read, "Use of Weakly Irregular Waveguide Theory to Calculate Eigen Frequencies, Q Values, and RF Field Functions for Gyrotron Oscillators," International Journal of Electronics, Vol. 51, No. 4, 1981, pp. 475-484.

27. A. W. Fliflet, M. E. Read, K. R. Chu, and R. Seeley, "A Self-Consistent Field Theory for Gyrotron Oscillators: Application to a Low Q Gyromonotron," International Journal of Electronics, Vol. 53, No. 6, 1982, pp. 505-521.

28. V. A. Flyagin, A. V. Gapanov, M. I. Petelin, and V. K. Yulpatov, "The Gyrotron," IEEE Transactions on Microwave Theory and Techniques, Vol. MTT-25, No. 6, 1977, pp. 514-521.

29. O. P. Gandhi, Microwave Engineering and Applications, Pergamon Press, Inc., Elmsford, New York, 1981.

30. A. K. Ganguly and S. Ahn, "Self Consistent Large Signal Theory of the Gyrotron Traveling-Wave Amplifier," International Journal of Electronics, Vol. 53, No. 6, 1982, pp. 641-658.

31. D. Golomb, Y. Goren, A. Ron, and J. L. Hirshfield, "Investigation of the Saturation Properties of Gyroamplifiers," IEEE Transactions on Microwave Theory and Techniques, Vol. 36, No. 6, 1988, pp. 934-938.

32. R. F. Harrington, Time Harmonic Electromagnetic Fields, McGraw-Hill Book Company, New York, 1961.

33. Hewlett Packard Company, Relocatable Libraries Reference Manual for HP 1000, Operating Systems RTE-4 and RTE-6/VM, Manual Part No. 92077-90377, 1987.

34. R. W. Hornbeck, Numerical Methods, Prentice-Hall, Inc., Englewood Cliffs, New Jersey, 1975.

35. H. P. Hsu, Vector Analysis, Simon and Schuster, New York, 1969.

36. J. D. Jackson, Classical Electrodynamics, Second Edition, John Wiley & Sons, Inc., New York, 1975.

37. C. C. Johnson, Field and Wave Electrodynamics, McGraw-Hill Book Company, New York, 1965.

38. D. S. Jones, _Methods in Electromagnetic Wave Propagation_, Oxford University Press, Inc., Fair Lawn, New Jersey, 1979.

39. R. M. Jones and M. W. Alcock, "The Power Transfer and Frequency Detuning in a Gyrotron," _International Journal of Electronics_, Vol. 57, No. 6, 1984, pp. 901-914.

40. J. A. Kong, _Electromagnetic Wave Theory_, John Wiley and Sons, Inc., New York, 1986.

41. E. J. Konopinski, _Electromagnetic Fields and Relativistic Particles_, McGraw-Hill Book Company, New York, 1981.

42. N. A. Krall and A. W. Trivelpiece, _Principles of Plasma Physics_, McGraw-Hill Book Company, New York, 1973.

43. K. E. Kreisher and R. J. Temkin, "Linear Theory of an Electron Cyclotron Maser Operating at the Fundamental," _Plasma Fusion Center Report_, Massachusetts Institute of Technology, Cambridge, Massachusetts, March 1980.

44. S. P. Kuo, S. C. Kuo, B. R. Cheo, and M. C. Lee, "Analysis of the Harmonic Gyrotron Traveling-Wave Amplifier," _International Journal of Infrared and Millimeter Waves_, Vol. 7, No. 4, 1986, pp. 635-651.

45. Y. Y. Lau, "Simple Macroscopic Theory of Cyclotron Maser Instabilities," _IEEE Transactions on Electron Devices_, Vol. ED-29, No. 2, 1982, pp. 320-335.

46. Y. Y. Lau and L. R. Barnett, "A Note on Gyrotron Traveling-Wave Amplifiers Using Rectangular Waveguide, _IEEE Transactions on Electron Devices_, ED-30, No. 8, 1983, pp. 908-912.

47. Y. Y. Lau and K. R. Chu, "Gyrotron Traveling-Wave Amplifier: III. A Proposed Wide-Band Fast Wave Amplifier," _International Journal of Infrared and Millimeter Waves_, Vol. 2, No. 3, 1981, pp. 415-425.

48. Y. Y. Lau, K. R. Chu, L. R. Barnett, and V. L. Granatstein, "Gyrotron Traveling-Wave Amplifier: I. Analysis of Oscillations," _International Journal of Infrared and Millimeter Waves_, Vol. 2, No. 3, 1981, pp. 373-393.

49. Y. Y. Lau, K. R. Chu, L. R. Barnett, and V. L. Granatstein, "Gyrotron Traveling-Wave Amplifier: IV. Analysis of Launching Losses," _International Journal of Infrared and Millimeter Waves_, Vol. 3, No. 1, 1982, pp. 45-62.

50. Y. Y. Lau, K. R. Chu, L. R. Barnett, and V. L. Granatstein, "Gyrotron Traveling-Wave Amplifier: II. Effects of Velocity Spread and Wall Resistivity," International Journal of Infrared and Millimeter Waves, Vol. 2, No. 3, 1981, pp. 395-413.

51. W. Lawson and C. D. Striffler, "A General Linear Growth Rate Formula for Large Orbit, Annular Electron Beams," Physics of Fluids, Vol. 28, No. 9, 1985, pp. 2868-2887.

52. C. S. Lee, S. W. Lee, and S. L. Chuang, "Normal Modes in an Overmoded Circular Waveguide Coated with Lossy Material," IEEE Transactions on Microwave Theory and Techniques, Vol. MTT-34, No. 7, 1986, pp. 773-785.

53. Q. F. Li, S. Y. Park, and J. L. Hirshfield, "Theory of Gyrotron Traveling-Wave Amplifiers," IEEE Transactions on Micrwoave Theory and Techniques, Vol. MTT-34, No. 10, 1986, pp. 1044-1058.

54. P. A. Lindsay, "Gyrotrons (Electron Cyclotron Masers): Different Mathematical Models," IEEE Transactions on Quantum Electronics, Vol. QE-17, No. 8, 1981, pp.1327-1333.

55. J. B. Marion and M. A. Heald, Classical Electromagnetic Radiation, Second Edition, Academic Press, Inc., New York, 1980.

56. A. N. Matveyev, Principles of Electrodynamics (L. F. Landovitz, Translator), Reinhold Publishing Corporation, New York, 1966.

57. P. M. Morse and H. Feshback, Methods of Theoretical Physics, McGraw-Hill Book Company, New York, 1953.

58. G. S. Nusinovich, "Linear Theory of a Gyrotron with Weakly Tapered Magnetic Field," International Journal of Electronics, Vol. 64, No. 1, 1988, pp. 127-135.

59. E. Ott and W. M. Manheimer, "Theory of Microwave Emission by Velocity Space Instabilities in an Intense Relativistic Electron Beam," IEEE Transactions on Plasma Science, Vol. PS-3, No. 1, March 1975, pp. 1-5.

60. W. H. Press, B. P. Flannery, S. A. Teukolvsky, and W. T. Vetterling, Numerical Recipes, Cambridge University Press, New York, 1986.

61. S. Ramo, J. R. Whinnery, and T. vanDuzer, Fields and Waves in Communication Electronics, Second Edition, John Wiley and Sons, Inc., New York, 1984.

62. G. N. Rapoport, A. K. Nemak, and V. A. Zhurakhovskiy, "Interaction Between Helical Electron Beams and Strong Electromagnetic Cavity Fields at Cyclotron Harmonic Frequencies," *Radio Electron Energy Physics*, Vol. 12, 1967, pp. 587-595.

63. G. Reiter, "Generalized Telegraphist's Equation for Waveguides of Varying Cross Section," *Proceedings of the Convention on Long Distance Transmission by Waveguide*, London, January 1959, pp. 54-57.

64. P. S. Rha, *Self-Consistent Theory and Simulation of High Harmonic Gyrotron and Peniotron Oscillators Operating in a Magnetron-Type Open Cavity*, PhD Dissertation, Department of Electrical Engineering, University of Utah, Salt Lake City, Utah, 1986.

65. E. J. Rothwell, "Analysis of Loss to Prevent Oscillations in the Slow Wave Cyclotron Amplifier," *International Journal of Electronics*, Vol. 53, No. 6, 1982, pp.715-727.

66. G. J. Sehn, *Relativistic Interaction Between a Rotating Electron Beam and a Microwave Field Inside a Waveguide at the Cyclotron Frequency*, PhD Dissertation, University of Colorado, Boulder, Colorado, 1967.

67. S. R. Seshadri, *Fundamentals of Plasma Physics*, American Elsevier Publishing Company, New York, 1973.

68. L. F. Shampine and M. K. Gordon, *Computer Solution of Ordinary Differential Equations*, W. H. Freeman and Company, San Francisco, California, 1975.

69. R. Shankar, *Principles of Quantum Mechanics*, Plenum Press, New York, 1980.

70. J. C. Slater, *Microwave Electronics*, D. Van Nostrand Company, New York, 1950.

71. L. Solymar, "Spurious Mode Generation in Nonuniform Waveguides," *IRE Transactions on Microwave Theory and Techniques*, Vol. 7, July 1959, pp. 379-383.

72. P. Sprangle and A. T. Drobot, "The Linear and Self-Consistent Theory of the Electron Cyclotron Maser Instability," *IEEE Transactions on Microwave Theory and Techniques*, Vol. MTT-25, No. 6, 1977, pp. 528-544.

73. P. A. Stark, *Introduction to Numerical Methods*, Macmillan Publishing Co., Inc., New York, 1970.

74. R. S. Symons, H. R. Jory, S. J. Hegji, and P. E. Ferguson, "An Experimental Gyro-TWT," IEEE Transactions on Microwave Theory and Techniques, Vol. MTT-29, No. 3, 1982, pp. 181-184.

75. R. S. Symons, H. R. Jory, S. J. Hegji, and P. E. Ferguson, "An Experimental Gyro-TWT," IEEE Transactions on Microwave Theory and Techniques, Vol. MTTS-29, No. 3, 1981, pp. 181-184.

76. A. W. Trivelpiece and R. W. Gould, "Space Charge Waves in Plasma Columns," Journal of Applied Physics, Vol. 30, No. 11, 1959, pp. 1784-1793.

77. P. Vitello, W. H. Miner, and A. T. Drobot, "Theory and Modeling of a Compact Low-Field, High-Frequency Gyrotron," IEEE Transactions on Microwave Theory and Techniques, Vol. MTT-32, No. 4, 1984, pp. 373-386.

78. J. L. Vomvoridis, "An Efficiency Doppler-Shifted Electron-Cyclotron Maser Oscillator," International Journal of Electronics, Vol. 53, No. 6, 1982, pp. 555-571.

79. J. M. Wachtel and E. J. Wachtel, "Backward-Wave Oscillation in the Gyrotron," Applied Physics Letters, Vol. 37, No. 12, 1980, pp. 1059-1061.

80. Chang-biao Wang, Jian-nan Tu, Hua-bei Jiang, and Yan Sun, "On the Two Methods of Kinetic Theory of ECRM," International Journal of Infrared and Millimeter Wves, Vol. 7, No. 7, 1986, pp. 1005-1035.

MISSION
of
Rome Air Development Center

RADC plans and executes research, development, test and selected
acquisition programs in support of Command, Control, Communications
and Intelligence (C^3I) activities. Technical and engineering support within
areas of competence is provided to ESD Program Offices (POs) and other
ESD elements to perform effective acquisition of C^3I systems. The areas
of technical competence include communications, command and control,
battle management, information processing, surveillance sensors,
intelligence data collection and handling, solid state sciences,
electromagnetics and propagation, and electronic, maintainability, and
compatibility.

END

FILMED

6-89

DTIC